


5-2016

Analysis of Bridge Deck Sections by Pseudo-compressibility method based on FDM and LES: Improving Performance through Implementation of Parallel Computing

Blandine Therese Mbianda Kemayou
University of Arkansas, Fayetteville

Follow this and additional works at: <http://scholarworks.uark.edu/etd>

 Part of the [Civil Engineering Commons](#), and the [Transportation Engineering Commons](#)

Recommended Citation

Mbianda Kemayou, Blandine Therese, "Analysis of Bridge Deck Sections by Pseudo-compressibility method based on FDM and LES: Improving Performance through Implementation of Parallel Computing" (2016). *Theses and Dissertations*. 1619.
<http://scholarworks.uark.edu/etd/1619>

This Thesis is brought to you for free and open access by ScholarWorks@UARK. It has been accepted for inclusion in Theses and Dissertations by an authorized administrator of ScholarWorks@UARK. For more information, please contact scholar@uark.edu, ccmiddle@uark.edu.

Analysis of Bridge Deck Sections by Pseudo-compressibility method based on FDM and LES:
Improving Performance through Implementation of Parallel Computing

A thesis submitted in partial fulfillment
of the requirements for the degree of
Master of Science in Civil Engineering

By

Blandine Therese Mbianda Kemayou
University of Douala
Bachelor in Industrial Engineering, 2011
University of Douala
Master of Science in Civil Engineering, 2013

May 2016
University of Arkansas

This Thesis is approved for recommendation to the Graduate Council

Dr. R. Panneer Selvam
Thesis Director

Dr. Ernie Heymsfield
Committee Member

Dr. Micah Hale
Committee Member

ABSTRACT:

The incidence of wind on bridges produces static and dynamic loading that must be adequately addressed when designing bridges. Dynamic loading is the primary concern, as the amplitude of the structures response to the applied loading may be greatly amplified. Ideally, the bridge's properties should be designed to avoid dynamic loading. Previous investigations of wind loading on bridges consisted of measuring forces produced on scaled models of bridges within wind tunnels. However, these wind tunnel tests are costly and time consuming due to cost to fabricate and instrument the bridge cross sections. Recent advancements in computational power of computers allow realistic simulation of wind flow over bridges via computational fluid dynamics (CFD). It is advantageous to study wind forces on bridge decks via computer simulation because parameters of the bridge and the wind field around it can be modified to evaluate their influences on the forces produced on the bridge. The present study introduces a new computer model that is used to simulate two-dimensional flow of wind around a bridge deck. This program is in parallel format, which substantially reduces computational time compared to time required for similar simulations on a single computer. Minimum grid refinement to adequately resolve the boundary layer is identified. A user manual is developed so that the program can be operated by a designer with minimal training. Finally, the model is validated by comparing the force coefficients that it predicts with force coefficients from wind tunnel experiments.

KEY WORDS: Wind loading, bridge aerodynamic, computational fluid dynamic, parallel computing

ACKNOWLEDGMENTS

Special thanks are extended to my advisor Dr. R. Selvam for his unconditional support, time and guidance during this work. I am thankful for the opportunity he gave me to work on the project upon my arrival, to use his “UofA Bridge code” program and his training on Tecplot software. I am grateful for the financial support of the Fulbright scholarship, GENEX and Harold R. Bosch.

I would also like to thank Dr. Selvam research group (Dr. Matt Strasser and Dr. Nawfal Ahmed) for their assistance in understanding the topic and reviewing my work. Many thanks to the faculty and staff at the Civil engineering department of the University of Arkansas for their commitment to students especially to my committee member Dr. Micah Hale and Dr. Ernie Heymsfield for their time spent in reviewing this thesis.

My thanks goes out to my family, my parents Kemayou Joseph and Kemayou Rose, my brother and sisters: Joel, Christelle and Stephanie for their word of encouragement, love and prayers.

TABLE OF CONTENTS

ANALYSIS OF BRIDGE DECK SECTIONS BY PSEUDO-COMPRESSIBILITY METHOD BASED ON FDM AND LES: IMPROVING PERFORMANCE THROUGH IMPLEMENTATION OF PARALLEL

COMPUTING.....	1
ABSTRACT:	2
ACKNOWLEDGMENTS.....	3
LIST OF TABLES.....	8
LIST OF FIGURES.....	9
1. INTRODUCTION.....	1
1.1. OVERVIEW	1
1.2. THESIS MOTIVATION.....	2
1.3. OBJECTIVES	3
2. LITERATURE REVIEW: BRIDGE AERODYNAMICS.....	6
2.1. INTRODUCTION	6
2.2. EXPERIMENTAL SIMULATION OF BRIDGES: WIND TUNNEL TESTS	6
2.2.1. <i>Wind tunnel tests with Full Bridge Model.....</i>	<i>6</i>
2.2.2. <i>Wind tunnel tests on the Taut Strip Model.....</i>	<i>7</i>
2.2.3. <i>Wind tunnel tests on the Section Model.....</i>	<i>8</i>
2.3. NUMERICAL SIMULATION OF BRIDGES	8
2.3.1. <i>General equation to be solved</i>	<i>8</i>
2.3.2. <i>Numerical method for solving governing flow equation</i>	<i>9</i>
2.4. COMPUTATIONAL FLUID DYNAMIC (CFD) METHOD.....	10
2.4.1. <i>Overview.....</i>	<i>10</i>
2.4.2. <i>CFD methods in bridge aerodynamic.....</i>	<i>14</i>
2.5. OTHER THAN CFD METHODS.....	24

2.5.1.	<i>The sparse third-order Volterra model</i>	24
2.5.2.	<i>Lattice Boltzmann Method (LBM)</i>	24
2.6.	ADVANCED METHODS	25
2.6.1.	<i>Linear and nonlinear approach</i>	25
2.6.2.	<i>Probabilistic/Statistical method (Stochastic model)</i>	25
2.6.3.	<i>CFD with aerodynamics countermeasures</i>	26
2.7.	CONCLUSION AND JUSTIFICATION OF THE THESIS	27
3.	WIND EFFECTS ON BRIDGE	28
3.1.	INTRODUCTION	28
3.2.	WIND LOAD	28
3.2.1.	<i>Wind Pressure</i>	29
3.2.2.	<i>Wind forces and moment</i>	29
3.3.	WIND INDUCED FORCES ON BRIDGES.....	32
3.3.1.	<i>Static effects</i>	33
3.3.2.	<i>Dynamics effects</i>	33
4.	COMPUTER MODELLING	38
4.1.	STRUCTURE AND FLOW PARAMETERS	38
4.1.1.	<i>Structure: Great Belt East Bridge (GBEB)</i>	38
4.1.2.	<i>Flow</i>	39
4.2.	GOVERNING EQUATIONS	41
4.2.1.	<i>Normalization</i>	41
4.2.2.	<i>Flow equation</i>	41
4.2.3.	<i>Boundary and initial conditions</i>	44
4.2.4.	<i>Numerical procedure to solve for the fluid equations</i>	45
4.2.5.	<i>Numerical diffusion and dispersion</i>	46
4.2.6.	<i>Parallel computing</i>	47

5. RESULTS	48
5.1. INTRODUCTION	48
5.2. PRESENTATION OF THE RESULTS	49
5.2.1. <i>Influence of Artificially Viscosity (AV) on force coefficients</i>	49
.....	54
5.2.2. <i>Parallel computing performance evaluation</i>	54
5.2.3. <i>Influence of grid refinement on force coefficients</i>	56
5.3. CONTOUR PLOT FOR DIFFERENT GRIDS	59
5.4. GENERAL REMARKS	70
5.4.1. <i>Vorticity contour and Strouhal number</i>	70
5.4.2. <i>Drag and lift coefficient</i>	74
5.4.3. <i>Pressure contour</i>	75
5.4.4. <i>Result summary</i>	76
6. CONCLUSION.....	80
6.1. SUMMARY AND CONCLUSION	80
6.2. MODEL LIMITATIONS AND RECOMMENDATION.....	82
7. USER MANUAL FOR “UOFA BRIDGE CODE” PACKAGE.....	83
7.1. INTRODUCTION	83
7.1.1. <i>Grid Generation</i>	83
7.1.2. <i>Bridge Solver</i>	84
7.1.3. <i>Visualization and Data Processing</i>	84
7.2. USER MANUAL FOR THE GRID GENERATION CODE.....	84
7.2.1. <i>Step 1: Pre-processing, preparation of the input data: acbrg-i.txt</i>	85
7.2.2. <i>Step 2: Pre-processing, preparation of the second input data inp.txt</i>	87
7.2.3. <i>Step 3: Processing, run the code acbrg.exe</i>	88
7.2.4. <i>Step 4: Post-processing, visualization of the output file</i>	89

7.2.5. Examples	89
7.3. USER MANUAL FOR THE BRIDGE CODE.....	93
7.4. USER MANUAL FOR POST PROCESSING	97
7.5. FLOWCHART OF THE DESIGN PROCESS USING THE PACKAGE “UOFA BRIDGE CODE”	101
REFERENCES	103
APPENDIX 1: GRID DETAILS WITH INNER AND OUTER POINTS.....	108
APPENDIX 2: SAMPLE INPUT AND OUTPUT FILE FOR MORE REFINED GRID.....	109

LIST OF TABLES

Table 1-1: Structural properties of Tacoma Narrow and GBEG bridge Picture from (Larsen & Walther, 1997)	3
Table 2-1: Percentile error for the forces coefficient (Cd, Cl,St,Cm,V) relative to wind tunnels experiments	21
Table 4-1: GBEB structural properties.....	39
Table 5-1: Change in force coefficient for different AV value and a single grid size GB1:333x90	50
Table 5-2: Change in force coefficient for different AV value and different grid size	51
Table 5-3: Running time for different processors	55
Table 5-4: Flow parameters for grids refined in radial direction.....	59
Table 5-5: Flow parameters for grid refined in tangential direction	59
Table 5-6: Error (in percentage), current work result with literature.....	77
Table 5-7: Summary of flow parameter for different studies.....	77
Table 5-8: <i>Comparison and contrast of the current work with Selvam & Govindaswamy (2002)</i>	79

LIST OF FIGURES

Figure 2-1: Full Model of Tacoma Narrows bridge (Parson,2015)	7
Figure 2-2 General view of a Taut Strip Model (Davenport et al., 1992).....	7
Figure 2-3: Deck Section Model (internal balance) of Messina bridge (Diana, et al. 2013)	8
Figure 2-4: CFD code procedures.....	10
Figure 2-5: CFD Methodology	13
<i>Figure 2-6:</i> Outline of published studies for the GBEB suspension span bridge.....	20
Figure 2-7 : Error in drag coefficient (C_d) versus minimum grid spacing B =bridge width	21
Figure 2-8: Error in Strouhal number (St) versus minimum grid spacing B =bridge width	22
Figure 2-9 : Error in lift coefficient (C_l) versus minimum grid spacing B =bridge width.....	22
Figure 2-10 : Error in critical wind velocity (V) versus minimum grid spacing B =bridge width.....	23
Figure 3-1: Wind load chain	28
Figure 3-2: Wind pressure representation on Great Belt East Bridge.....	29
Figure 3-3: Variation of drag coefficient (a) with Reynold number for a circular cylinder (Morgenthal & Mcrobbie, 2002) (b) with aspect ratio of cross section D/B for rectangular cylinder (Liu, 1991)	30
Figure 3-4: Wind force on bridge.....	32
Figure 3-5: Wind effect on bridges (Ubertini, 2008)	32
Figure 3-6: Classes of vortex formation observed with increasing elongation of different prismatic bodies: Class I, Leading-edge vortex shedding; Class II, Impinging leading-edge vortices; Class III, Trailing-edge vortex shedding (Deniz and Staubli 1997 in Morgenthal's work, 2000)	35
Figure 3-7: Illustration of (a) negative damping, (b) positive damping	37

Figure 4-1: Great Belt East Bridge a) suspension span cross section (dimension are in mm, Selvam & Govindaswamy, 2001); b) elevation (modified from iClickfun,2015).....	38
Figure 4-2: Structured grid coordinates system	44
Figure 4-3: Computational domain and boundary conditions.....	44
Figure 5-1: Mean drag and Strouhal number versus Artificial Viscosity coefficient plot (left to right).....	50
Figure 5-2: Vorticity plot for different AV value and single grid GB5:333x90	52
Figure 5-3: Vorticity plot for different AV=10 ⁻² and AV=10 ⁻⁴ value and three grids (GA4:549x70, GA5:549x80 and GA6:549x90).....	53
Figure 5-4: Vorticity plot for different AV=10 ⁻⁵ and AV=10 ⁻⁶ value and three grids (GA4:549x70, GA5:549x80 and GA6:549x90).....	54
Figure 5-5: Computation time (T) versus number of processor (N) plot for grid GB5: 333x90.	56
Figure 5-6: Schematic of the radial grid points development	57
Figure 5-7: Schematic of the tangential grid point developments.....	58
<i>Figure 5-8: Vorticity contour for grid refined in tangential direction full view.....</i>	60
Figure 5-9: Vorticity contour for grid refined in tangential direction close up view	61
Figure 5-10: Vorticity plot for grid refined in the radial direction, full view	62
Figure 6-11: Vorticity contour for grid refined in radial direction, close up view.....	63
Figure 5-12: Vorticity plot for grid refined in radial direction.....	63
<i>Figure 5-13: Pressure contour for grid refined in the tangential direction</i>	64
<i>Figure 5-14: Pressure contour for grid refined in the radial direction</i>	65
<i>Figure 5-15: Drag and lift coefficient plot for grid refined in tangential direction</i>	66
<i>Figure 5-16: Drag and lift coefficient plot for grid refined in radial direction</i>	67

Figure 5-17: Frequency and amplitude plot for grid refined in tangential direction.....	68
Figure 5-18: Frequency and amplitude plot for grid refined in radial direction	69
Figure 5-19 Vorticity plot from Selvam & Govindaswamy (2002): top grid 216x63;bottom grid 312x57.....	71
Figure 5-20: Minimum tangential spacing on bridge deck	72
Figure 5-21: Variation of Strouhal number with radial grid spacing	73
Figure 5-22: Variation of Strouhal number with tangential grid spacing, B is the bridge width	73
Figure 5-23: Variation of mean drag coefficient with tangential grid spacing, B is the bridge width	74
Figure 5-24: Variation of mean drag coefficient with radial grid spacing, B is the bridge width	75
Figure 5-25: Mean drag coefficient chart for different studies, B is the bridge width.....	77
Figure 5-26: Strouhal number chart for different studies, B is the bridge width	78
Figure 7-1: General window interface for pre and post processing	85
Figure 7-2: Window interface for the acbrg-i.txt file generation.....	86
Figure 7-3: Grid generation input file 2 window interface	87
Figure 7-4: Dos windows to run acbrg.exe code	88
Figure 7-5: Sample Grid domain and boundary points	89
Figure 7-6: Schematic of the radial grid points development	91
Figure 7-7: Sample grid visualization	92
Figure 7-8: Sample creation of a folder in Linux account	94
Figure 7-9: File transfer window 1	95
Figure 7-10: File transfer window 2	96
Figure 7-11: Windows interface for the dft-i.txt post processing file generation	98

Figure 7-12: Frequency versus amplitude plot from fr-o.plt file 100

1. INTRODUCTION

1.1. Overview

The world is experiencing a population growth and this leads to more demand for human facilities and therefore transportation means. Bridges span physical barriers such as valleys, rivers, and allow passage over these obstacles as roads, railroads, paths. To design such a civil engineering structure, and three main requirements need to be considered: durability or long service life, serviceability, and human safety. The construction of bridges with respect to the above criteria requires a proper investigation of wind induced load on bridges by engineers. Long span, slender, cable-stayed and suspension bridges because of their shape and weights are most vulnerable to wind load; henceforth, the major concern for bridge designers is to ensure the stability of their structures.

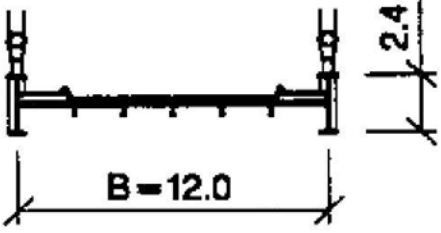
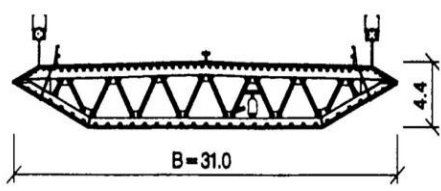
In the past, wind tunnel tests were the sole tool used by engineers to understand the response of bridge to wind load and assess their design; however, these experiments are time and cost consuming. Up to 6 to 8 weeks are needed to perform a typical wind tunnel test (Larsen & Walther, 1997). Moreover, experiment costs range from \$50,000 to \$100,000 per bridge girder cross section (Selvam et al., 2001). The development of computer technology in recent years has led to the trend of computer modelling to design bridges. A plethora of numerical methods based on computational fluid dynamics (CFD) has been developed to conduct wind analysis on bridge. Results which previously needed eight weeks to be obtained take only a couple of weeks with computer modelling (Selvam & Govindaswamy, 2002). This noticeable improvement in time and cost provides benefit for the different groups (Consulting firms, clients, project managers etc.) involved. Computational fluid dynamics (CFD) simulations are typically governed by a formulation of the incompressible continuity and Navier Stokes (NS) equations. Numerous

numerical methodologies are utilized to discretize and solve the governing equations. Force coefficients predicted for similar flow over similar cross sections vary because different grid refinements are utilized in different work. The literature contains no systematic investigation of the grid refinement to realistically resolve the flow around the bridge deck as is necessary to accurately compute forces on the deck.

1.2. Thesis Motivation

The collapse of the Tacoma Narrows Bridge due to wind loading (Washington, 1940) 4 months after its opening, brought the awareness to the worldwide bridge designers of the necessity of aerodynamic analysis. The failure was due to flutter instability, a phenomenon triggers when the wind speed is greater than the critical velocity; excessive increase of bridge deflection (negative damping) occurs and lead to the collapse of the bridge. Normally, with positive damping, deflection of a structure due to wind should decrease. The Great Belt East Bridge (GBEG), the focus of the present work, has a critical wind speed 78 mph (Reinhold et al., 1992);approximately twice of the 40mph wind speed at which the Tacoma Narrow Bridge failed. In addition, the GBEG has higher structural properties when compared to the Tacoma Narrow Bridge (Table1-1). Design of bridge to resist wind requires careful aerodynamic instability study and good choice of structural characteristics (shape, weight, damping parameter, natural frequency etc.). The former constitute the focus of the present work.

Table 1-1: Structural properties of Tacoma Narrow and GBEG bridge Picture from (Larsen & Walther, 1997)

Bridge	<i>Old Tacoma Narrow Bridge</i>	<i>Great Belt East Bridge</i>
Structure type:	suspension bridge	suspension bridge
Status	reconstructed & in use since 1950	In use since 1998
Location	Washington	Denmark
Material	Steel	Steel
Shape	H- shape & plate girder	Streamlined& Box girder
Main span length	2800 ft	5328.1 ft
Mass(Plf)	$2.85 \cdot 10^3$	$15.225 \cdot 10^3$
Inertia Psf/ft	$1.28 \cdot 10^6$	$17.82 \cdot 10^6$
Cross section(dimension in m)		

1.3. Objectives

The first goal of the present research is to investigate the computer model “*UofA Bridge Code*” developed to analyze bridges based on an improved Finite Difference Model, structural mechanics and CFD principles. The second goal is to demonstrate how the current model improves the Selvam & Govindaswamy (2002) model. Finally, once the model is assessed through wind tunnel experimental results for the Great Belt East Bridge (GBEG) and other recent works, a grid resolution study will be done to provide accurate grid range spacing to predict accurate force parameters. The tasks below will be followed to achieve our objectives:

TASK 1: Validate the model and evaluate the parallel computing performance

This part intends to assess “*UofA Bridge Code*” by comparing flow parameters predicted by the simulation of the GBEG suspension span with wind tunnel test and previous models (Reinhold et al. (1992), Bruno & Chris (2002), Selvam et al. (2002), Braun & Auruch (2008) and Patro et al. (2013)). By using the “*UofA Bridge Code*” model, the goal is to ensure the model can give results in comparison with previous work. The task will be approached by the following phases:

- ✓ Estimation of the discrepancy between the results obtained from the “*UofA Bridge Code*” model and previous models.
- ✓ Comparison of the running time using 1 to 6 processors for a specific grid size, and assessment of the efficiency of parallel computing
- ✓ Enumeration of the limitations of the current model “*UofA Bridge Code*”

TASK 2: Demonstrate the user friendliness of the model and write a user manual

The “*UofA Bridge Code*” is an improved version of Selvam & Govindaswamy (2001) Model. This task aimed to present the limitation of the Selvam & Govindaswamy (2001) model solved and reduced by the current model and provide a user guide. Fixed Bridge will be used and the task will be achieved by:

- ✓ Comparing and contrasting the current model for fixed bridge with that of the Selvam & Govindaswamy (2001) model
- ✓ Writing a user manual for the “*UofA Bridge Code*” package

TASK 3: Conduct a grid resolution and artificial viscosity study

Complementary to task 1, the goal of task 3 is to guide engineers in proper grid and artificial viscosity (AV) factor choice during their design. The steps are:

- ✓ Optimization of the grid resolution in tangential and radial direction and evaluation of the grid dependency of the result
- ✓ Study the influence of the artificial viscosity coefficient on flow parameters

The numerical modelling of bridge using the “*UofA Bridge Code*” package is an efficient tool for bridge designers to do a quick and accurate simulation of any type of bridge. With the parallel computing, this tool speeds up the designing process. For instance, a decrease in time for the modelling of GBEB suspension span is observed; initially, 8 weeks were needed with wind tunnel test. With the Selvam and Govindaswamy (2001) model few days run. Now with the current model only less than 30 minutes is required. This improvement in computational time decreases considerably the cost of the project. Moreover, with a friendly usage of the “*UofA Bridge Code*” package, designers with no background in grid generation process can smoothly conduct a bridge simulation.

2. LITERATURE REVIEW: BRIDGE AERODYNAMICS

2.1. Introduction

In this literature review, methods used to model bridges aerodynamic behavior under straight line wind are presented. A focus is made on computer modelling of a bridge subjected to wind flow. This approach is gaining popularity in recent years as compared to wind tunnel tests used in the past. The first part of this chapter present a brief overview to understand wind tunnel tests; the second part focuses on the numerical method used in bridge analysis (the equations to be solved and solving methods). The chapter is summed up with a conclusion about the thesis motivation.

2.2. Experimental simulation of bridges: wind tunnel tests

Wind tunnel tests were the sole mean used to design a bridge in the past; the goal is to physically and effectively represent a bridge and investigate its behavior under wind storm using any of the three types (full bridge, taut strip and section model) of wind tunnel tests (Simiu & Scanlan, 1986):

2.2.1. Wind tunnel tests with Full Bridge Model

Full Bridge Model is geometrically similar to the real bridge and is usually scaled to the order of 1/300 (Simiu & Scanlan, 1986). Parameters such as mechanical damping and mass distribution must be physically realistic. Figure 2-1 shows an example of the Tacoma bridge model.



Figure 2-1: Full Model of Tacoma Narrows bridge (Parson,2015)

2.2.2. Wind tunnel tests on the Taut Strip Model

The basic structure is made up of two wires stretched between anchor blocks. This model is effective in determining the response of long span bridges in turbulent boundary layer flow (Davenport et al., 1992); the Taut Strip Model correspond to the laboratory wind flow in a manner similar to the suspension bridge center span (Simiu & Scanlan, 1986).

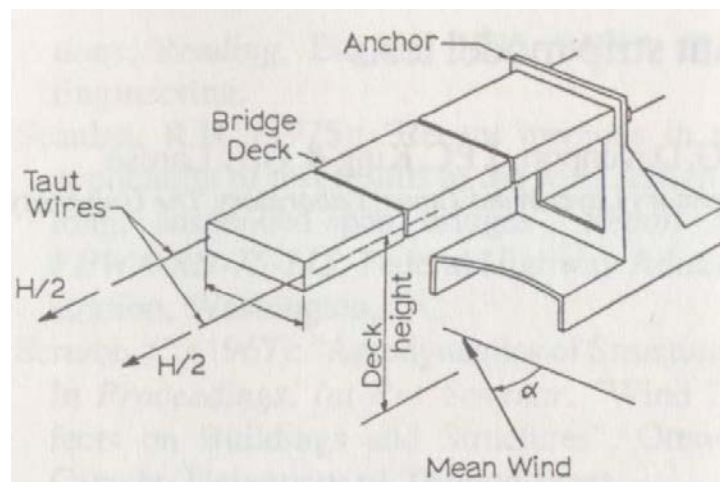


Figure 2-2 General view of a Taut Strip Model (Davenport et al., 1992)

2.2.3. Wind tunnel tests on the Section Model

Constructed with a scale of 1/50 to 1/25 to reduce the discrepancies between full-scale and section model (Simiu & Scanlan, 1986), the Section Model offers the advantage of being inexpensive as compared to the full bridge model. The Section Model is useful for making initial assessment for the aeroelastic stability and to measure aerodynamic characteristics of a bridge deck section.



Figure 2-3: Deck Section Model (internal balance) of Messina bridge (Diana, et al. 2013)

2.3. Numerical simulation of bridges

2.3.1. General equation to be solved

Bridge aerodynamics are bridge subjected to oscillate due to wind effects or wind induced loads; its analysis requires the investigation of surrounding wind flow, bridge structural motion and wind flow interaction with the structure. Thus, equations use for this purpose are:

- The Navier Stokes equations to solve for the wind flow pressure and velocity around the bridge
- The equations of motion for heaving and pitching to study the bridge translational and rotational motion and get its position at each time step

The fluid structure interaction is modeled by solving simultaneously both structural and flow equations. However, it brings the issue of Lagrangian and Eulerian coordinates. Lagrangian coordinates, a particle-following coordinates system, is used for the structural equation formulation; Eulerian coordinates, a fixed in space coordinates system, is on the other hand used for the fluid equation formulations (Selvam & Govindaswamy, 2001).

2.3.2. Numerical method for solving governing flow equation

Solving flow equations enables to determine the aerodynamic/flow parameters (flow parameters are discussed in chapter 4), wind velocity and pressure essential for a bridge design. A various number of numerical methods have been developed to solve the Navier Stokes equations and are discussed in the following sections.

- Computational Fluid Dynamics (CFD) methods;
- Complementary and other than CFD methods;
- Advanced methods developed in recent years

2.4. Computational Fluid Dynamic (CFD) method

2.4.1. Overview

CFD is a branch of fluid mechanics that uses numerical simulation to solve and analyze fluid flow problems and Navier Stokes equations as previously mentioned. The procedure and methodology used in CFD codes are described in Figure 2-5 and Figure 2-4.

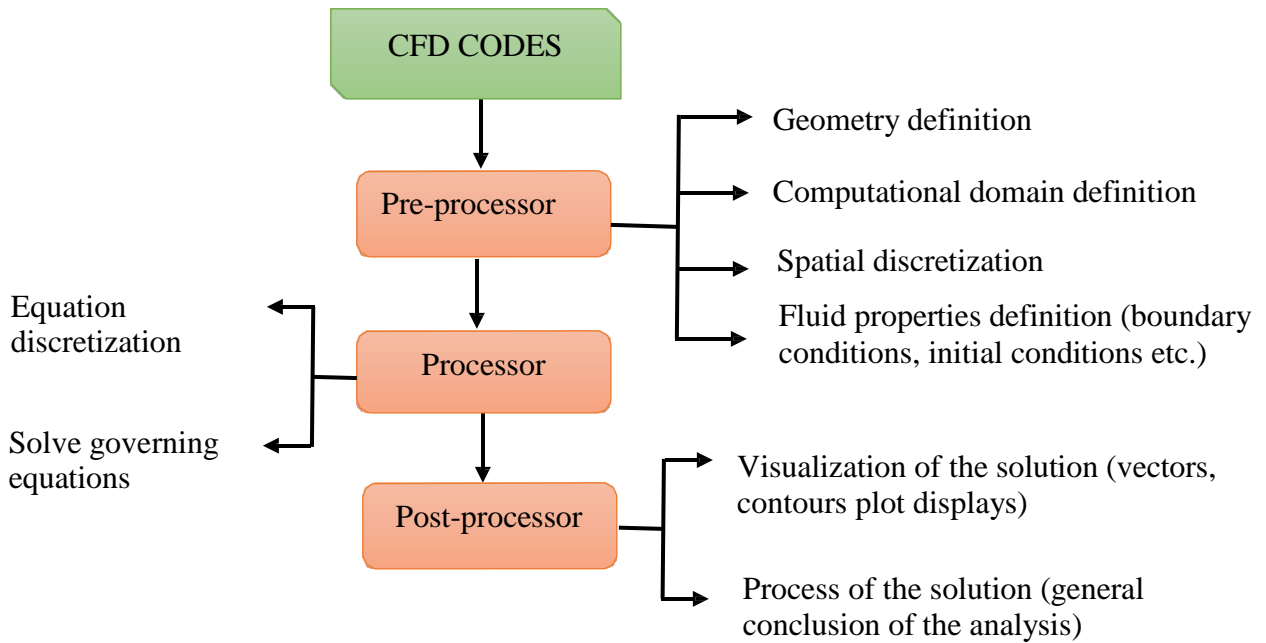


Figure 2-4: CFD code procedures

Discretization methods and turbulence models formed the main part of CFD methodology.

2.4.1.1. *Discretization methods*

The method involves all the process of transforming a continuous fluid flow into separate and distinct numerical data. This is done through equation, spatial and time discretization. In spatial discretization, partial differential equations are approximated as systems of linear equations that a computer can easily process. Finite Element Method (FEM), Finite

Difference Method (FDM), Finite Volume Method (FVM), Boundary Element Method (BEM) and Spectral Element Method (SEM) are used for equations discretization (described in Anderson (1995), Ferziger & Peric (1999) and Lewis (1991)). Domain discretization is also used to break up the study domain in discrete sub-domains to form the mesh as mentioned in section 1.2. Temporal discretization splits the time in the flow into distinct time step using either explicit or implicit methods. Explicit and implicit methods, fully detailed in Blazek (2001), use respectively a forward and backward difference in time; implicit methods use large time step (Fan Liaw, 2005).

2.4.1.2. *Turbulence Models*

In most CFD applications, the flow regime is characterized by chaotic property changes (pressure, velocity) at a point in time; this is the turbulent flow regime. Unlike turbulent regime, the flow is smooth and adjacent layers of fluid slide one over the other in laminar regime. The transition from laminar to turbulent depends upon the type of flow and body. Turbulent flow is modeled by Large Eddy Simulation (LES), Reynold Average Navier-Stokes equations (RANS), Direct Numerical Simulations (DNS) and Detached Eddy Simulation (DES) Figure 2-5.

❖ Large Eddy Simulation(LES)

The model is classified and formulated from space filtered equations. In space filtered equations, eddies larger than the grid size (or length scale) are resolved directly while smaller eddies are approximated using model such as eddy viscosity model (Selvam, 1997). LES uses time dependent equations and requires a large amount of computer time and storage. The model was used by Selvam & Govindaswamy (2001) to analyze the GBEB deck section and will be used in the present work with FDM.

❖ **Reynold Average Navier-Stokes equations (RANS)**

Unlike LES, RANS models all aspect of the unsteady flow using time averaged equations (Selvam, 2014). Using time-independent equations (Selvam & Govindaswamy, 2001) in RANS models, the flow is split into time average mean and fluctuating components. The original Navier Stokes equations remains unchanged with mean values as variables and unknown extra terms called Reynolds stresses. The different turbulent models that depend upon the relationship developed for the Reynold stresses are: zero equation model-mixing length, two equation models k- ϵ , Reynold stress equations and Algebraic equations (Selvam , 2014), details are found in Chen & Jaw, (1998).

❖ **Direct Numerical Simulations (DNS)**

Here, the Navier stokes equations are solved without any turbulence model; to capture all the eddies' size developed, more refined grids are necessary and this is challenging. DNS is restricted to a certain range of Reynolds number (Selvam, 2014).

❖ **Detached eddy simulation(DES)**

DES model switches between RANS and LES, it employs LES in the wake of the region and RANS model near the solid boundaries (Fan Liaw, 2005). When using LES, DES reduces computational effort; DES is used by commercial software like ANSYS-CFX (Menter & Kuntz, 2001).

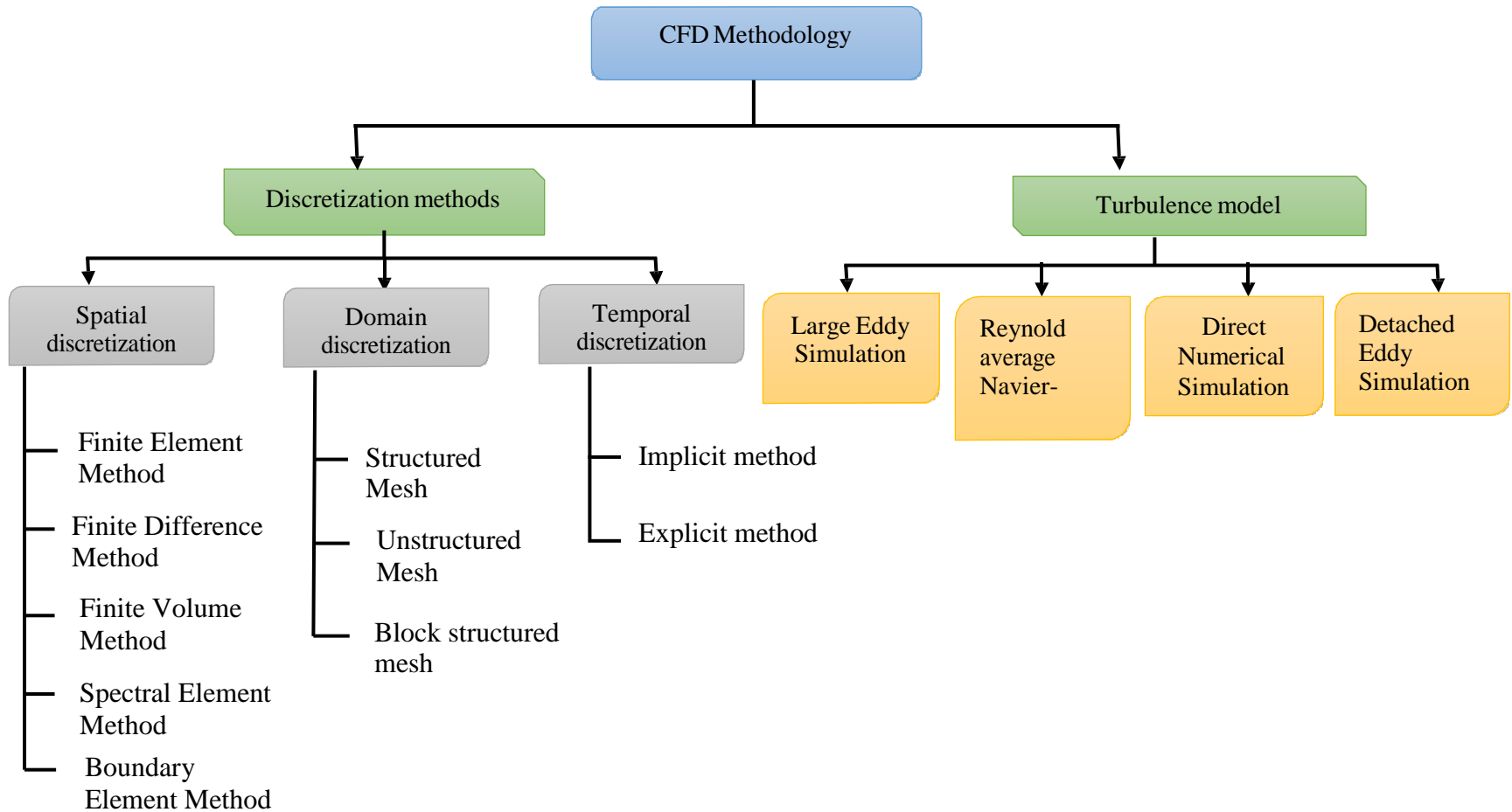


Figure 2-5: CFD Methodology

2.4.2. CFD methods in bridge aerodynamic

A computational domain representing the bridge and its surrounding fluid flow is necessary when solving the Navier stokes equations. Indeed, this domain helps to transform the partial differential equations to a form understandable by computers and to break up the continuous fluid flow into discrete elements; the grid or mesh is used for this purpose in CFD problems. Generally, the solution accuracy can be influenced by the grid characteristics (type, size, number of nodes, and distance between nodes in x, y and z direction). Numerous methods in CFD are grid dependent or not; a review of these methods follows.

2.4.2.1. *Grid based method*

A classification is done for fixed and movable bridges; for fixed bridges, only the vortex shedding can be extracted through aerodynamic parameters while for movable bridges in addition to the vortex shedding, flutter analysis can be done. Vortex shedding, flutter and aerodynamic parameters are discussed in chapter 3 and 4.

2.4.2.1.1. Fixed bridges

In fixed bridge computer modelling, the bridge cross-section is restrained against any rotational or translational motion and the grid velocity is zero on the bridge boundary. Previous works on grid based method and fixed bridge are detailed in following paragraphs:

- Selvam et al. (1998) and Selvam (1998), used FEM 2D and 3D model with LES turbulence model to compute the drag and Strouhal number of the GBEB approach span. Selvam et al. (1997b) and Tamura et al. (1993) used the FDM 2D model for the same GBEG. With 2% less grid than Tamura's work, Selvam et al. (1998) were

also able to obtain good results for the 3D model, demonstrating that the FEM is more accurate for modelling than the FDM. In the Selvam & Govindaswamy (2001) model, although the number of nodes was 7 times higher than that of Selvam et al. (1998), the FEM with LES model for the GBEB (suspension span) gave reasonable Strouhal number results and a lower drag coefficient than the predicted wind tunnel test results. The grid refinement and number of nodes increase the computational time; but, the FEM efficiency was again demonstrated. Selvam et al. (2010), used 60 times the number of nodes of Selvam et al. (1998) when comparing the GBEB (suspension span) 2D and 3D model. They concluded that FDM 3D model is not appropriate to predict aerodynamic parameters even with more refined grids. This may be due to the geometry of the bridge (suspension span vs approach span). From all the above mentioned studies, the grid generation is challenging for the design because engineers need to make appropriate grid characteristic choice; the grid generation process takes more time than to run the model (Patro et al. ,2013). The issue was overcome when the authors developed an adaptive mesh refinement or h-adaptive FEM & LES to analyze the GBEB (suspension span). Adaptive mesh refinement is based on velocity and vorticity gradient error for the mesh generation. With triangles elements, grid node points and computational time decrease in comparison to quadrilateral elements used in previous works (Selvam et al. 1998, 1997b ; Selvam & Govindaswamy, 2001; Selvam ,1998).

- Bai & Sun (2010), computed the aerodynamic forces coefficient for a 2D and 3D model of a U-shape beam and two generic bridges deck cross section. They developed a block iterative coupling method for the FSI and an improved CFD mesh

control method to generate an O type grid. The method was claimed to be accurate and in good agreement with the wind tunnel experiment of Larsen & Walther (1997,1998). Similarly, Selvam et al. (2010) used a different grid shape for their 3D analysis, the authors recommended a 2D CFD simulation instead of 3D for stable structures. However, some may ask at what range of flow characteristic a structure is considered stable. Selvam et al. (2010) were specific “At a high value of the Re (>50000)” when they made the above mentioned recommendation.

2.4.2.1.2. Movable bridges

Movable bridges are modelled considering a nonzero grid velocity. The bridge structural equation is solved to know the exact position of the bridge at each time step; the solution is incorporated when solving the continuity and momentum component of the Navier Stoke equations. The force coefficients are determined and in addition to that, the flutter analysis is done through forced or free oscillations. In the former technique, a set of frequency dependent flutter derivatives (H^*_i and A^*_i with $j=1, 2, 3$) are computed and critical flutter velocity is thus deduced. In the latter technique, the flutter velocity is observed directly with the flow equation. Many works using grid based method and movable bridges exist in the literature.

- Selvam et al. (2002), used the free oscillation technique for the GBEB suspension span. The pressure was solved for a given bridge position, the predicted pressure was then applied to the same bridge to find its new position and solve the flow equation again. This iterative process was repeated until the solution convergence is reached; the process was claimed to be less time consuming; however, details of the grid generation was lacking.

- Braun & Awruch (2003) used the pseudo-compressibility approach and FEM 2D flow to compute the Strouhal number of the GBEB suspension span. With an explicit scheme and Fluid Structure Interaction(FSI), the Strouhal number obtained was comparable with experimental tests. The approach was different from the semi-implicit procedure and the rigid body moving technique for FSI used by Selvam & Govindaswamy (2001). The processing time was not efficient and details about the grid generation process was missing. In 2008 , Braun & Awruch idealized the same GBEB section with Jersey barriers and safety wire fences and used the same 2003 numerical method for the Guama River Bridge (Para State,Brazil). It was demonstrated that the wire fences have negligible influence on bridges aerodynamic behavior, and no improvement in the computational time was specified.
- Frandsen (2004), computed the flutter limit of the same GBEB using spectrum analysis, FEM and self-excited motion. Using unstructured mesh and two different grids, a mesh dependency for the accurate flutter predictions was stated. Indeed, the more refined the boundary layers are, the more accurate the flutter velocity is predicted. Futhermore, flow obstructions such as wind screens and guide vanes decrease flutter limit and suppress large vortex-induced vibrations. It should be noted that, Frandsen fairly represented the boundary layer confirming the flate plate theory of Theodorsen (1935): “accurate model of boundary layer is not critical for the flutter phenomenon”. With comparable results with wind tunnel test, the mechanism of grid formation was unclear.
- Bai & Sun (2010), computed the flutter derivatives for a 2D and 3D model of two generic bridge decks using a forced vibration technique. In the method, a frequency

and amplitude was assigned to the bridge to initiate its oscillation in pitching and heaving sinusoidal motions. In the free vibration technique, neither initial force nor frequency were applied to the bridge; the bridge cross section was elastically suspended in the flow and its stability was observed for various wind speeds. Patro et al. (2009) used the free vibration method for the flutter analysis of the GBEB suspension span and the Alternate Chesapeake and Delaware Canal Bridge (ACDCB). The h-adaptative mesh generator offered the advantage of reducing the number of nodes with finer grid resolution.

2.4.2.1.3. Issues of grid based methods

From the above literature review, information regarding the technique for proper mesh generation and grid parameter choice is lacking. Moreover, few studies stated the impact of grid refinement and grid spacing close to the bridge perimeter on the accuracy of the computed aerodynamic force coefficients. Figure 2-6 gives a summary of published studies for the GBEB suspension span bridge; Figure 2-7 to Figure 2-9 give the discrepancy plot versus minimum grid spacing for the aerodynamic coefficients and flutter velocity. The drag (C_d), Lift (C_l) and Moment (C_m) coefficient, Strouhal (St) number and Reynolds (Re) are dimensionless parameters. The grid spacing is a function of the bridge width (B); the percentile error was computed using wind tunnels results as reference.

It can be observed that grid spacing closed to the bridge boundaries do not always guarantee results in agreement with wind tunnel experiments (Figure 2-7). Theoretically more refined grid should lead to more accurate results of the force parameters; many factors for instance numerical diffusion, computational techniques may be responsible for the discrepancy.

Referring to the chart on Figure 2-8 , grid spacing less than $0.0002B$ have 20% and lower discrepancy for the Strouhal number. On the otherhand, for approximaatively the same grid spacing the lift and drag coefficient discrepancies are higher than 20% (Figure 2-7,Figure 2-9).

Selvam (2010), stated that an increase of grid refinement close to the bridge boundaries lead to an increase of accuracy for the predicted force coefficients. This is verify according to the graph in Figure 2-8; however, from the other plots a question raised: what is the limit or the grid spacing below which results may start to diverge from the exact solution? This is one issue the present research attempt to resolve; find a range of grid spacing near to the structure boundaries to expect accurate result of the force coefficients.

Figure 2-6: Outline of published studies for the GBEB suspension span bridge

Researchers	Numerical Methods and Geometry	Turbulence Model/ Strategy	Re	Grid Characteristics			Aerodynamic Parameters				Flutter Velocity (Uc) in m/s	Angle of Attack in degree
				Min spacing	Nodes	Element	Cd	Cl	St	Cm		
Larsen & Jacobsen(1992)	Wind Tunnel test experimental	Section Model and turbulent flow	-	Not applicable			0.57 & 0.59& 1.21	0.067 & -0.050 & -0.18	-	0.028 & 0.013	70-74	0
Reinhold et al(1992)			10 ⁵				0.08	0.01	0.109-0.158	0.04	74.2 & 78.4	0
								1.18	0.75	0.2	0.2	
Selvam et al (2002)	FEM	LES	10 ⁵	0.0015 B	14805	14570	0.062	-	0.14	-	69	-
Bruno & Chris (2003)	2D CVM	Laminar flow	-	0.002B	-	-	0.05	-0.227	0.17	-	-	0
			-	0.00022B	-	-	0.054	-0.288	0.186	-	-	0
	2D Statistical Approach	RSM(Reynold Stress Model)	10 ⁵	0.00022B	-	-	0.058	0.026	0.289	-	-	0
	2D CVM	LES	10 ⁵	0.00022B	-	-	0.071	-0.195	0.124-0.164	-	-	0
Braun & Auruch(2003)	FEM	ALE	10 ⁵ & 3x10 ⁵	0.003B	8400	8175	0.68	0.01	0.18	0.04	69 & 73	0
Frandsen 2004	2D FEM	ALE	6.2x10 ⁶	0.0079B	3768	3420	0.51	-0.08	0.28	-	50	-
			1.65x10 ⁷	0.032B	3438	7128	-	-	0.11	-	70	-
Braun & Auruch(2008)	FEM	LES and ALE	10 ⁵ & 3x10 ⁵	0.003B	8400	8175	0.65	0.05	?	0.05	69 & 73	0
							1.12	0.74	0.18	0.23		10
Selvam (2010)	p-adaptive FEM	LES	10 ⁵	0.00044B	24820	-	0.0675	-	0.112-0.182	-	-	0
	2D FEM	LES	10 ⁵	0.00012B	60840	-	0.0641	-	0.16	-	-	0
Bai and Sun(2010)	2D CFD and ANSYS - CFX solver	DES(Detached Eddy Simulation)	-	-	-	-	1.6	0.5	-	0.15	-	-
	3D CFD and ANSYS - CFX solver	DES(Detached Eddy Simulation)	-	-	-	-	0.9	0.25	-	0.7	-	-
Selvam et al (2010)	2D FDM	Laminar flow	2000-10 ⁵	0.001B	2434100	-	0.05	-	0.182	0.05	-	0
Patro et al (2013)	h-adaptive FEM	LES	10 ⁵	0.001B	18615	-	0.063	-	0.11-0.19	-	69	0

Table 2-1: Percentile error for the forces coefficient (Cd, Cl, St, Cm, and V) relative to wind tunnels experiments

Researchers	Cd (%)	Cl (%)	St (%)	Cm (%)	V (%)
IT Selvam et al (2002)	22.5	-	11.39	-	1.42
Bruno &Chris (2003)	37.5	95.59	7.59	-	-
	32.5	96.52	17.72	-	-
	27.5	61.19	82.91	-	-
	11.25	94.87	3.79	-	-
Braun & Auruch(2003)	15.25	0	13.92	0	1.35
Frandsen 2004	10.52	60	77.21	-	32.43
	-	-	0.91	-	0
Braun & Auruch(2008)	10.16	25.37	?	25	1.42
	5.08	1.33	10	15	1.61
Selvam (2010)	15.62	-	2.75	-	-
	19.87	-	1.26	-	-
Bai and Sun(2010)	35.59	33.33	-	25	-
	23.72	66.66	-	71.42857	-
Selvam et al (2010)	37.5	-	15.18	25	-
Patro et al (2013)	21.25	-	20.25	-	1.42

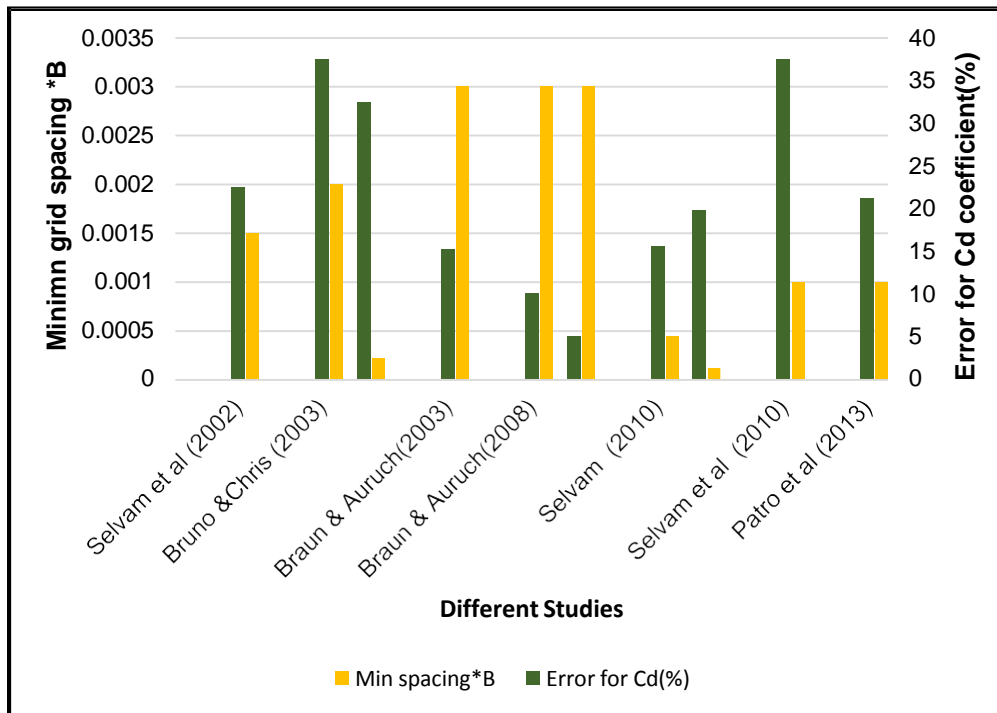


Figure 2-7 : Error in drag coefficient (Cd) versus minimum grid spacing B=bridge width

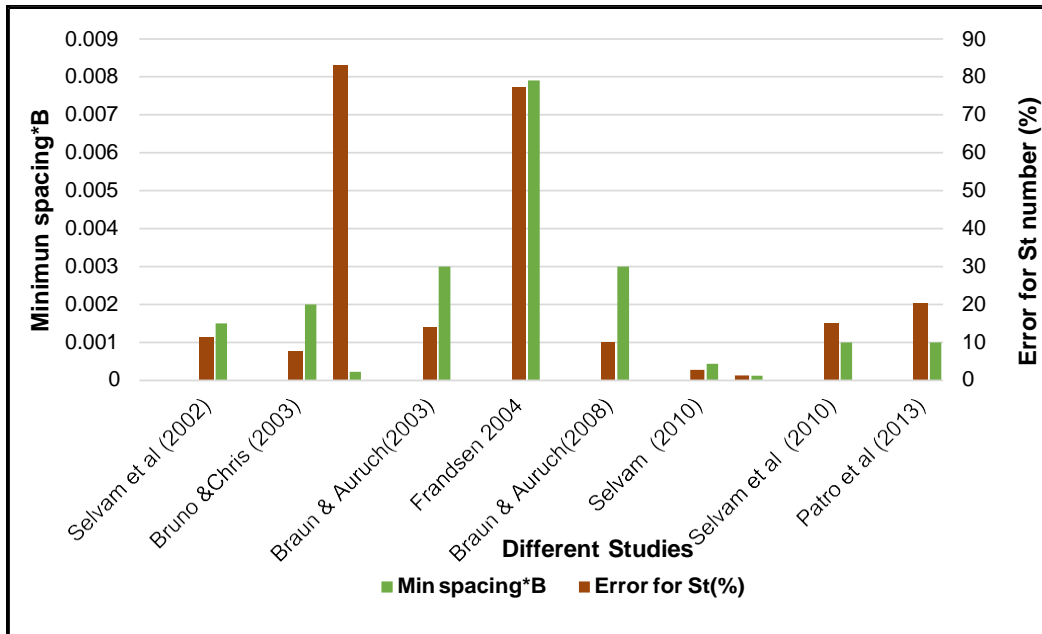


Figure 2-8: Error in Strouhal number (St) versus minimum grid spacing B=bridge width

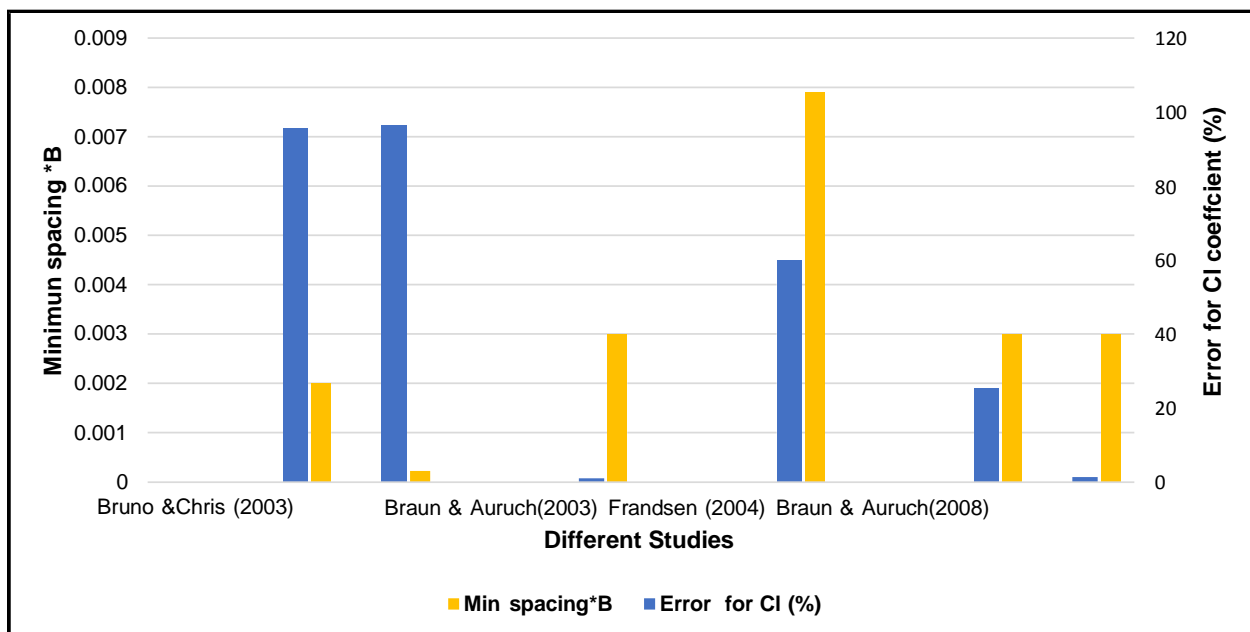


Figure 2-9 : Error in lift coefficient (CI) versus minimum grid spacing B=bridge width

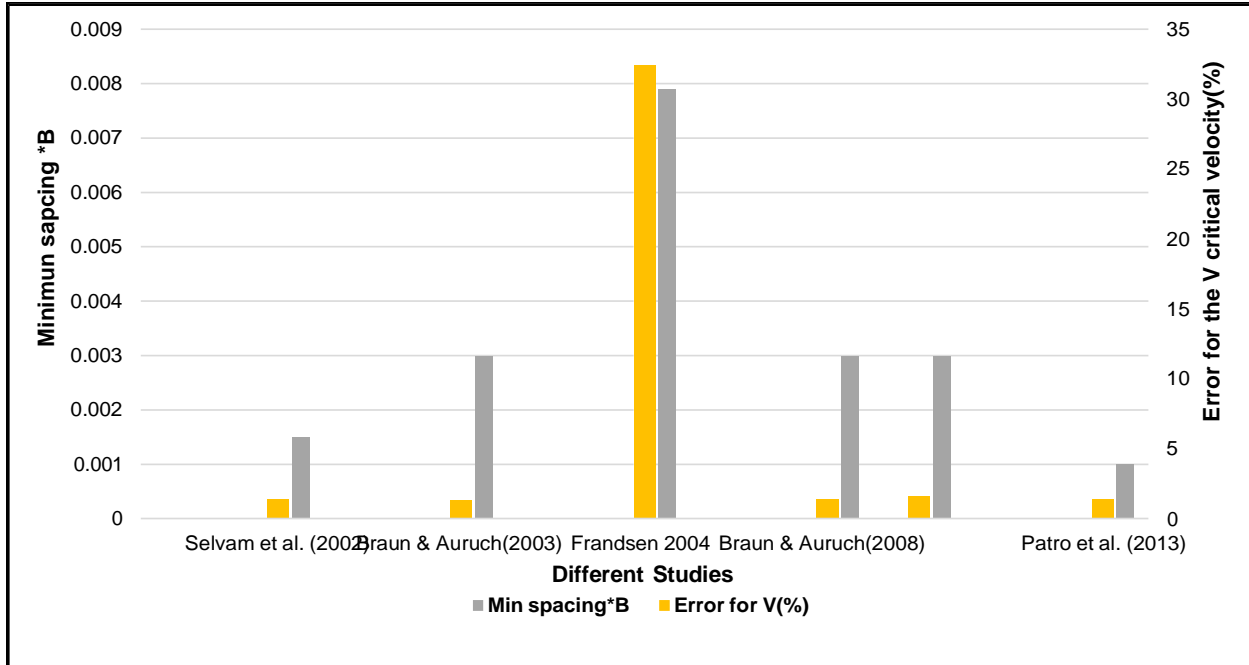


Figure 2-10 : Error in critical wind velocity (V) versus minimum grid spacing B=bridge width

2.4.2.2. *Grid free methods*

These methods, known as particle methods, offer the advantage of easy data input because there is no need of a grid generator; however, they required an immense computational effort since all mutual vortex interactions have to be considered at each time step (Morgenthal, 2000). An example of grid free method is the Discrete vortex method (DVM) used for fixed and moving bridges.

The DVM is widely used for the following reasons (Bruno & Khris, 2003):

- Usage of Lagrangian approach with appropriate mesh quality, numerical diffusion, modeling of all details of the deck section as in Grid based method,
- Reduction of computational effort due to the usage of potential flow method to describe the flow.

The DVM approach, an example of boundary element method, as stated by Morgenthal, (2000) was used for viscous flow (Taylor & Vezza, 1999 and Larsen & Walther ,1997&1998), inviscid flow (Bienkiewicz & Kutz,1993). Morgenthal & Mcrobbie (2002) developed the DVM to compare various numerical method used in bridge design. Larsen &Walther, (1997,1998) analyzed four stationary and movable 2-D bridges cross-section. The results for the flutter aerodynamics derivatives, drag coefficient and Strouhal number were in good agreement with the wind tunnel test results for some sections. The computation time for the simulation was not mentioned; the analysis was limited to 2D flow and bluff bodies, which need more investigation to determine if the method could be expand for streamlined bodies and 3D flow around the structure.

2.5. Other than CFD Methods

2.5.1. The sparse third-order Volterra model

Wu & Kareem, (2014) used the Volterra theory to model a 2-D nonlinear bridge deck response under an arbitrary aerodynamic input. Indeed, the bridge deck response consists of sum of multidimensional convolution integrals of increasing order and coefficient (Volterra Kernels). The kernel coefficients are identified with a pair of general input (vertical wind fluctuation) and output (vertical/torsional displacement of bridge deck) obtained through numerical and experimental simulations. Once the kernel coefficients are known, the bridge deck response can be identified. The method is comparable with wind tunnels test and effective for moving bridge simulation.

2.5.2. Lattice Boltzmann Method (LBM)

The LBM is a complementary of CFD method even though it is based on CFD techniques. Unlike CFD, LBM used Lattice Boltzmann equations for the flow (further equations

details in McNamara & Zanetti, 1998) instead of Navier Stokes equations. As reported in Uphoff et al.,(2012), the method offers the advantage of being efficiently parallelized and effective for bridge 3-D simulation and turbulent flow. Upholl et al.,(2012) worked on the 3-D GBEG to evaluate the behavior of the multi-relaxation time (MRT) LBM with a Smagorinsky LES model. Their study focused on the pressure coefficient around a bridge using the law of the wall for the domain discretization and nested time technique for the grid refinement. The predicted results compared with Selvam et al., (2010) study and related the span wise extension of vertical structure around bridge for Reynold number ranging from 2000 to 15000.

2.6. Advanced Methods

2.6.1. Linear and nonlinear approach

Hysteresis loop for numerical and experimental simulations and aerodynamics forces prediction of bridge deck were used by Diana et al. (2008). They outlined the effect of non linear model (various angle of attack of wind, reduced velocity, amplitude of instataneous angle of incidence) on aerodynamic behavior of bridge decks. The authors found a discrepancy between linear and nonlinear models for the force coefficients and thus recommended to take into account nonlinear approach for experimental and numerical bridge models.

2.6.2. Probabilistic/Statistical method (Stochastic model)

Probabilistic method is based on reliability theory in which bridge failure modes are analyzed to estimate wind response of the structure. Reliability analysis outputs are values of the critical wind speed and bridge aerodynamic parameters which correspond to the real structure target failure probability. The later mentioned probability value is provided in some codes, depending on the safety class of the bridge. In general, the method provided random

design parameters and it suffered from uncertainty of main parameter like the structural properties (damping, mass and stiffness) and the mean wind speed estimation (Ostenfeld & Larsen, 1992).

Madsen & Ostenfeld, (1992) computed the critical wind speed of the GBEB; their model suffered from uncertainty in the distribution type for wind speed and the assumption that the Reynold number effect is negligible. Unlike Madsen & Ostenfeld, (1992), Strommen, (2010) related the Reynold number with the vortex shedding; the study described how to determine cross sectional forces, analyze wind effect (buffeting, galloping, flutter, vortex shedding) on a bridge using stochastic model. Bruno & Khris, (2003) used a different turbulent model with a statistical approach for the GBEG analysis. It was found that the k- ϵ model (RANS turbulence model) failed to predict unsteady flow as compared to the Reynold Stress turbulent Model (RSM). Even with a grid spacing closed to the bridge deck of 0.00022B (B=1 the bridge width), the model could not achieve good result due to the statistical approach yielding good result only for massively separated flow in which periodic fluctuations predominate.

2.6.3. CFD with aerodynamics countermeasures

Sarwar & Ishihara, (2010) used 3-D LES turbulence model to compute reduced velocity and investigate the model performance for a box girder bridge using aerodynamics countermeasures (fairings, double flaps). Aero elastic instability of rectangular and box girder sections was investigated with a width to depth (B/D) aspect ratio of 4 and 3.81. Aerodynamic countermeasures in force oscillation computations are found to alter the aerodynamic characteristics of box girder bridges. Indeed, unlike fairing, double flaps in a bridge section reduced to half the amplitude of vortex induced vibrations. This is done by diminishing the

vortex formation on the bridge upper surface. Fairing, on the other hand, produced strong vortex formation and large vibration amplitude. A concept of sliding mesh was also introduced to represent condition similar to wind tunnel test but there were not mention of the grid refinement level reached to achieve the results.

2.7. Conclusion and justification of the thesis

In the CFD and grid based method for bridges, the grid refinement is a key component of the 2-D and 3-D analysis that considerably affects the aerodynamic parameters like the Strouhal number and the drag coefficient. Selvam, (2010) reported that an increase in tangential grid refinement led to the capture of several vortices on the top and bottom of a bridge deck. Henceforth, the radial and tangential grid refinement affects the Strouhal number which depends on those vortices and the drag coefficient that is affected by the vortices developed on the side of the bridge deck.

Proper grid choice and computational time are issues when designing bridges. Theoretically, the increase in grid refinement leads to an increase in computer storage, performance and time for the bridge analysis. The present work which is focused on grid based CFD (FDM and LES) method attempt to resolve the following points:

- Improve Selvam & Govindaswamy, (2001) model by creating a user friendly package for bridge analysis
- Reduce the computationnal time for the bridge analysis by implementing parallel computing
- Propose a range of grid spacing close to the bridge boundaries for accurate results

- Study the viability of the FDM based pseudo compressibility method for flow modeling.

3. WIND EFFECTS ON BRIDGE

3.1. Introduction

Slender and suspended-span bridges have become a worldwide trend in bridge design. These type of bridges are light, cost and can span long distance. However, the counterpart of these benefits is the wind-sensitivity of the bridge. In this chapter, a general overview of wind load characteristic and induced forces on structure especially suspension bridges are presented. Wind has dynamic and static effect on bridges, but the dynamic effect, which is critical for the bridge design requirement (durability and serviceability) will be reviewed in depth.

3.2. Wind Load

The wind load on a structure depends on many factor illustrated in the chain (Figure 3-1) below:

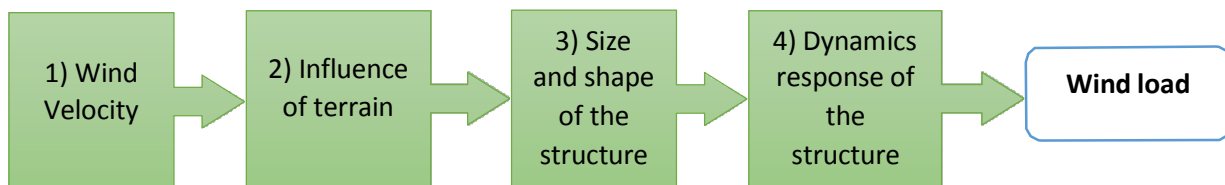


Figure 3-1: Wind load chain

All the factors shown in the chain are the combined effect needed to be determined for a safe and stable design of any structure susceptible to failure due to wind action. Wind velocity is predicted by meteorological data; the terrain influence depends on the surrounding topography. The effects of dynamic depends on the shape of the structure and existence or not of damping components. Wind load is defined by wind pressure and wind force or moment.

3.2.1. Wind Pressure

Wind pressure can be defined as the force exerted by the wind on a surface per units area. Around any surface subjected to wind, negative pressure or suction acts away from the surface while positive pressure acts toward the surface. The former surface is called leeward face and the later windward face.

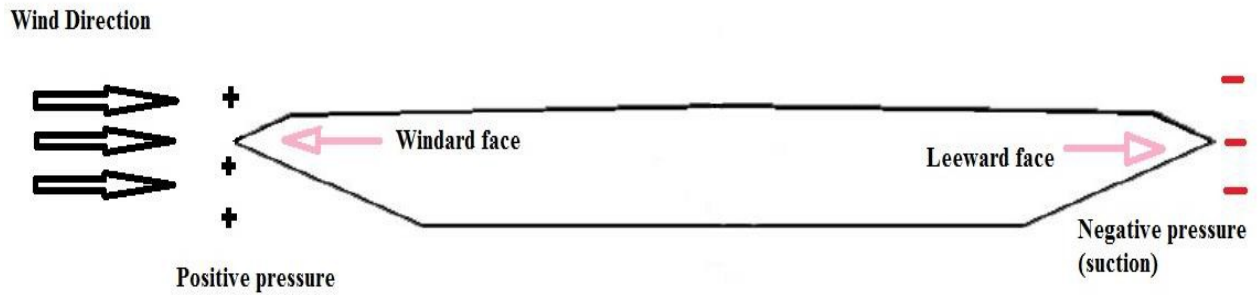


Figure 3-2: Wind pressure representation on Great Belt East Bridge

3.2.2. Wind forces and moment

Drag, lift force and overturning moment and shear are induced by wind on a bridge (Liu, 1991).

- **Drag force**

It is the force that resists the movement of a solid object through a flow and acts in the flow direction. The drag force (F_D) can be determined from:

$$F_D = C_d \rho V^2 B / 2 \quad (3-1)$$

Where:

B: bridge deck width

C_d: drag coefficient

V: mean wind speed

W: bridge length in the Z direction

ρ : fluid density

The drag coefficient C_d is a flow parameter that depends on the structure geometry and the Reynolds number (Re) (Figure 3-3). For a cylinder having plane surface, the dependence of the drag coefficient with Reynolds number is much lower than that of cylinders having round surfaces (Liu, 1991).

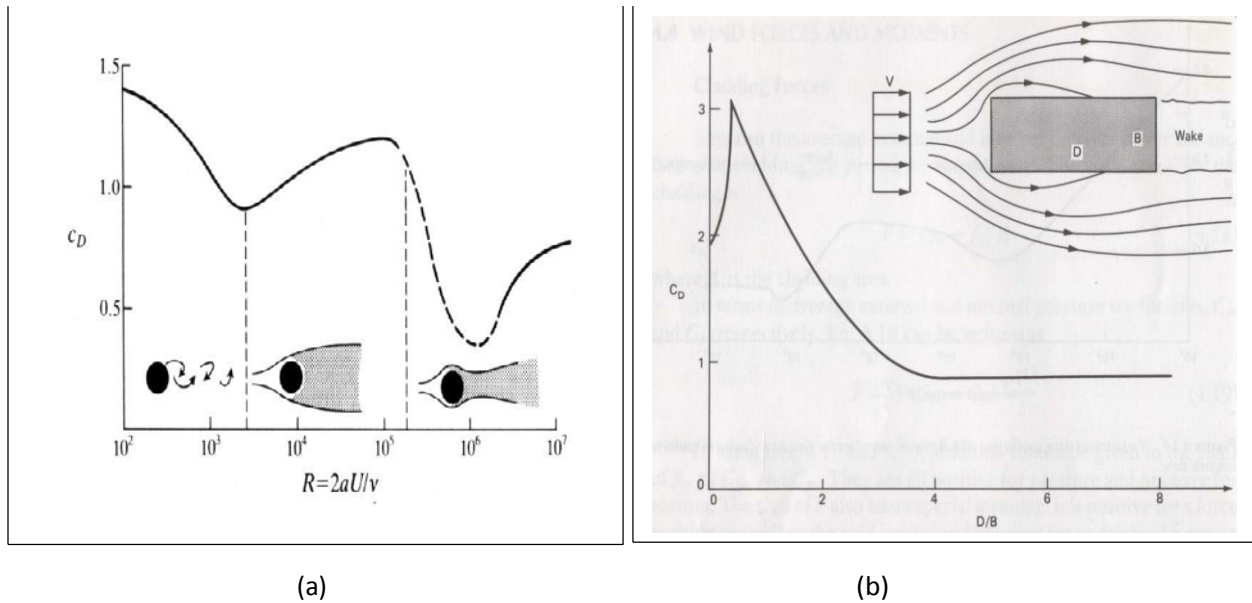


Figure 3-3: Variation of drag coefficient (a) with Reynold number for a circular cylinder (Morgenthal & Mcrobbie, 2002) (b) with aspect ratio of cross section D/B for rectangular cylinder (Liu, 1991)

- **Lift force**

Being the force developed on an object in the across-flow directions, the lift force is also affected by the body shape and the Re . Henceforth, the more a body is streamlined the higher is the lift force and lower is the drag force (Simiu & Scanlan, 1986). The lift force can be found

using the steady and unsteady state. In the steady-state lift, the force is developed for asymmetric object with wind not parallel to their symmetric axis. For unsteady state, when vortices are created on both side of an object, large dynamic lift are developed. The root-mean – square of the dynamic lift force ((F_L)_{rms}) is then obtained in that case.

$$F_L = C_L \rho V^2 / 2 \quad (3-2) \quad \text{for a Steady-state lift}$$

$$(F_L)_{rms} = C'_L (\rho V^2) / 2 \quad (3-3) \quad \text{for an unsteady lift}$$

Where

C_L: lift coefficient

C'_L: dynamic lift coefficient

F_L: lift force

(C'_L)_{rms}: root mean square of C'_L

- **Vertical overturning moment and horizontal twisting moment (Torsion)**

The Vertical overturning moment (M) is the moment generated by the drag and/or lift force at a distance above the ground (moment arm) (Liu, 1991). It can be obtained from:

$$M = C_m \rho V^2 / 2 \quad (3-4)$$

Where C_m is the coefficient moment.

- **Shear (Fluid friction)**

Fluid friction forces are tangential to the structure surface and in the flow direction. Also termed “skin drag” or “frictional drag “ (Liu, 1991) , this force can sometimes be neglected safely.

of gravity, F_l, F_d and M the lift, drag force and moment respectively.

The illustration of the winds' forces on a bridge is shown in Figure 3-4 where CG is the center

of gravity, F_l , F_d and M the lift, drag force and moment respectively.

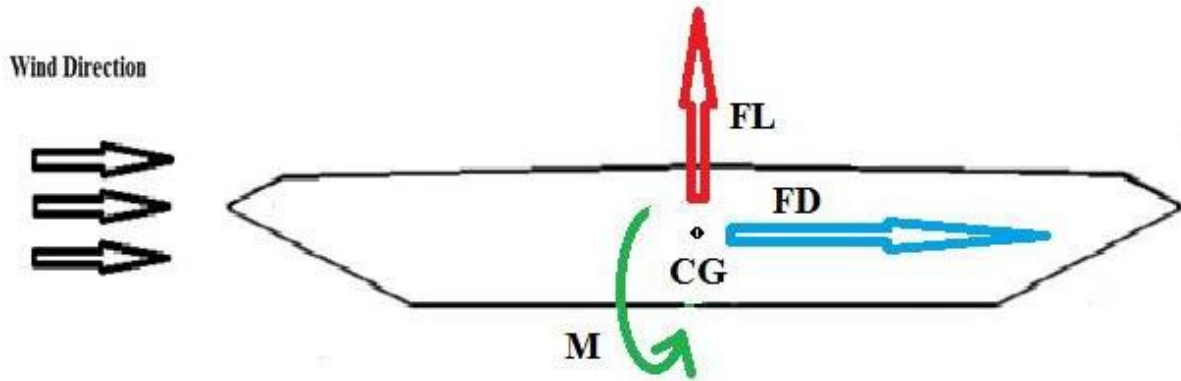


Figure 3-4: Wind force on bridge

3.3. Wind induced forces on bridges

As cited by Ubertini,(2008) , the response and stability problems are the two major subdivisions of wind effect on cable –supported bridges (Figure 3-5).While in response problems, there is a dynamic equilibrium between the body and wind forces, in stability problems, interchanging energy between the body motion and the aero elastic forces leads to loss of equilibrium.

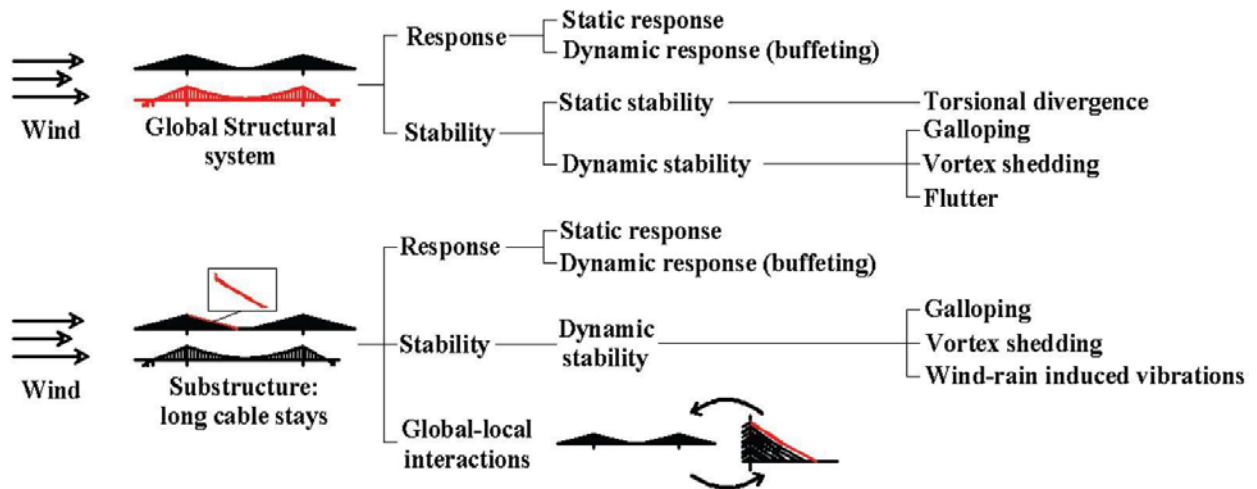


Figure 3-5: Wind effect on bridges (Ubertini, 2008)

In Figure 3-5, static and dynamic response/stability are predominant in wind effects on bridges, hence, a review of these effects is done in the following sections.

3.3.1. Static effects

Static behaviors of bridge due to wind can be predicted through theoretical calculations but require aerodynamic force coefficients. As reported in Tanaka, (1992) these static effects are:

- ❖ **Overturning moment**, which is responsible for the twisting of a bridge ,is discussed in section 3.2.2 and shown in Figure 3-4
- ❖ **Excessive lateral deflections** are responsible for the cracking of partitions and external cladding, mechanical systems misalignment and possible permanent deformations on the bridge.
- ❖ **Lateral buckling or torsional divergence**, occurs when the wind critical divergence velocity (U_c) is reached. As the wind velocity increases the wind forces on bridge (refer to section 3.2) increases too but particularly the twisting moment and therefore the wind angle of attack α (Simiu & Scanlan, 1986). Depending on the bridge deck flexibility aerodynamic moment as well as twist and torsional divergence will develop till the bridge failure.

3.3.2. Dynamics effects

Aerodynamic phenomena are responsible for the bridge dynamic response to wind. Vortex shedding excitation, galloping and stall hysteresis, flutter instability and buffeting vibration may cause a structure to oscillate.

3.3.2.1. *Vortex shedding excitation*

Vortex shedding instability, which occurs usually in low wind speed and turbulence conditions (Holmes, 2001), causes lateral vibration on a bridge. The wind flow pattern around a structure is flow separation at the structure edge corner, production of suction and pressure force and vortices formation in the wake (downstream side) of the structure. The Strouhal number (S) is used to study the vortex shedding frequency, which also depends on the Reynold number (details in section 4-2-2). As cited by Morgenthal, (2002), key physical parameters of a 2-D body exhibiting vortex induced oscillations are the size and the shape of the after body (downstream part of the cross section). In Figure 3-6, a structure with short after body will be weakly excited while another with long after body will experience considerable oscillations under the same conditions.

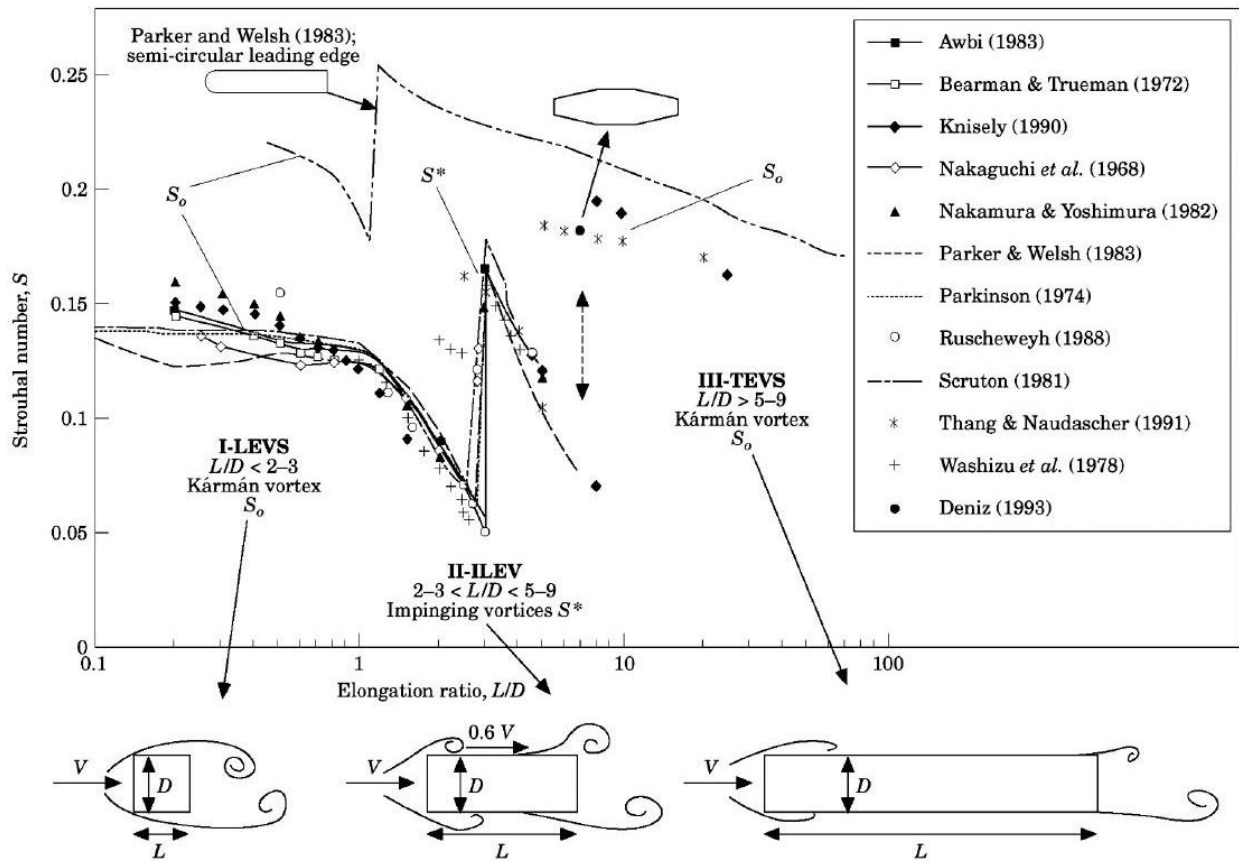


Figure 3-6: Classes of vortex formation observed with increasing elongation of different prismatic bodies: Class I, Leading-edge vortex shedding; Class II, Impinging leading-edge vortices; Class III, Trailing-edge vortex shedding (Deniz and Staubli 1997 in Morgenthal's work, 2000)

3.3.2.2. Galloping

Galloping is typical to almost any lightweight, slender and flexible cylindrical (prismatic) structures except those of circular cross section exposed to wind (Liu, 1991) and effective section of some ice-coated power line cables (Simiu & Scanlan, 1986). Galloping arises from an asymmetry in the flow, which produced vertical oscillations of the bridge deck.

There are two types of galloping: across-wind and wake galloping.

3.3.2.2.1. Across-wind galloping

Across-wind galloping occurs when a structure develops a large amplitude of oscillation in the direction normal to the flow at a frequency lower than the wake frequency. The knowledge of lift, drag coefficients obtained in static conditions and wind angle of attack α enables the analytical description of this phenomenon (Simiu & Scanlan, 1986). Thus, by evaluating the time averaged lift and drag coefficient of a slender prismatic structure and by assessing the sign of $\left(\frac{dC_l}{d\alpha} + \frac{C_D}{D} \right)$, one can determine the initial tendency toward a

structure galloping instability (Simiu & Scanlan, 1986). Simui & Scanlan (1986) stated that across-wind galloping instability may occur for a negative $\left(\frac{dC_l}{d\alpha} + \frac{C_D}{D} \right)$ at $\alpha=0$.

3.3.2.2.2. Wake galloping

Wake galloping was studied for the case of two cylinders with one located upstream the other. The instability occurred when the downstream cylinder frequencies were low as compared to its wake frequency and those of the upstream cylinder. Structural parameters for instance the structure spring constant influences the wake galloping phenomenon (Simiu & Scanlan, 1986).

3.3.2.3. Flutter instability

Many types of flutter exist: classical flutter, stall flutter, panel flutter and single degree of freedom flutter (Liu, 1991). Classical flutter shall be discussed herein, as it is the most common in bridge engineering. Classical flutter is an aero elastic phenomenon due to wind effect on a structure during the instability, two degrees of freedom involving rotation and vertical translation are coupled together (Simiu & Scanlan, 1978). When a structure is subjected

to any disturbance due to the structural damping, the amplitude of oscillation will decay (positive damping, Figure 3-7a), while during flutter phenomenon, the flow regime feeds energy into the structure and counteract the structural damping, thus the oscillation increase (negative damping, Figure 3-7 b) till the structure failure. Flutter can be analyzed through forced and free oscillation.

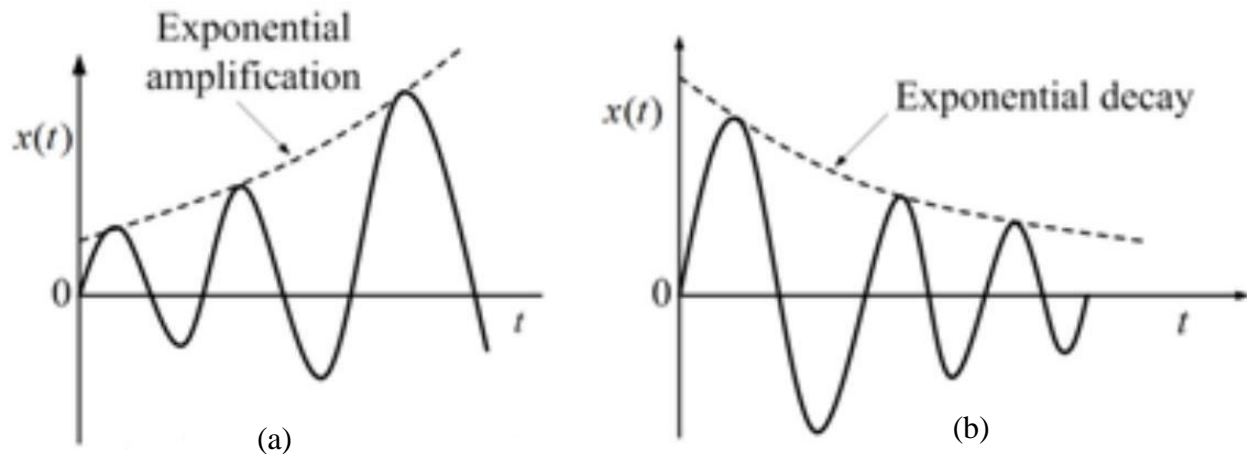


Figure 3-7: Illustration of (a) negative damping, (b) positive damping

3.3.2.4. *Buffeting vibration*

Buffeting is a non-self-induced vibration as compared to self-induced turbulence which are stronger and smooth flow (across galloping and vortex shedding but not wake galloping). Buffeting is a natural turbulence or gustiness in the free stream flow; two types of buffeting exist (Liu, 1991):

- Buffeting caused by free-stream turbulence
- Wake buffeting or interference caused by disturbance arising from an upwind neighboring structure or obstacle

4. COMPUTER MODELLING

4.1. Structure and flow parameters

4.1.1. Structure: Great Belt East Bridge (GBEB)

The case study is the Great Belt East Bridge (GBEB), the second longest bridge in Denmark with a length of 6,790 m after the Oresund Bridge 7,845 m. Located in the city of Storebælt, the GBEG opened in 1998 and consisted of a 3 spans box girder with span lengths of 535 m-1624 m-535m. The bridge carried a four lanes highway across the Eastern channel and offered safe crossing of the international shipping channel (Larsen & Jacobsen, 1992).

The bridge cross section and the structural properties are given in Figure 4-1 and Table 4-1. The GBEG was used by many researchers to carry wind tunnel experiments (Larsen & Jacobsen (1992), Larsen (1996), Reinhold et al. (1992), Tolstrup (1992)) and numerical simulations (Selvam & Govindaswamy (2001), Selvam (2010)). This bridge constitutes a benchmark problem for the assessment of the present work.

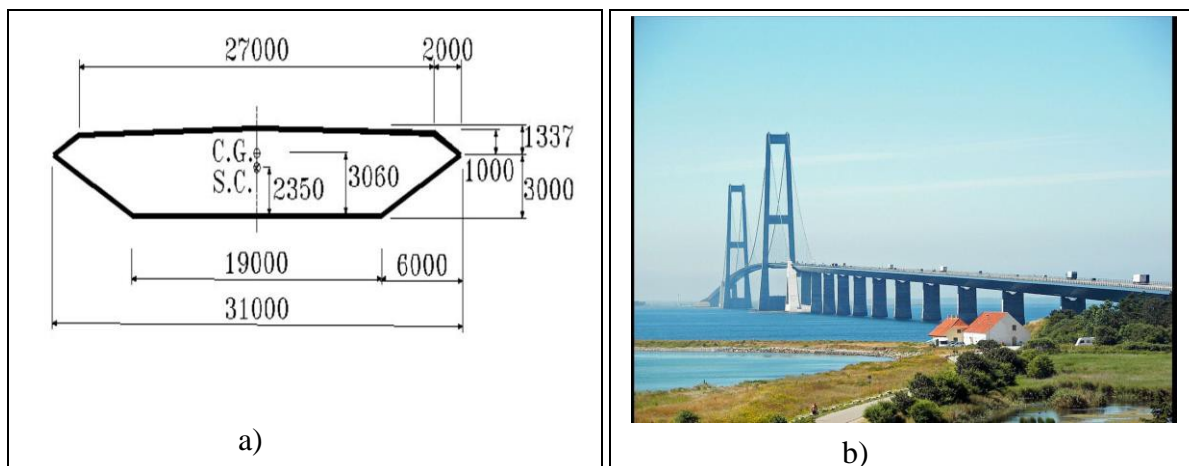


Figure 4-1: Great Belt East Bridge a) suspension span cross section (dimension are in mm, Selvam & Govindaswamy, 2001); b) elevation (modified from iClickfun, 2015)

Table 4-1: GBEB structural properties

Structural properties	value	Units
Mass	2338.1	kg/m
Inertia	261.82	kgm ² /m

4.1.2. Flow

To carry out comprehensive studies on a bridge deck, fundamental aerodynamic characteristics need to be known. These characteristics are the Reynold number, the drag, lift and moment coefficient, flutter derivatives and the Strouhal number.

- **The Reynold number** is a dimensionless number that quantifies the relative importance of internal and viscous forces. Liu, (1991) defined range for the Reynold number: Subcritical range ($300 < Re < 2 \times 10^5$), Critical Reynold number ($Re = 2 \times 10^5$), Supercritical range ($2 \times 10^5 < Re < 4 \times 10^6$), Hypercritical range ($Re > 4 \times 10^6$). The Reynold number is defined as follow:

$$Re = VB / \nu \quad (4-1)$$

Where:

B: bridge deck width

V: mean wind speed

ν : kinematic viscosity

- **The drag, lift and moment coefficients** usually depend on the angle α between the horizontal and bridge deck plane and are defined per unit span as:

$$C_D = F_D / 0.5 \rho U^2 \infty B \quad (4-2)$$

$$C_M = F_M / 0.5 \rho U_\infty^2 B \quad (4-3)$$

Where:

B: bridge deck width

C_D, C_L and C_M: drag, lift and moment coefficient

F_D, F_L and F_M: drag, lift force and moment

U_∞: reference velocity

ρ: fluid density

- *The motional aerodynamics coefficients or flutter derivatives* characterize the self – excited forces acting on the oscillating bridge (Simiu & Scanlan, 1986). The coefficients are H_i^* and A_i^* (i=1,2,3),
- *The Strouhal number (S)*, is a dimensionless number which depends on the Reynold number and helps to study the vortex shedding frequency. The number can be get from:

$$S = fH / U_\infty \quad (4-5)$$

Where

f :the shedding frequency

H : the bridge height

4.2. Governing equations

4.2.1. Normalization

Normalization is widely used in CFD; it is a unit-transformations process that gives dimensionless and normalized variable use in the equations. This process help to easily conduct calculations avoid huge value and apply a numerical model to different design types rather than a specific one. Simiu & Scanlan, (1986) reported that non-dimensional forms enabled the transfer of experimental results to full scale and established reference values for cataloguing properties of a given geometric form in the numerical method. The non-dimensionalized representation of variables as proposed by Selvam, (2014) is:

- Velocity in x and y direction U and V: $U^*=U/U_\infty$, $V^*=V/U_\infty$
- Vertical and horizontal displacement x and y: $x^*=x/B$, $y^*=y/B$
- Time t: $t^*=tU_\infty/B$,
- Pressure p: $p^*=p/\rho U_\infty^2$,

The astrisk represents the normalized values and U_∞ is the reference velocity. In the present work, all variables are dimensionalized with respect to the bridge width B which is equal to 1.

4.2.2. Flow equation

In mid-18th century, the French engineer Claude-Louis Navier and Irish mathematician Georges G. Stokes derived the worldwide known Navier-Stokes equations to describe the fluid motions based on fundamental governing equations of fluid dynamic. These equations, described how the velocity, pressure, temperature and density of a moving fluid are related.

- **Continuity equation**: based on mass conservation in which the mass change in a control volume is equal to the difference between the entering and leaving mass

through the control volume's faces. The equation is defined in tensor for an incompressible flow as follows:

$$\nabla \cdot \mathbf{u} = 0 \quad (4-6)$$

- **Momentum equations:** derived from Newton's second law and expressed in term of pressure and viscous stresses acting on a particle in a fluid.

$$\rho_f \frac{d\mathbf{u}}{dt} = -\nabla p + \nabla \cdot \mathbf{T} \quad (4-7)$$

Where:

p: flow pressure

\mathbf{u}_i : mean flow

velocity

u: kinematic viscosity

ρ_f : fluid density

The commas represent differentiation and t the time; i=1, 2 and 3 are variables in the x, y and z direction respectively

- **Energy equation:** the fluid particle's energy rate of change is equivalent to the work done on that particle due to surface, heat and body forces.

The non-dimensional 2-D Navier-Stokes flow equation, used in this work, is in conservative form for an artificial compressibility method.

$$\frac{\partial U}{\partial t} + \frac{\partial F}{\partial X} + \frac{\partial G}{\partial Y} = 0 \quad (4-8)$$

Where: $U = [p, u, v]^T$

$$F = [\beta u, u^2 + p - (\partial u / \partial X) * (1/Re), uv - (\partial v / \partial X) * (1/Re)]^T$$

$$G = [\beta v, uv - (\partial u / \partial Y) * (1 / Re), v^2 + p - (\partial v / \partial Y) * (1 / Re)] T$$

Here $\beta=1/M^2$ with $M=u/c$ the Mach number,

u, v: wind velocity in x and y direction

c: speed of sound

A structured and non-orthogonal mesh, associated with coordinates system called (ξ, η) (Figure 4-2) is used; the transformed equation (4-8) will be as reported in (Rhie & Chow,1983 and Sorensen, 1995):

$$\partial U1/\partial t + \partial F1/\partial X + \partial G1/\partial Y = 0.0 \quad (4-9)$$

Where:

$$U1 = JU$$

$$F1 = F(\partial Y/\partial \eta) - G(\partial X/\partial \eta)$$

$$G1 = -F(\partial Y/\partial \eta) + G(\partial X/\partial \eta)$$

$$J = X_\xi Y_\eta - X_\eta Y_\xi$$

$$F1 = [\beta U_c, uU_c + Y_\eta p - uvX_\eta - (Au_\xi - Bu_\eta)/(JRe), vU_c - X_\eta p - (Av_\xi - Bv_\eta)/(JRe)]$$

$$G1 = [\beta V_c, uV_c - Y_\xi p - (Cu_\eta - Bu_\xi)/(JRe), vV_c + X_\xi p - (Cv_\eta - Bv_\xi)/(JRe)]$$

$$U_c = uY_\eta - vX_\eta, \quad V_c = -uY_\xi + vX_\xi$$

$$A = X_\eta^2 + Y_\eta^2, \quad B = X_\xi X_\eta + Y_\xi Y_\eta, \quad C = X_\xi^2 + Y_\xi^2$$

$Re = 1/\nu$ since dimensionless value are used

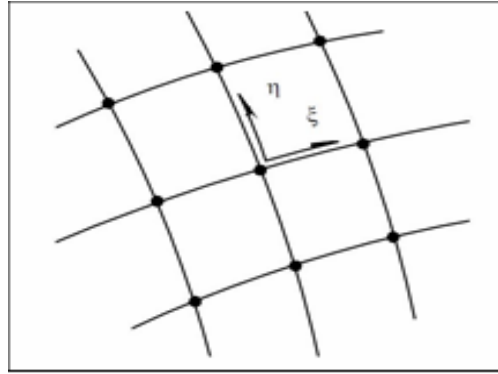


Figure 4-2: Structured grid coordinates system

4.2.3. Boundary and initial conditions

Boundary and initial conditions are values of pressure and velocity specified at a computational domain surface and at the beginning of numerical calculations. Figure 4-3 illustrates the computational domain and boundary conditions for the GBEB.

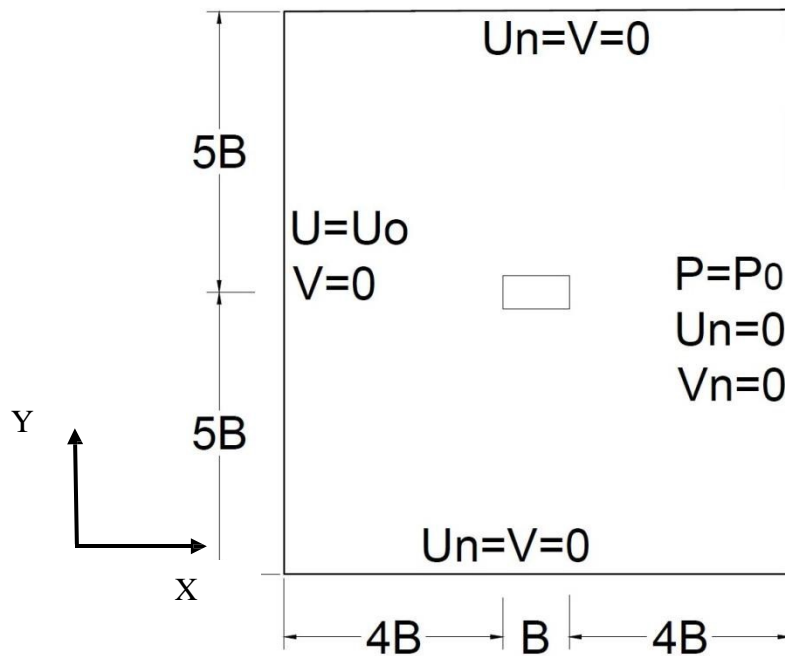


Figure 4-3: Computational domain and boundary conditions

In this figure, B represents the bridge width, U and V the velocity in x and y direction respectively. U_n and V_n are the normal gradient velocity in x and y direction respectively and U_0 is the free stream x velocity.

- The computational domain upstream boundary has a velocity of one in the x direction and zero in the y direction.
- The computational domain top and bottom boundaries have zero v normal gradient velocity in x direction and zero velocity in y direction (slip boundaries).
- The downstream side has a normal velocity in x and y direction equal to zero (traction free).
- The bridge wall has no slip boundaries condition.

4.2.4. Numerical procedure to solve for the fluid equations

Finite Difference Method (FDM) and Large Eddy Simulations for the turbulence model are used in the present work. To couple velocity and pressure in the governing equations and solve them simultaneously, pseudo-compressibility or artificial compressibility method is used. Artificial compressibility formulation is derived by introducing an artificial compressibility relation $\rho = p/\beta$ in the continuity equation (Kwak et al., 1986) to speed up the convergence. When non-dimensional form is used, β can be derived from: $\beta = 1/M^2$. The MacCormack scheme, a second order FDM is applied to convection and pressure terms, Central Difference is used for diffusion. The Navier Stokes equations in the present work are solved explicitly by getting new velocities and pressures from equation (4-8) for each grid point using MacCormack scheme written as follow:

- **Predictor forward difference**

$$U_{ij}^* = U_{ij}^n - dt[F_{i+1j}^n - F_{ij}^n]/dx - dt[G_{ij+1}^n - G_{ij}^n]/dy \quad (4-10)$$

- **Corrector backward difference**

$$U_{ij}^{(n+1)} = \{U_{ij}^n + U_{ij}^* - dt[F_{ij}^* F_{(i-1)j}^*]/dx - dt[G_{ij}^* G_{i(j-1)}^*]/dy\}/2 \quad (4-11)$$

A Mach number M of 0.3 is used for the simulation. For explicit procedure Selvam, (2014) suggested a time restriction of : $dt < h/(u+c)$, with $h = (h_1 h_2 h_3)^{0.333}$ for 3-D and $h = (h_1 h_2)^{0.5}$, for 2-D. The parameters h_i ($i=1,2,3$) is the control volume spacing in x, y and z directions. To reduce dispersion errors, a second order artificial viscosity (AV) is introduced in the above procedure as reported in Anderson, (1995).

4.2.5. Numerical diffusion and dispersion

Diffusion and dispersion are some issues encountered in flow computer simulations and in the present model. Numerical diffusion and dispersion reflect on the properties of the spatial discretization employed. From physical point of view, diffusion is the capacity of smoothing a sharp interface; numerically, it indicates that the space discretization operator will tend to smooth out sharp front discontinuities. Thus a sharp interface over a cell will be spread over a few cells by the space discretization operator. Numerical dispersion on the other hand, refers to the properties of the space discretization operator in not generating too high gradient. Dispersion is a dependence of wave speed on their wavelength; as the direction of propagation of the wavelength/ wave frequency and/or the mesh vary, the accuracy of the numerical solution varies. Because of these numerical instabilities the accuracy of the solution is affected and the exact representation of the actual flow is not done properly.

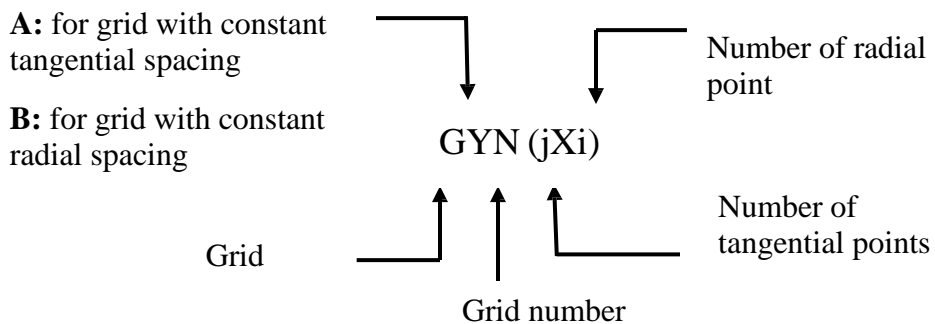
4.2.6. Parallel computing

The computations, involved in solving the previous equations are heavy for a computer in term of number of data processing, computer storage, capacity and computational time. For this reason, parallel modelling is implemented. Indeed, the computational domain is split in the radial direction; each subdomains are assigned to a specific processor when the code is ran. This enables a reduction of heavy calculations and increase of the running time by using several processors simultaneously. More details about parallel computing in Computational Fluid Dynamics problems can be found in Chetverushkin, et al., (2004).

5. RESULTS

5.1. Introduction

The bridge analysis of the GBEG cross section Figure 4-1 was performed using the Finite Difference Method and Large Eddy simulation. The Navier Stokes equations are solved numerically resulting in pressure, vorticity and velocity parameters at each domain node for a time step of 10^{-4} and a total duration of 60 time units. These parameters were later used in the solver to compute forces acting on the bridge using equations (4-2), (4-3), (4-5) of section 4.1.2. The solution strategies used to solve the equations are grid dependent and sensitive to numerical errors given the fact that a lot of numerical iterations were involved in the computation. For this reason, different grids with variable parameters (number of node, spacing between node in radial and tangential direction) were used and the results were compared with available literature. Numerical errors were minimized by using an artificial viscosity coefficient, the influence of this parameter on force coefficient is presented in the chapter. The grid generation process, model parallel performance and current model's advantage as compared to The Selvam & Govindaswamy (2002) are discussed in this chapter. In the next section each grid is named with the following term:



5.2. Presentation of the results

5.2.1. Influence of Artificially Viscosity (AV) on force coefficients

Numerical dispersion and diffusion are common when solving equations using computer modelling. The Artificial Viscosity (AV) coefficient is often used to reduce unsightly oscillation and control the solver for numerical stability. However, without a proper choice of the AV coefficient value, the result accuracy can be destroyed. Six different values of AV coefficient ranging from $AV1=10^{-1}$ to $AV6=10^{-6}$ are used to study a single grid size GB1:333x90. The grid has 29970 nodes with a minimum spacing of 0.0007B and 0.0016B respectively in radial and tangential direction; B is the bridge width. The result summaries are displayed in the Table 5-1 and Figure 5-1. Here WT refer to Wind tunnel experiments, Clrms is the root mean square of the lift coefficient.

The plot of the vorticity contour for the bridge section, as illustrated in Figure 5-2, shows that for an artificial viscosity coefficient greater or equal to 10^{-3} (case AV1, AV2 and AV3), there is no vortex shedding; for an AV between 10^{-4} and 10^{-5} (case AV4, AV5 and AV6) vortices are formed in the wake of the bridge. The absence of vortices is due to high diffusion; furthermore for AV less than 10^{-5} (case AV6), there is high flow dispersion. Only a range of AV between 10^{-4} and 10^{-5} gives reasonable vortex shedding path. To have a better understanding of the AV coefficient influence, three grids were investigated. Grid GA4:549x70, GA5:549x80 and GA6:549x90 were investigated for an AV coefficient ranging from $AV1=10^{-2}$ to $AV4=10^{-6}$. The same flow behavior were observed: For $AV=10^{-2}$, there is no vortex shedding and for $AV=10^{-6}$ there is high flow diffusion (Table 5-2, Figure 5-2 and Figure 5-3). An AV coefficient of 10^{-4} is used in this work and a range of AV coefficient between 10^{-4} and 10^{-5} is recommended

first to control the numerical instability of the solving process and second to avoid altering the solution.

Table 5-1: Change in force coefficient for different AV value and a single grid size GB1:333x90

Study	AV value		Force coefficients		
			St	Cdmean	Clrms
Present work (PW)	AV1	1.0E-01	0.011	0.5213	0.00766
	AV2	1.0E-02	0.386	0.0849	0.00872
	AV3	1.0E-03	0.073	0.0460	0.00174
	AV4	1.0E-04	0.193	0.0583	0.02005
	AV5	1.0E-05	0.148	0.0568	0.01286
	AV6	1.0E-06	0.386	0.0534	0.09230
WT: larsen& Walther (1998)			0.17	0.08	0.07

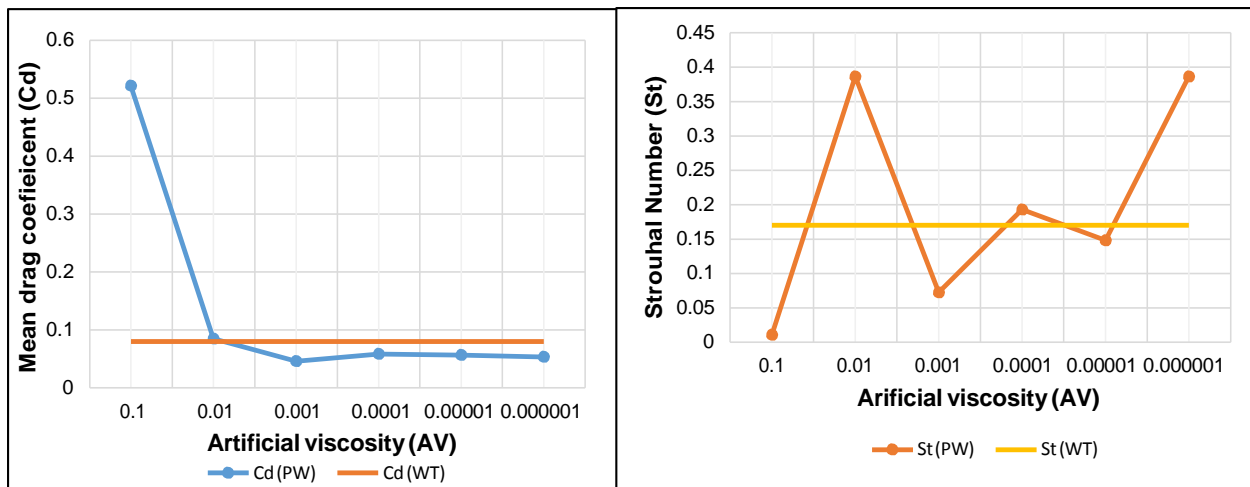


Figure 5-1: Mean drag and Strouhal number versus Artificial Viscosity coefficient plot (left to right)

Table 5-2: Change in force coefficient for different AV value and different grid size

Grid Details grid size	Minimum spacing		AV value	Force coefficients		
	Radial	Tangential		St	Cdmean	Clrms/Cl
549x70	0.002B	0.001B	1.E-02	0.014	0.0852	0.00024
			1.E-04	0.151	0.0575	0.0002
			1.E-05	0.229	0.0576	0.00024
			1.E-06	0.286	0.0588	0.00022
549x80	0.0016B	0.001B	1.E-02	0.017	0.0758	0.00023
			1.E-04	0.238	0.0624	0.00019
			1.E-05	0.148	0.0603	0.00019
			1.E-06	0.372	0.0633	0.000214
549x90	0.0013B	0.001B	1.E-02	0.017	0.0697	0.00021
			1.E-04	0.148	0.0623	0.00018
			1.E-05	0.188	0.0610	0.000186
			1.E-06	0.235	0.0606	0.0002
Wind tunnel test Larsen & Walther (1998)				0.17	0.08	0.07

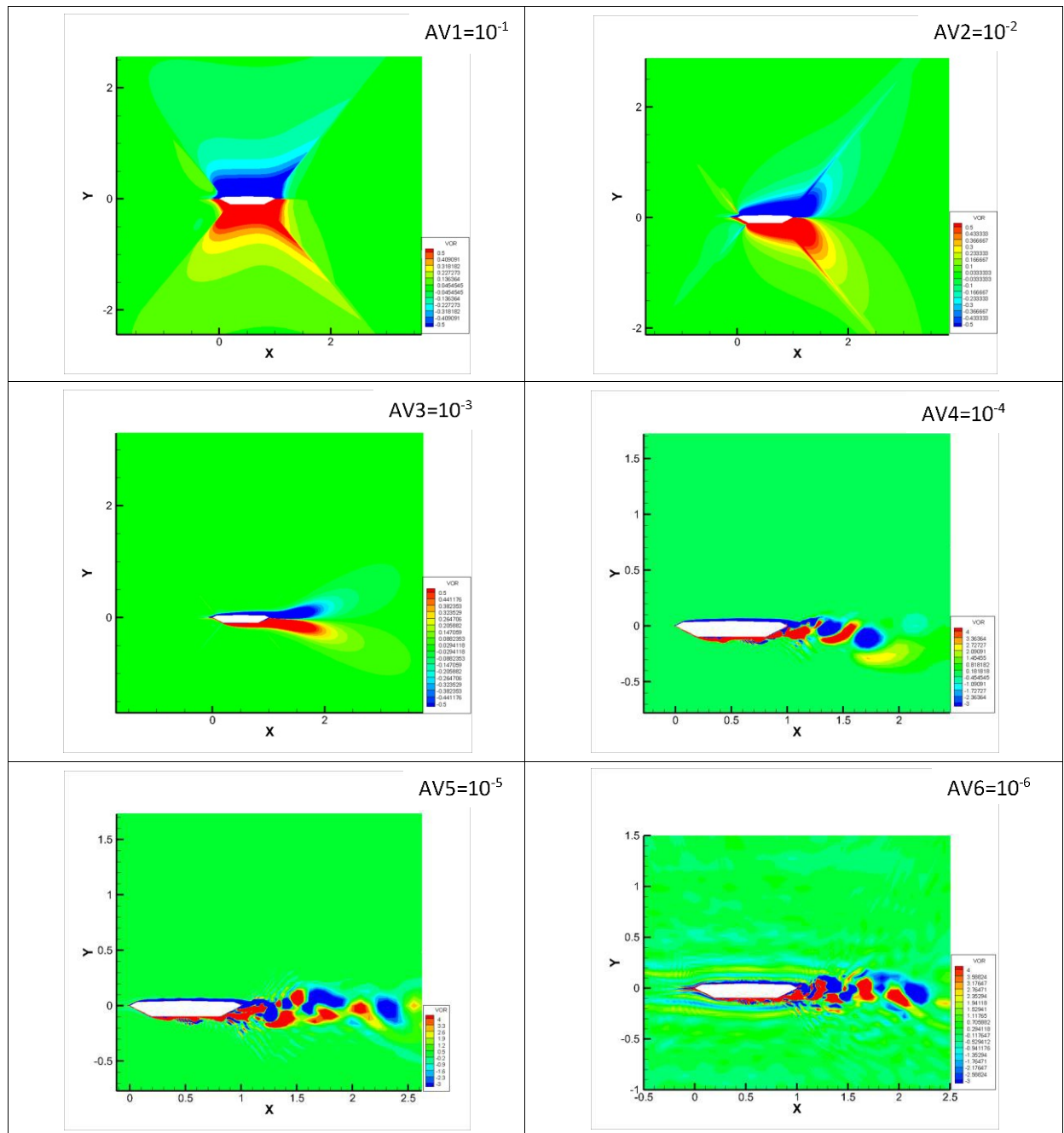


Figure 5-2: Vorticity plot for different AV value and single grid GB5:333x90

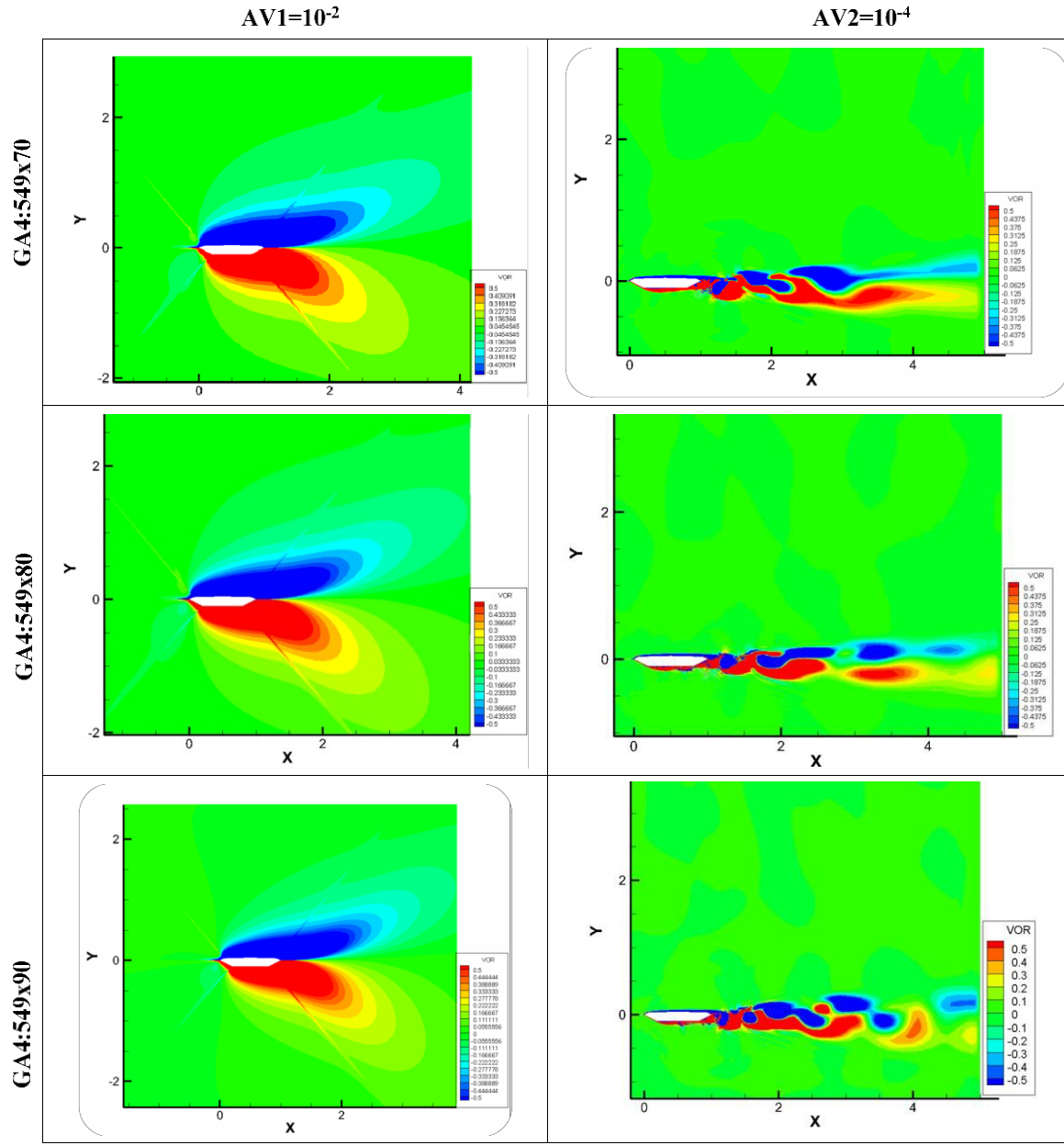


Figure 5-3: Vorticity plot for different $AV=10^{-2}$ and $AV=10^{-4}$ value and three grids (GA4:549x70, GA5:549x80 and GA6:549x90)

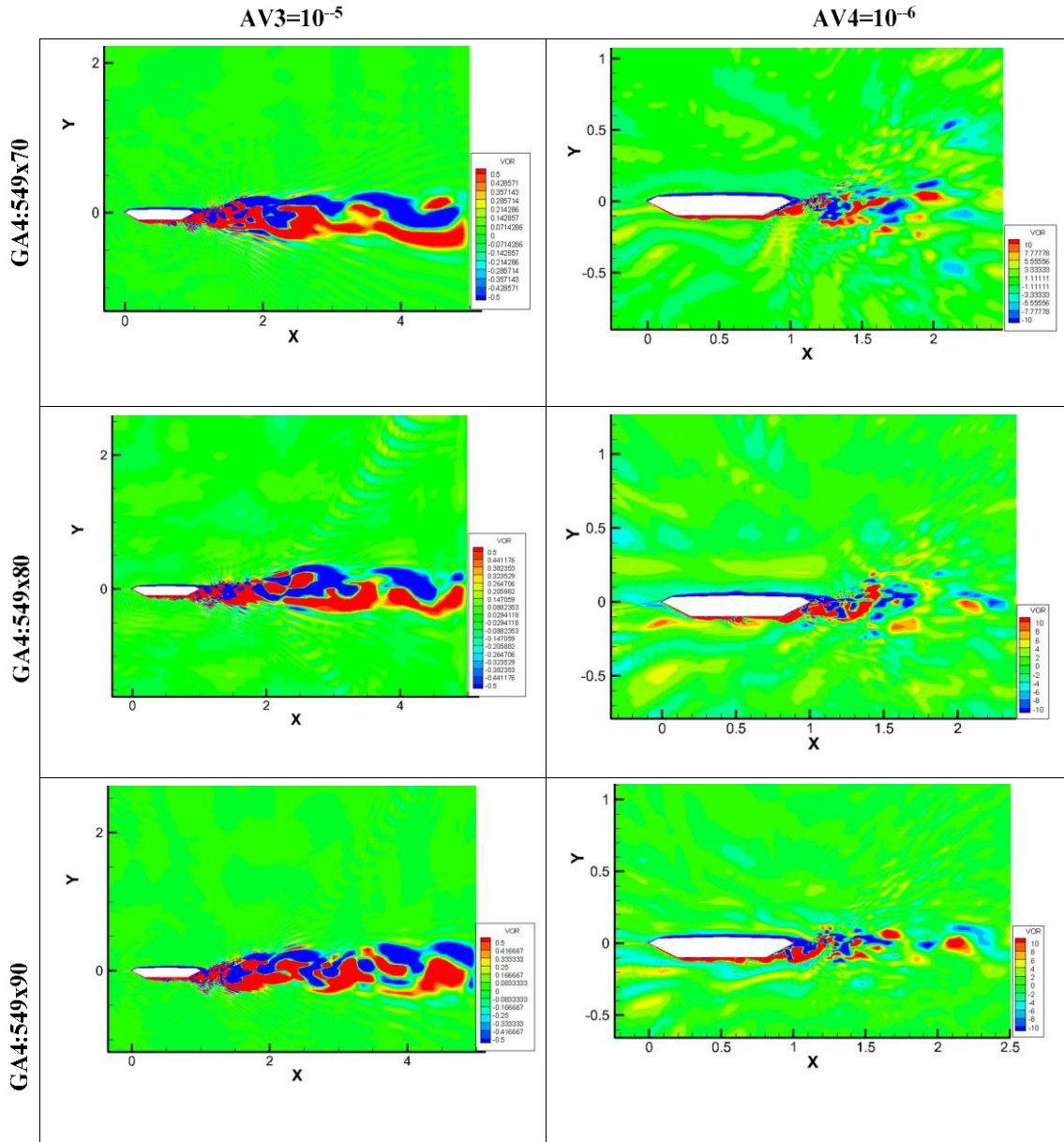


Figure 5-4: Vorticity plot for different $AV=10^{-5}$ and $AV=10^{-6}$ value and three grids (GA4:549x70, GA5:549x80 and GA6:549x90)

5.2.2. Parallel computing performance evaluation

The parallel modelling of the fluid solver is assessed by analyzing the time required to run a single grid GB5:333x90 for a different number of processors. The speed up(s), efficiency

(e) and time decrease percentage are calculated to assess the running time; the parameters are defined in equation (5-1) to (5-3). The time decrease percentage is estimated by using T1 as a reference; T1 is the time required to run the model using one processor.

$$s = T_1 / T_N \quad (5-1)$$

$$e = T_1 / (T_N * N) \quad (5-2)$$

$$\%decrease = (T_1 - T_N) * 100 / T_1 \quad (5-3)$$

With: N: the number of processors and

T_i (i=1 to N): the CPU time.

A total of six processors were used; all the computations were conducted on a Linux CentOS base operating system with 2 CPU (2 sockets); each socket has an Intel Xeon E5-2630 v2 (for a total of 24 threads) memory: 64GB and hard drive: 3TB. Table 5-3: Running time for different processors and Figure 5-5: Computation time (T) versus number of processor (N) plot for grid GB5: 333x90 displayed a considerable decrease in computational time and efficiency with a higher number of processor used. With six processors, there is 79% decrease of time as compared to a single processor. The more processors are used for the bridge analysis, the faster the analysis is completed.

Table 5-3: Running time for different processors

Number of processors	CPU Time (s)	Percentage decrease	s	e
1	5408.28	-	1.00	1.00
2	2867.61	46.98	1.89	0.94
3	2015.43	62.73	2.68	0.89
4	1607.26	70.28	3.36	0.84
5	1289.77	76.15	4.19	0.84
6	1106.73	79.54	4.89	0.81

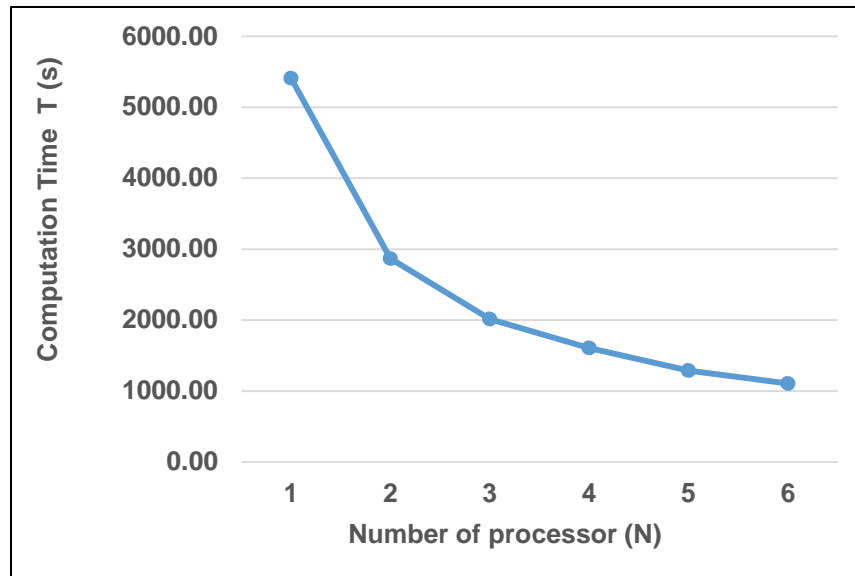


Figure 5-5: Computation time (T) versus number of processor (N) plot for grid GB5: 333x90

5.2.3. Influence of grid refinement on force coefficients

5.2.3.1. Grid generation overview

To generate the domain and the bridge structure, keys bridge points coordinate and domain are defined. In this work, eight bridge points and their corresponding points in the domain were specified; these points are respectively inner and outer points with d use as subscript for the domain point. A rectangular domain shape with $9B \times 10B$ dimension was used, B is the bridge width. The mesh is structured and body fitted, and the spacing between nodes were provided for the mesh pattern in the radial and tangential direction Figure 5-6 and Figure 5-7 below. It is important to note that non-dimensional values were used for the grid generation.

- **Radial grid point development**

The first radial node (R1) is located at the bridge perimeter (points 1, 2 etc. in Figure 5-6). The first radial spacing (Δr_0) is specified, thereby setting the location of the second radial node (R2). Spacing between the second and third radial node (R3) is computed as:

$$\Delta r_1 = \Delta r_0 * G_f = (R_2 - R_1) * G_f \quad (5-4)$$

Where: Gf: growth factor ($1 < G_f < 1.2$)

Utilizing this format, the grid radial dimension were increased to a maximum spacing Δr_{max} . In this work, $G_f = 1.1$, $\Delta r_0 = 0.001$ and $\Delta r_{max} = 0.1$. To form the mesh, the aforementioned spacing is proportionally distributed within the distance from each bridge inner to the outer points (for instance from point 1 to 1d, 2 to 2d in Figure 5-6).

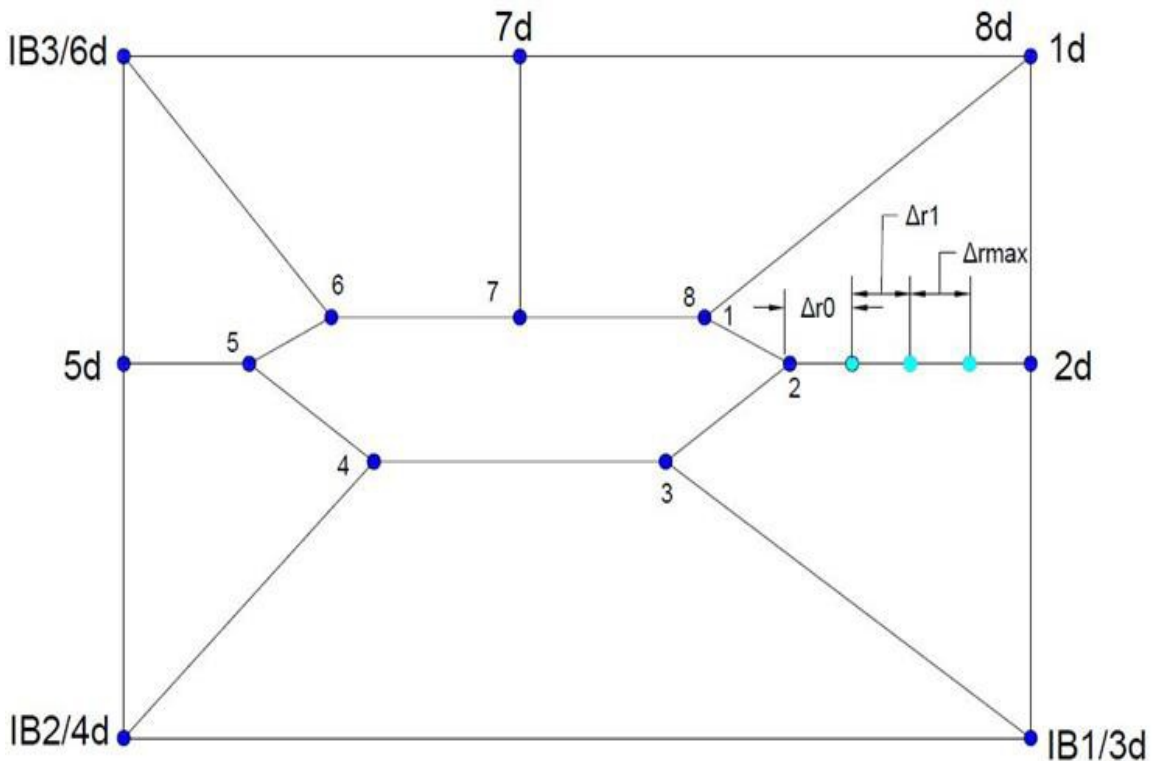


Figure 5-6: Schematic of the radial grid points development

- **Tangential grid point developments**

Tangential nodes are generated by simply providing a number of spaces between the bridge inner points for instance between point node 1 and 2, 2 and 3, 3 and 4 etc. in Figure 5-7.

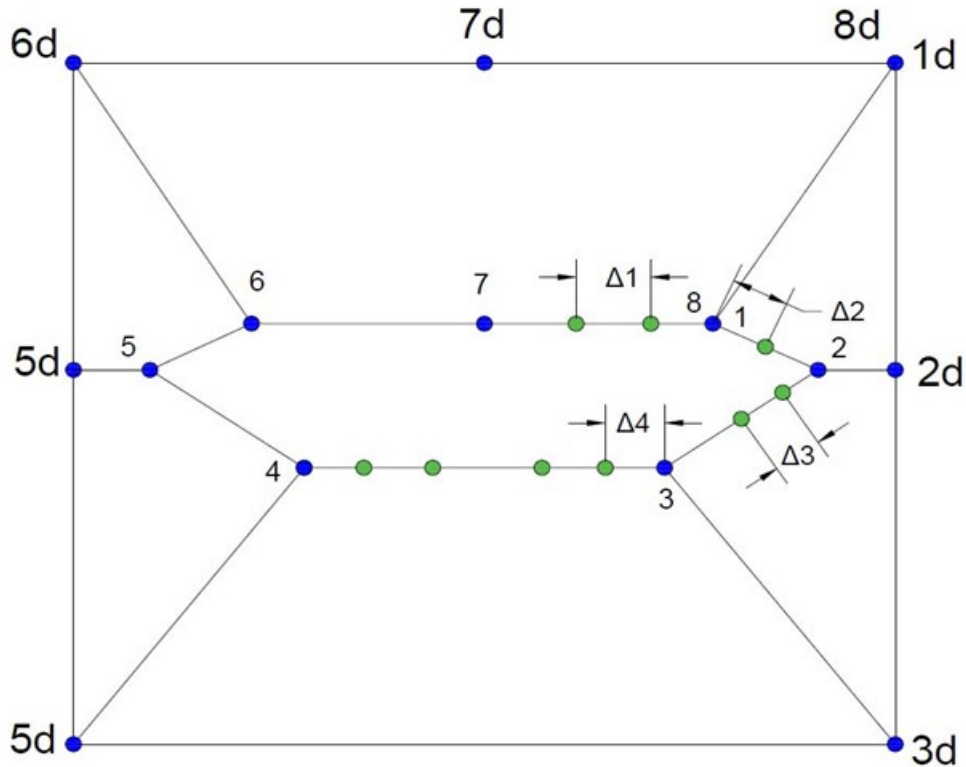


Figure 5-7: Schematic of the tangential grid point developments

5.2.3.2. Force coefficients for different grids

Variables like the domain size, the Reynold number, the artificial viscosity coefficient etc., can influence the force coefficients; therefore, depending on the purpose of the study, some variables need to be set as constant values. In the present work the Reynold number is 10^5 , $AV=10^{-4}$; domain size is $9B \times 10B$, and six processors were used. For this study the grids refined in radial direction, have a constant spacing of $0.001B$ in the tangential direction; reciprocally a

constant radial spacing of 0.0013B was kept for grids refined in tangential direction. The maximum radial and tangential points were respectively 90 and 549.

Table 5-4: Flow parameters for grids refined in radial direction

Grid	Number of nodes	Min radial grid spacing	Flow parameters		
			St	Cdmean	Cl
GA1:549x40	21960	0.0109B	0.230	0.0373	0.00024
GA2:549x50	27450	0.0048B	0.230	0.0416	0.00022
GA3:549x60	32940	0.0029B	0.185	0.0514	0.00021
GA4:549x70	38430	0.002B	0.151	0.0575	0.0002
GA5:549x80	43920	0.0016B	0.238	0.0624	0.00019
GA6:549x90	49410	0.0013B	0.148	0.0623	0.00018
Wind Tunnel Tests (WT)	Reinhold et al(1992)		0.109-0.158	0.08	0.01
	Larsen and Walter(1998)		0.17	0.08	0.07

Table 5-5: Flow parameters for grid refined in tangential direction

Grid	Number of nodes	Min tangential grid spacing	Flow parameters		
			St	Cdmean	Cl
GB1:449x90	40410	0.0015B	0.151	0.0625	0.00023
GB2:489x90	44010	0.0012B	0.109	0.0639	0.00021
GB3:529x90	39690	0.001B	0.193	0.0631	0.00019
GB4:549x90	36090	0.0001B	0.112	0.0645	0.0002
Wind Tunnel Tests (WT)	Reinhold et al(1992)		0.109-0.158	0.08	0.01
	Larsen & Walter(1998)		0.17	0.08	0.07

5.3. Contour plot for different grids

With the bridge solver post processing, visualization are made and general conclusion and remarks are deduced. The visualization includes different plots and graph: vorticity and pressure contours drag and lift coefficient and frequency versus amplitude graph.

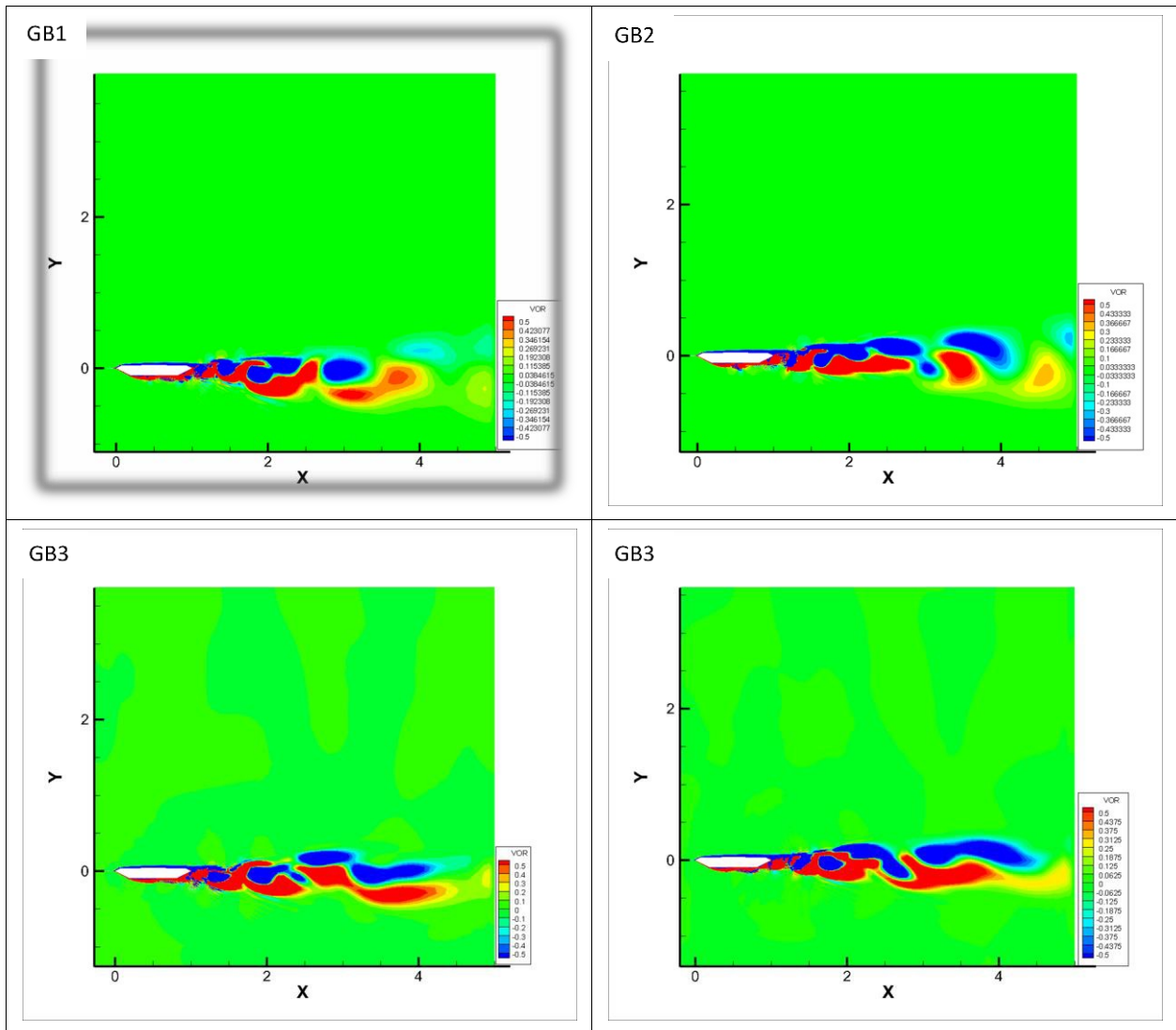


Figure 5-8: *Vorticity contour for grid refined in tangential direction full view*

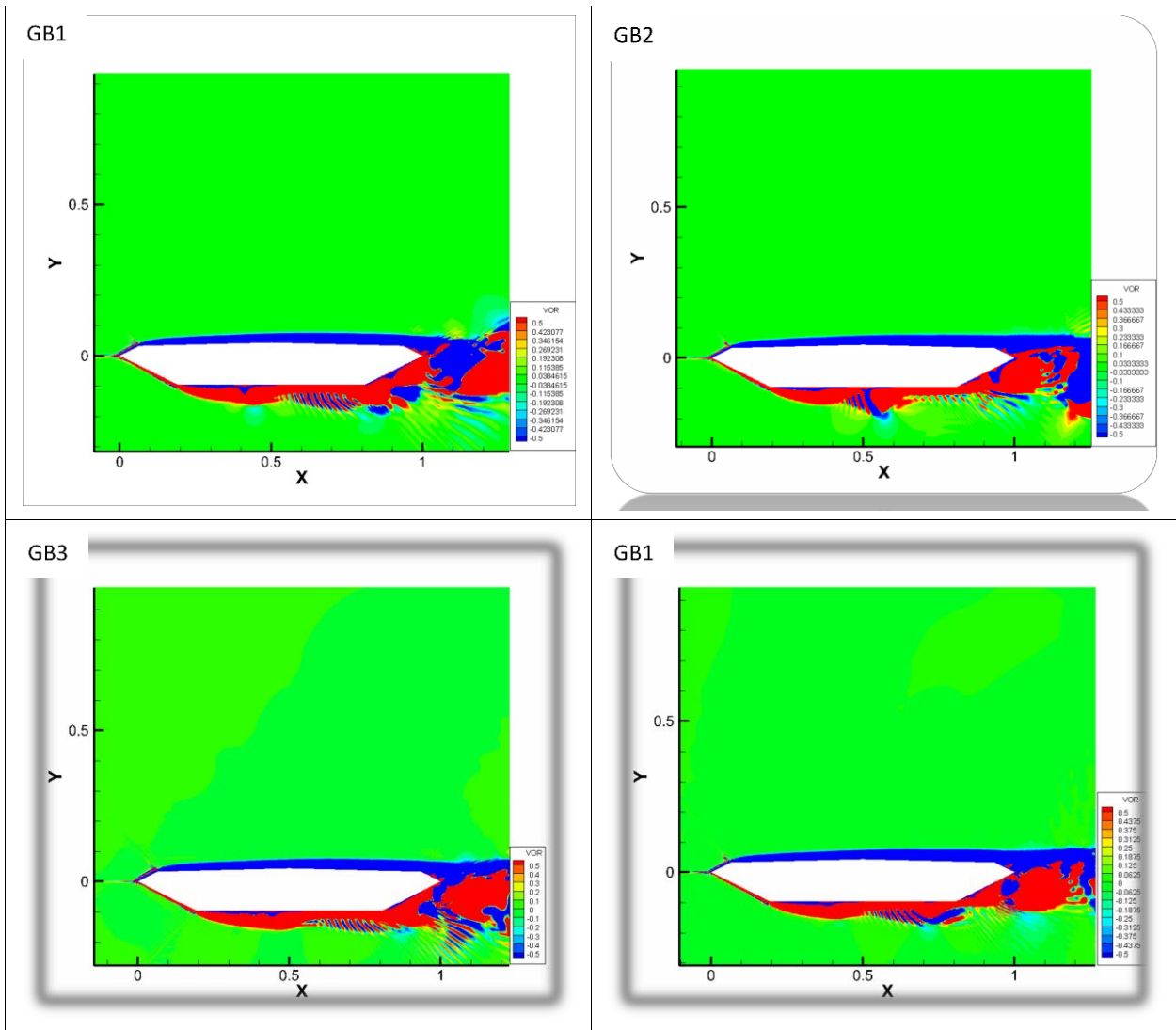


Figure 5-9: Vorticity contour for grid refined in tangential direction close up view

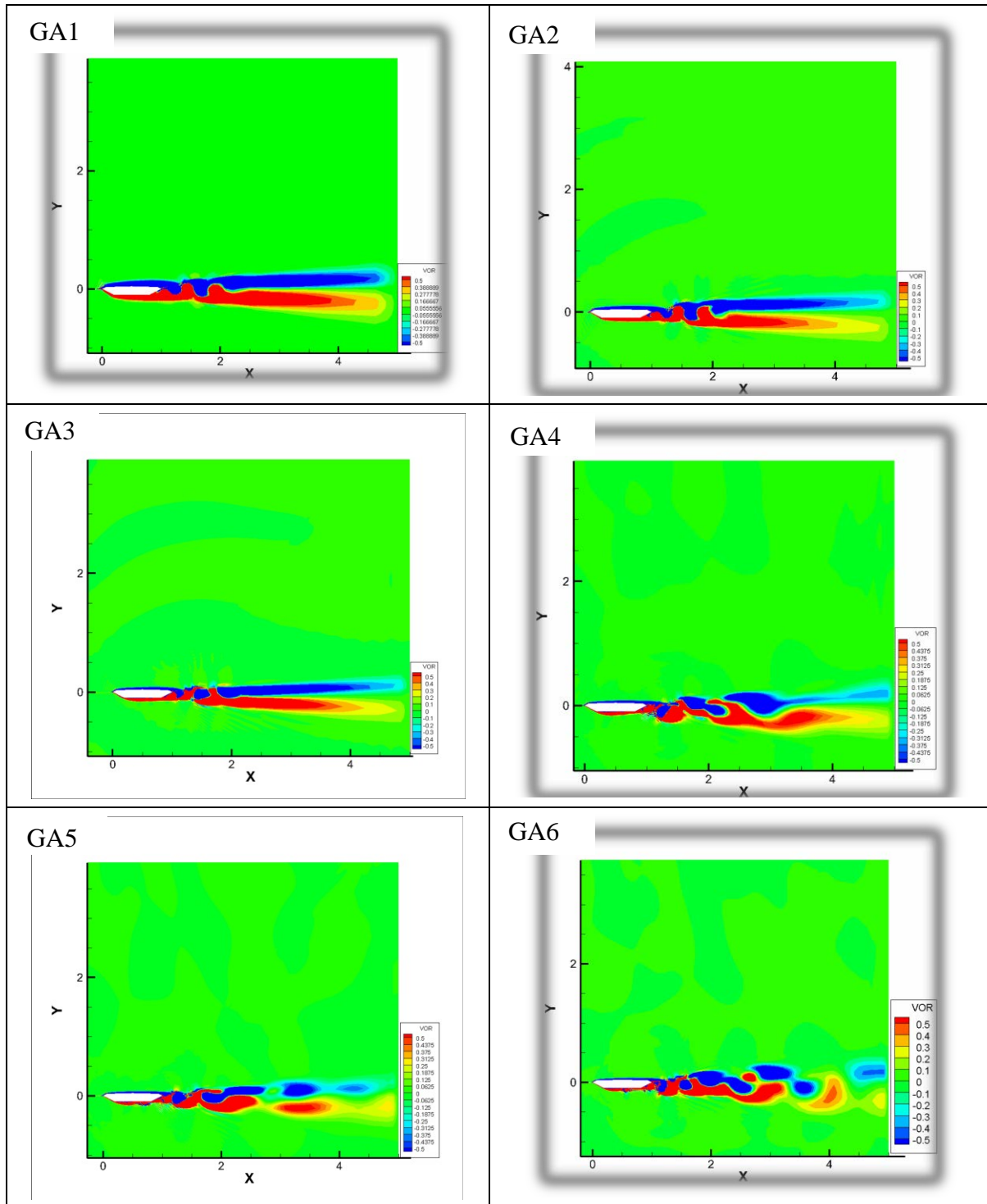


Figure 5-10: Vorticity plot for grid refined in the radial direction, full view

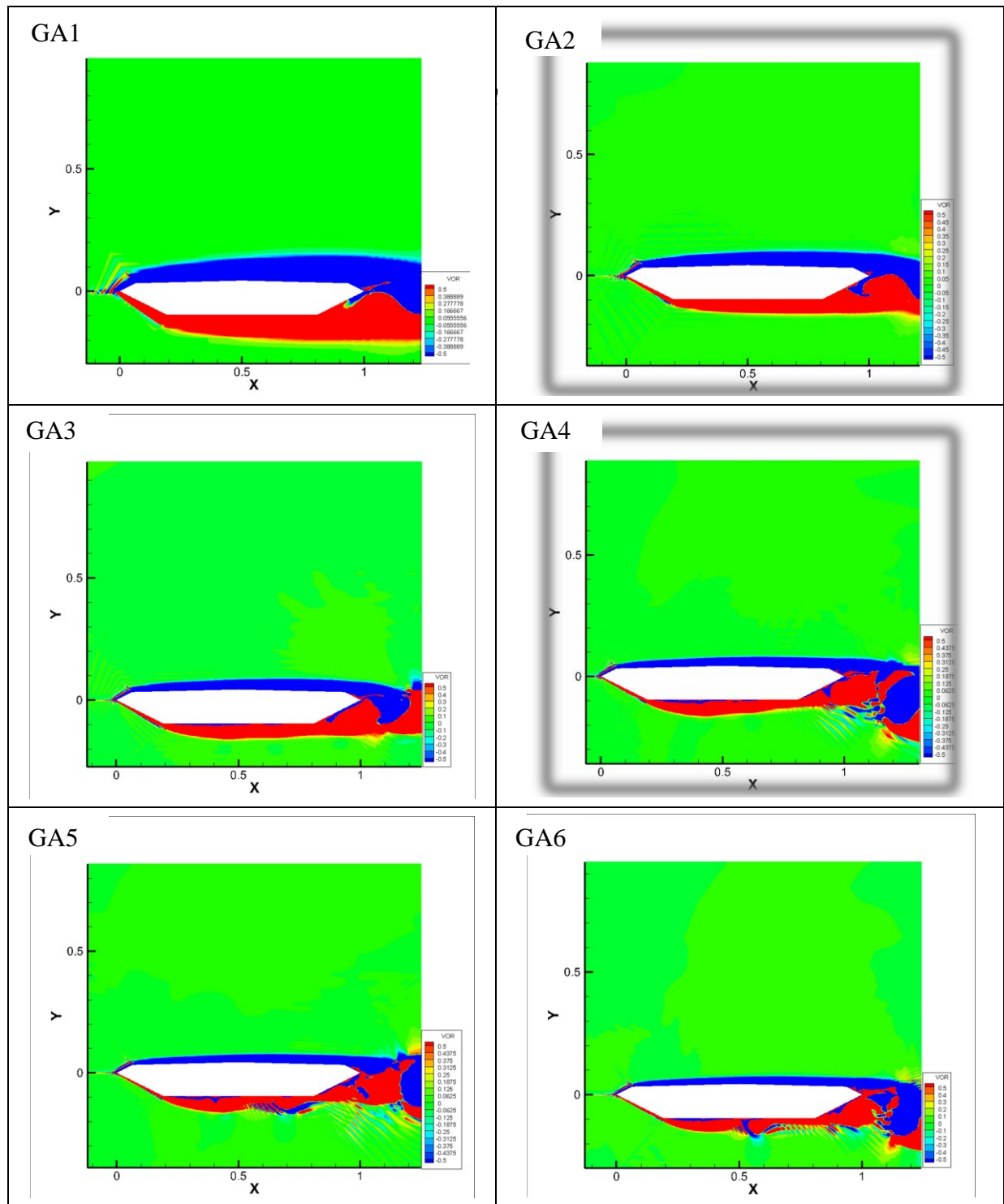


Figure 5-11: Vorticity plot for grid refined in radial direction, close up view

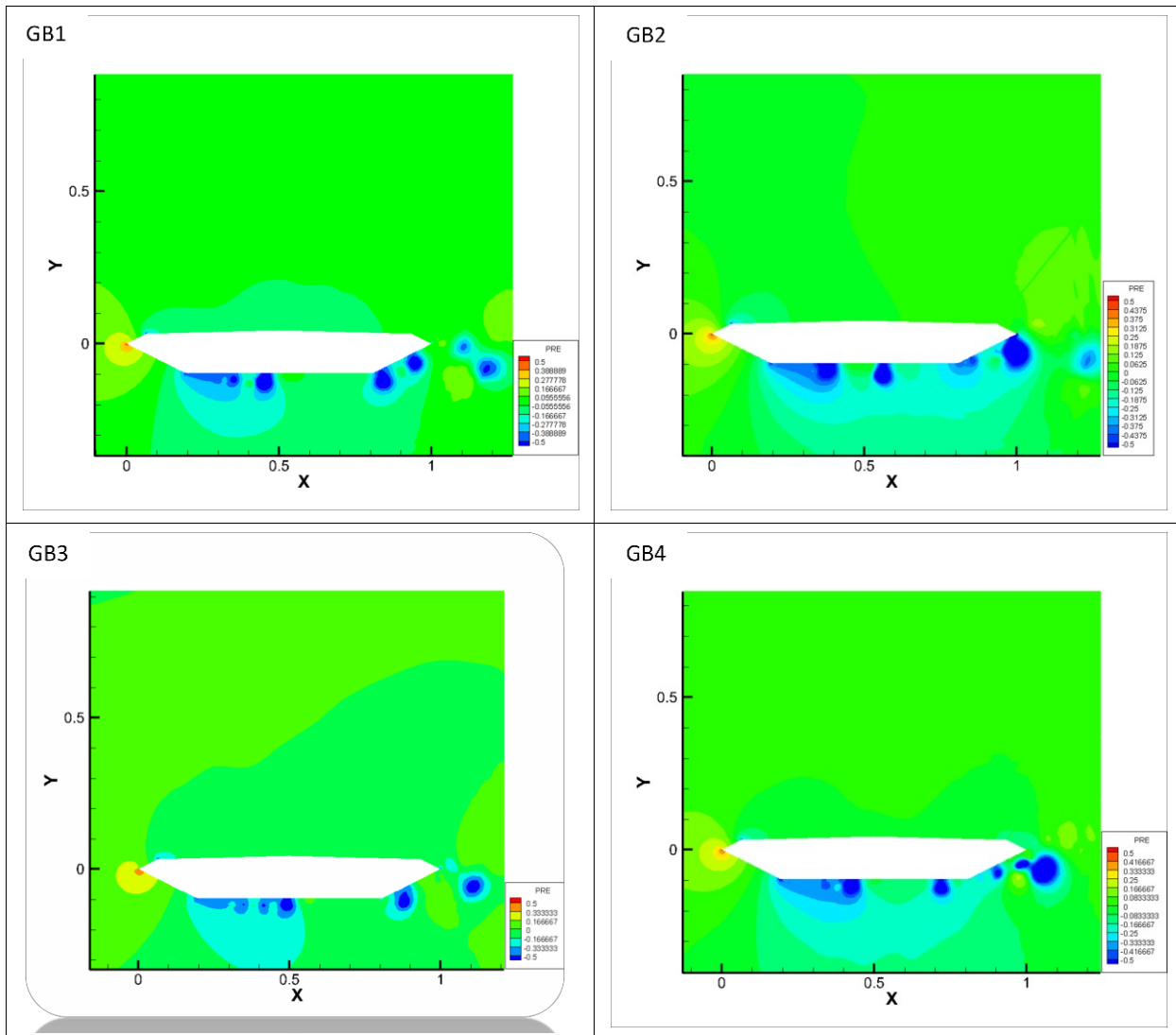


Figure 5-12: Pressure contour for grid refined in the tangential direction

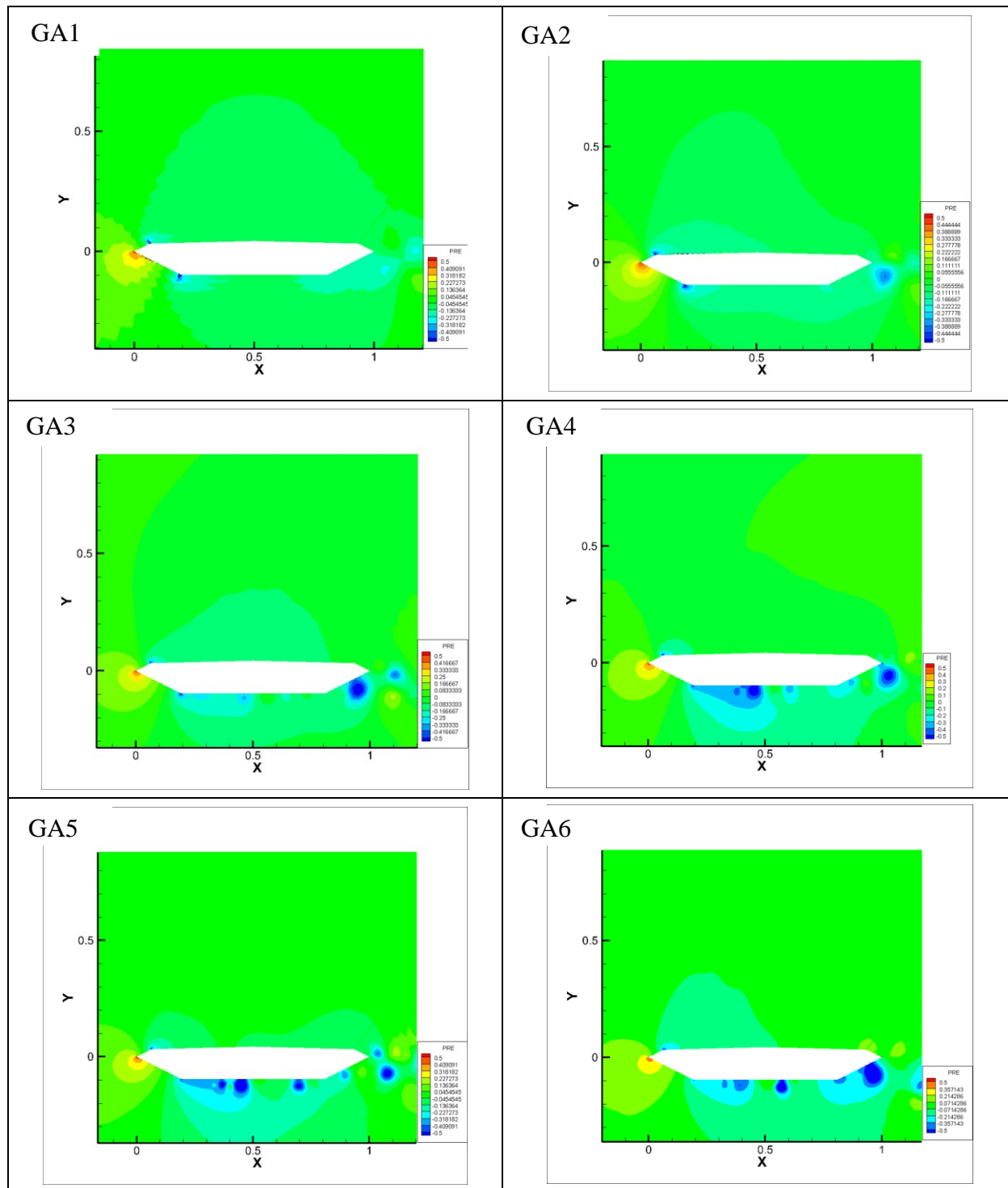


Figure 5-13: Pressure contour for grid refined in the radial direction

5.3.1.2. Drag and lift coefficient

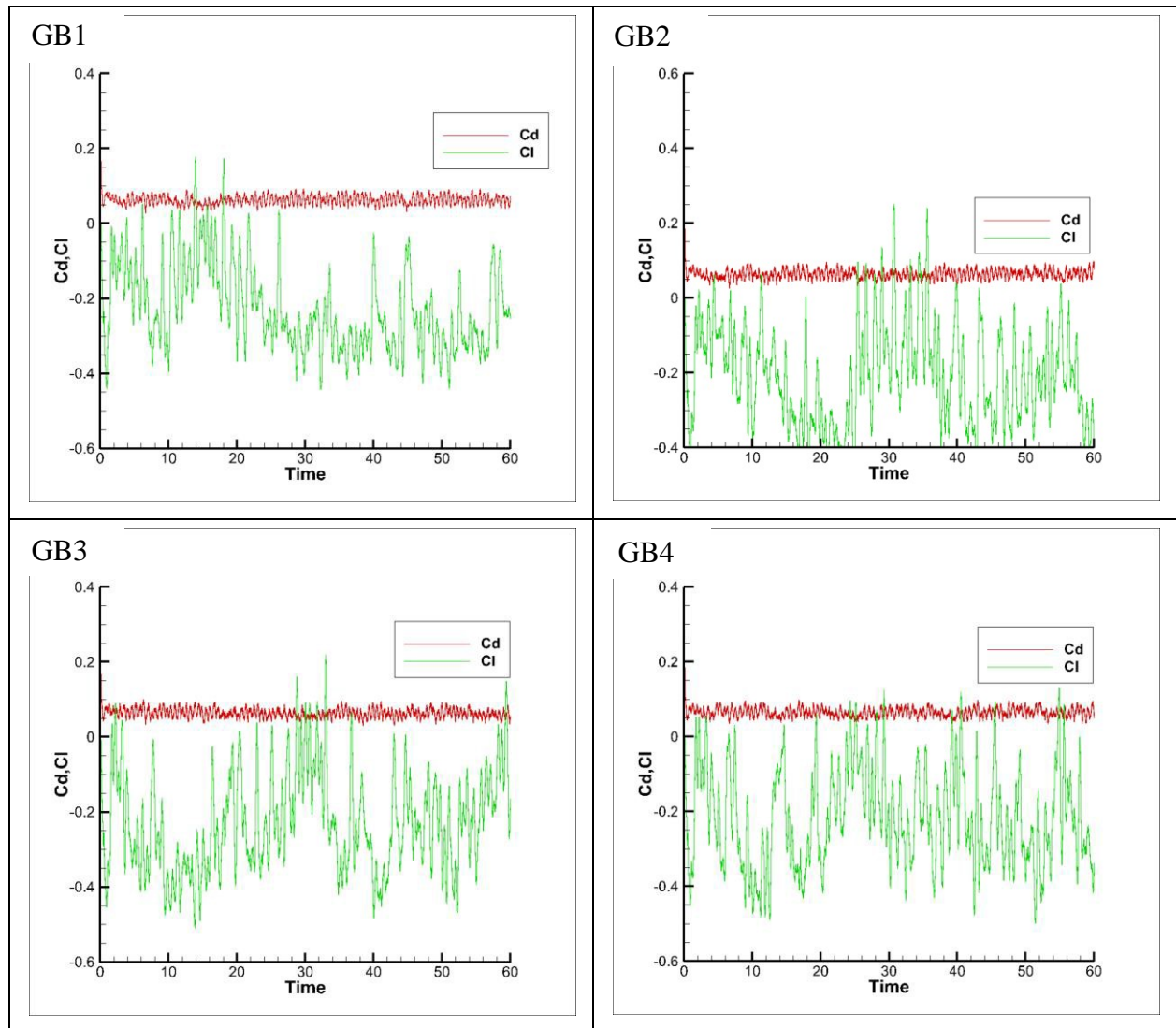


Figure 5-14: Drag and lift coefficient plot for grid refined in tangential direction

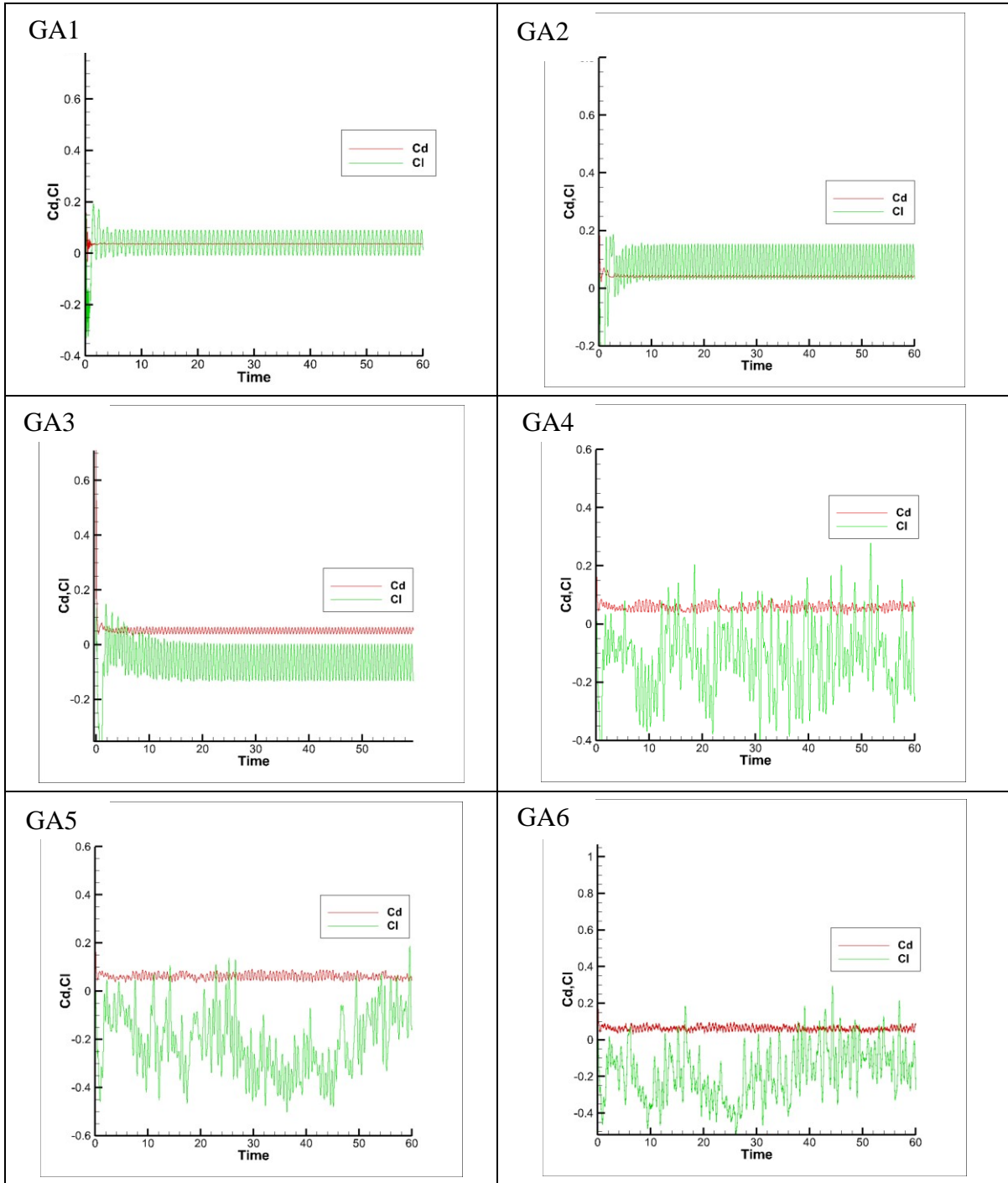


Figure 5-15: Drag and lift coefficient plot for grid refined in radial direction

5.3.1.3. *Frequency and amplitude plot*

The Discrete Fourier Transform method is used to represent the amplitude against frequency plot. The Strouhal number is obtained from Figure 5-16 and Figure 5-17, the frequencies of the fifth most predominant amplitude were used to compute the Strouhal number using the equation:

$St = Hf/V$, $V=1$ the reference velocity. Normalizing the bridge height with respect to the width $H/B=4.4/31=0.14$, thus $St=0.14f$ in non-dimensional form. Follow are the plot of the frequency versus amplitude for grid refined in the radial and tangential direction.

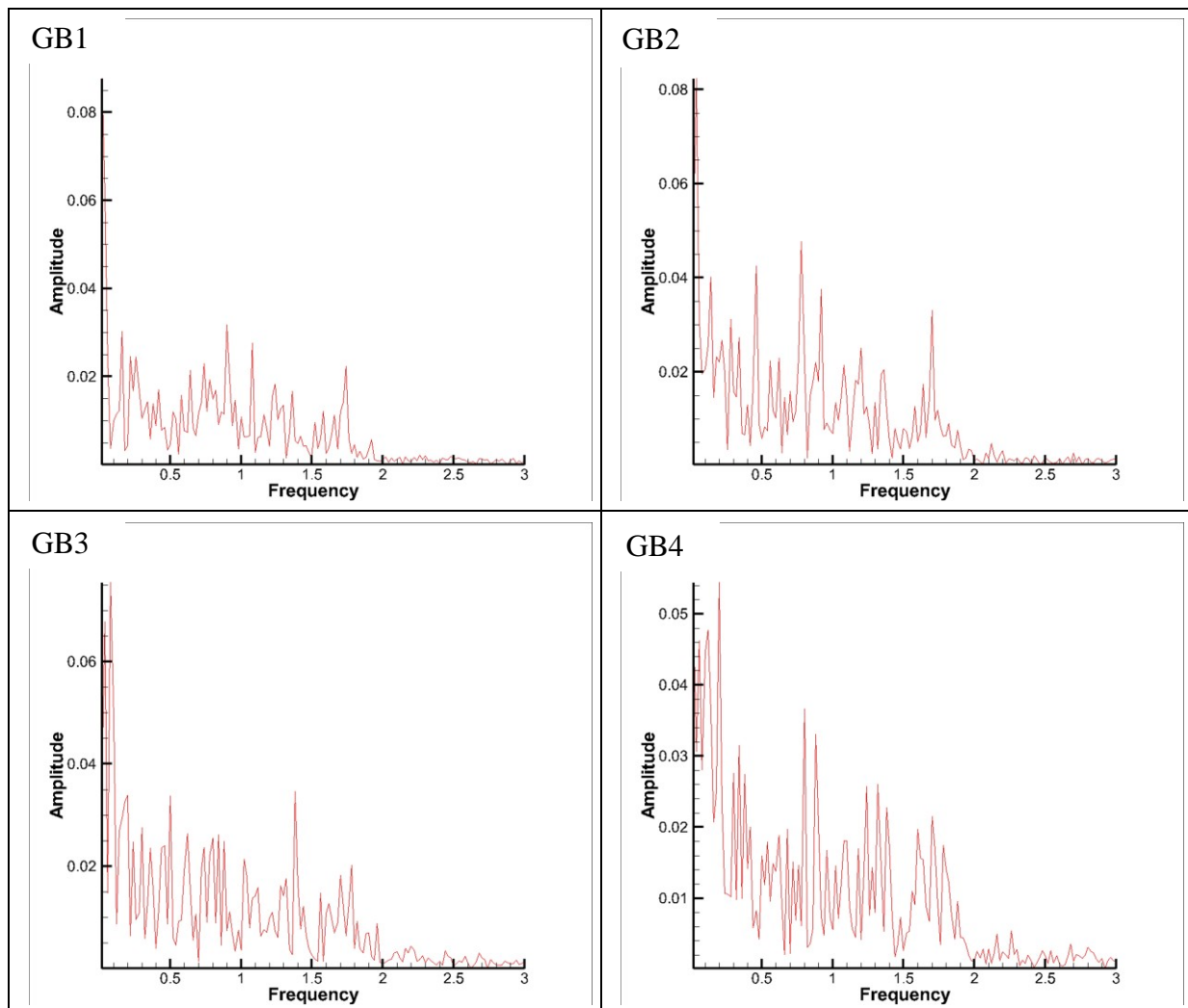


Figure 5-16: *Frequency and amplitude plot for grid refined in tangential direction*

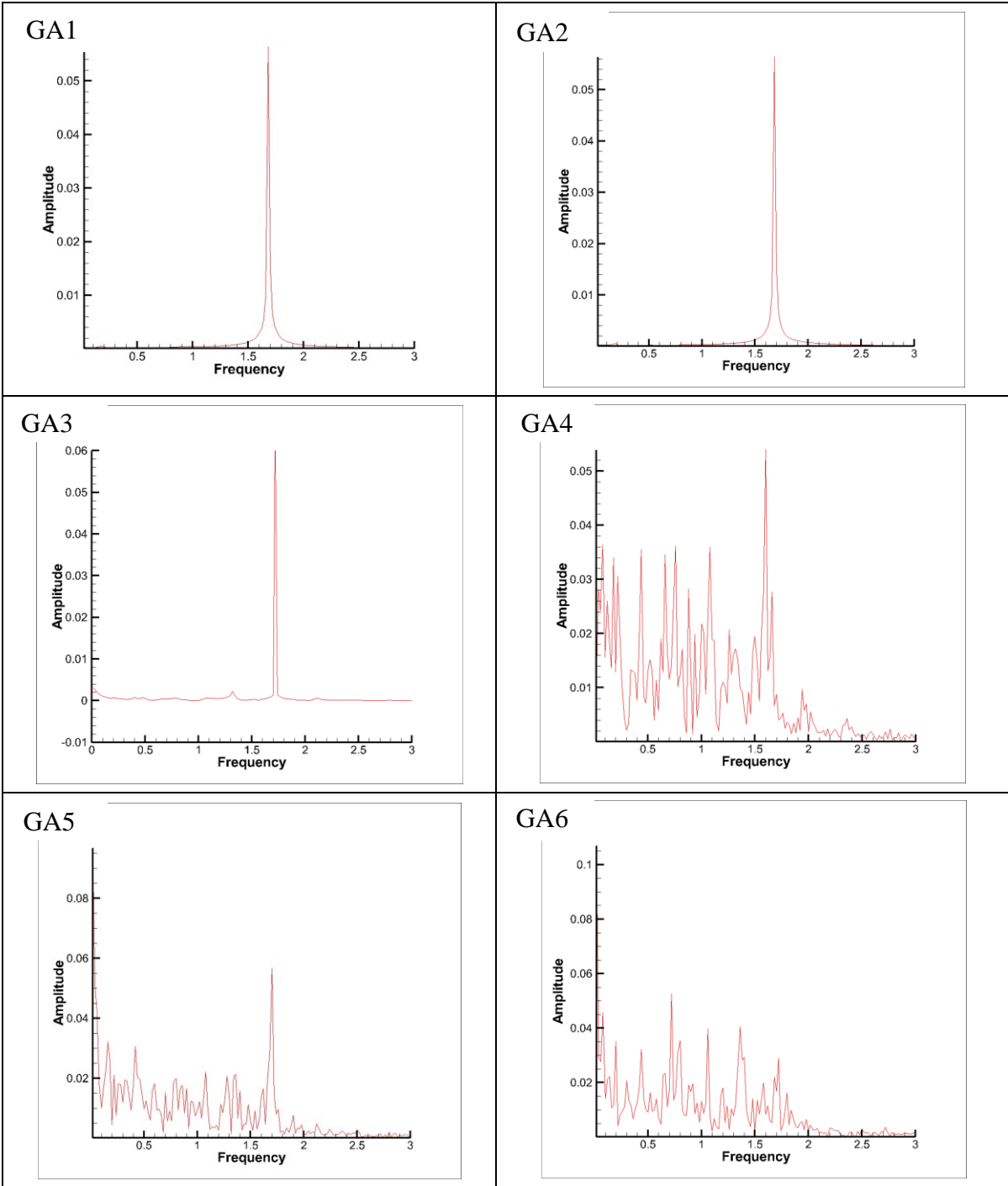


Figure 5-17: Frequency and amplitude plot for grid refined in radial direction

5.4. General remarks

5.4.1. Vorticity contour and Strouhal number

When the wind flow hits the bridge wall (wind flow direction from left to right), it is separated around the bridge corner and reattached in the wake of the bridge, resulting in vortices formation. The phenomenon of vortex shedding can be observed in Figure 5-8 and Figure 5-10. For grids refined in the tangential direction, a maximum number of 90 radial points supported by the solver were used; reciprocally a maximum number of 549 tangential points were used for grids refined in the radial direction. In Figure 5-8, four (4) circles of vortices detachments are observed for all the cases while in Figure 5-10, the number of vortices circles increases with the radial refinement. Respectively 2, 3 and 4 vortices detachments are observed for the grids pair GA2: (549x50) and GA3: (549x60), GA4: (549x70) and GA5: (549x80), GA6: (549x90) and GA1: (449x90). It can be concluded that vortices formations are more influenced by the radial refinement: the more a grid is refined in the radial direction, more vortices are developed in the wake of the bridge. Slight vortices formation at the bridge bottom perimeter started to develop as the radial refinement increase till the maximum 90 radial points (Figure 5-11). Unlike the Selvam & Govindaswamy (2002) model, no vortices are developed at the bridge top perimeter. Using grids of 14805 (216x63) and 18807 (312x57) points, with respectively 0.001B and 0.00065B minimum grid spacing close to the bridge wall, Selvam & Govindaswamy (2002) were able to develop those vortices (Figure 5-18 Vorticity plot from Selvam & Govindaswamy (2002): top grid 216x63); They used approximatively half of the grid points utilized in the present work. The absence of vortices might be due to the space discretization method implemented: specifically Selvam & Govindaswamy (2002) used FEM and in the present work FDM. Moreover, the absence of vortices might be related to the grid refinement on the bridge

top perimeter to accurately represent the boundary layer. Indeed, in this work the tangential grid spacing provided is the minimum between the $\Delta i(i=1,2,3,4)$ distances in Figure 5-19:

$$s^t = \min(\Delta 1, \Delta 2, \Delta 3, \Delta 4).$$

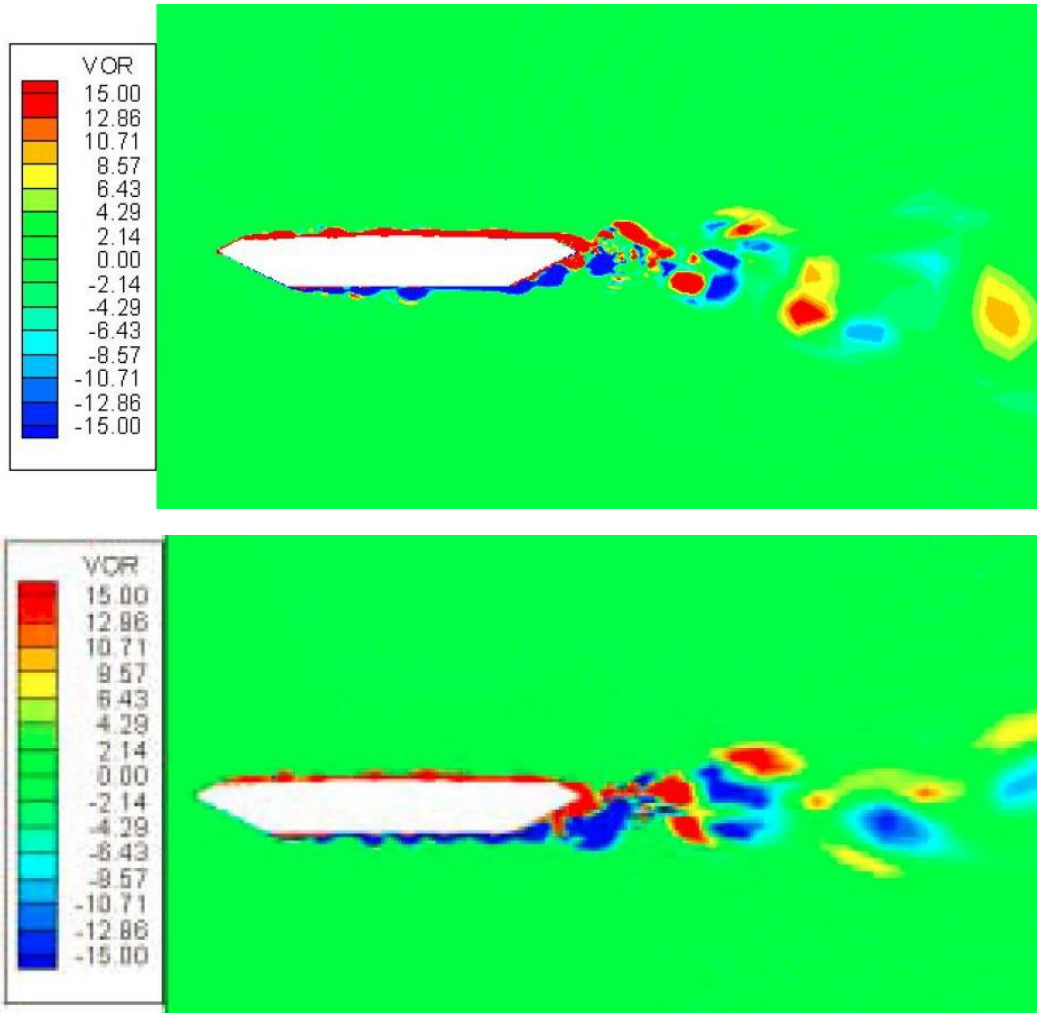


Figure 5-18 Vorticity plot from Selvam & Govindaswamy (2002): top grid 216x63;bottom grid 312x57

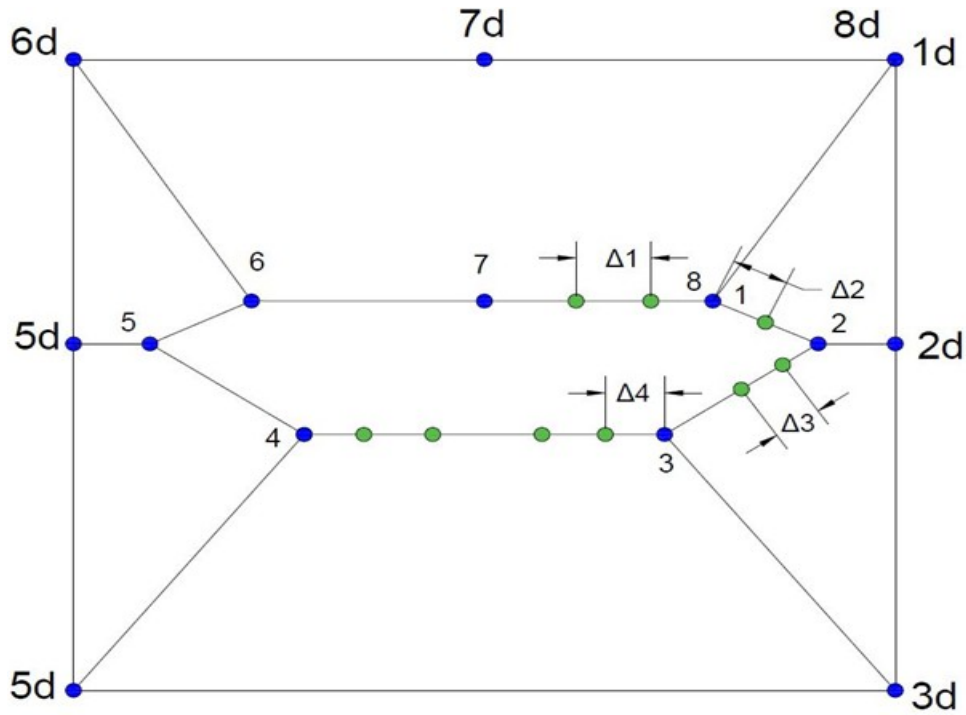


Figure 5-19: Minimum tangential spacing on bridge deck

The variation of the the Strouhal number with the minimum grid spacing close to the bridge wall, is not clearly understood at this stage. Indeed, as the minimum spacing decrease both in radial and tangential direction the Strouhal number decreases too getting closer to the wind tunnel result ; however, there is a sudden change in strouhal number value for grids GA5:549x80 and GB3:529x90 (Figure 5-20, Figure 5-21). Nevertheless these changes, the Strouhal number is in good agreement with wind tunnel tests for grid refined in both radial and tangential direction; in Table 5-7, the Strouhal number fall within the result range of wind tunnel experriments conducted by Reinhold et al(1992).

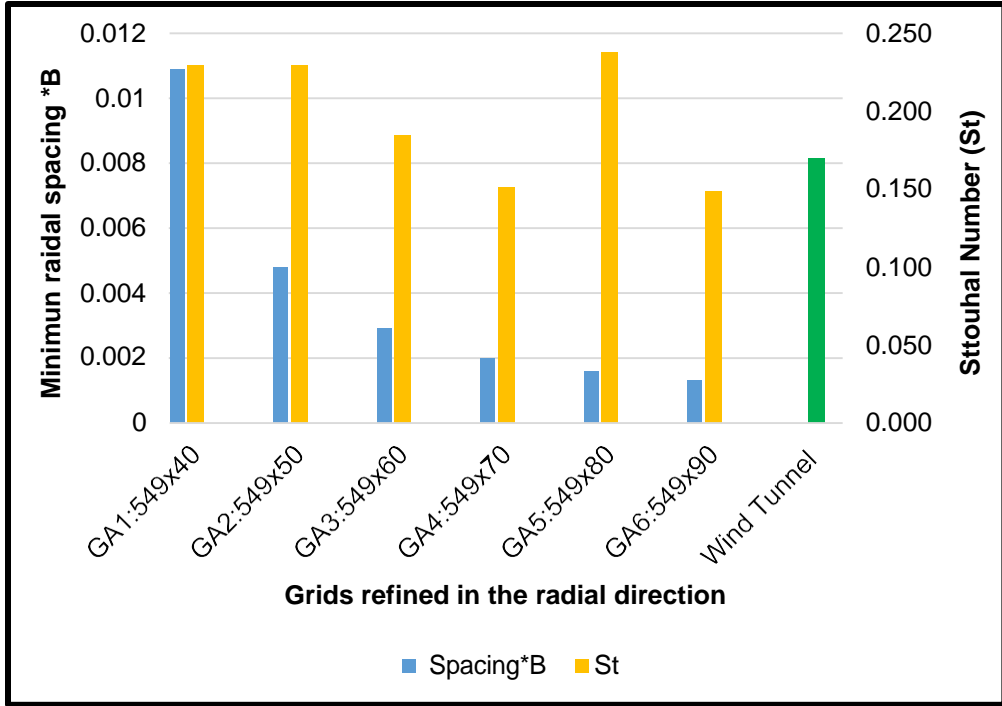


Figure 5-20: Variation of Strouhal number with radial grid spacing

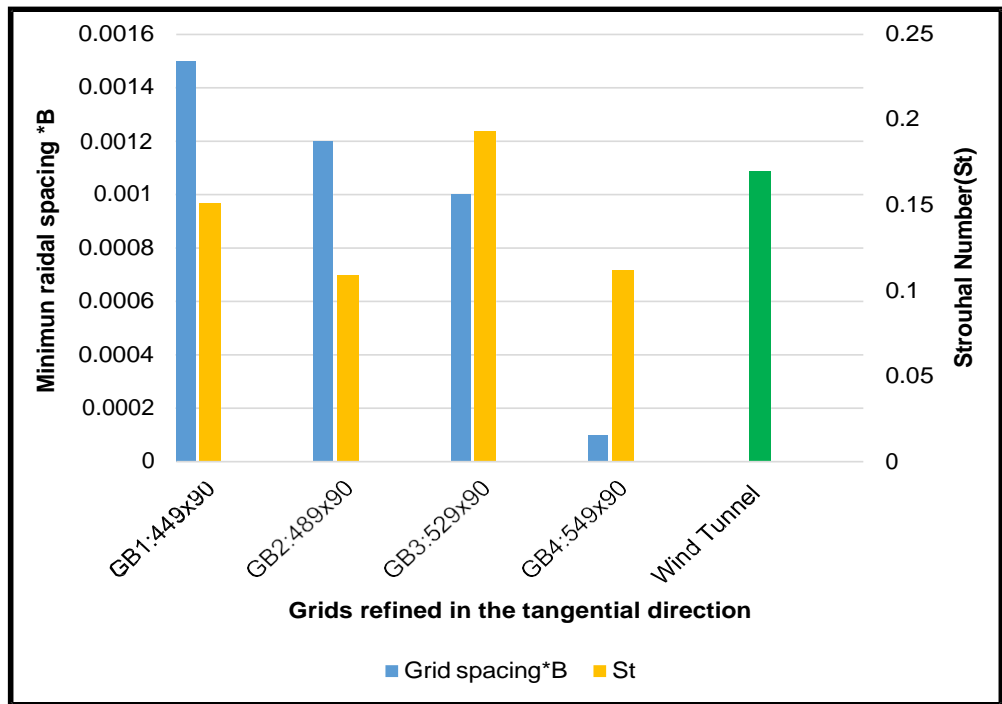


Figure 5-21: Variation of Strouhal number with tangential grid spacing, B is the bridge width

5.4.2. Drag and lift coefficient

For grid refined in the tangential direction, the drag coefficient varies slightly while for grid refined in the radial direction, the mean drag coefficient increase with the decrease of the minimum grid spacing (Figure 5-22 and Figure 5-23). The lift coefficients are not in comparison with wind tunnels experiment; there is not a clear understanding of the lift coefficient behavior with respect to the grid refinement since good results could not be obtained.

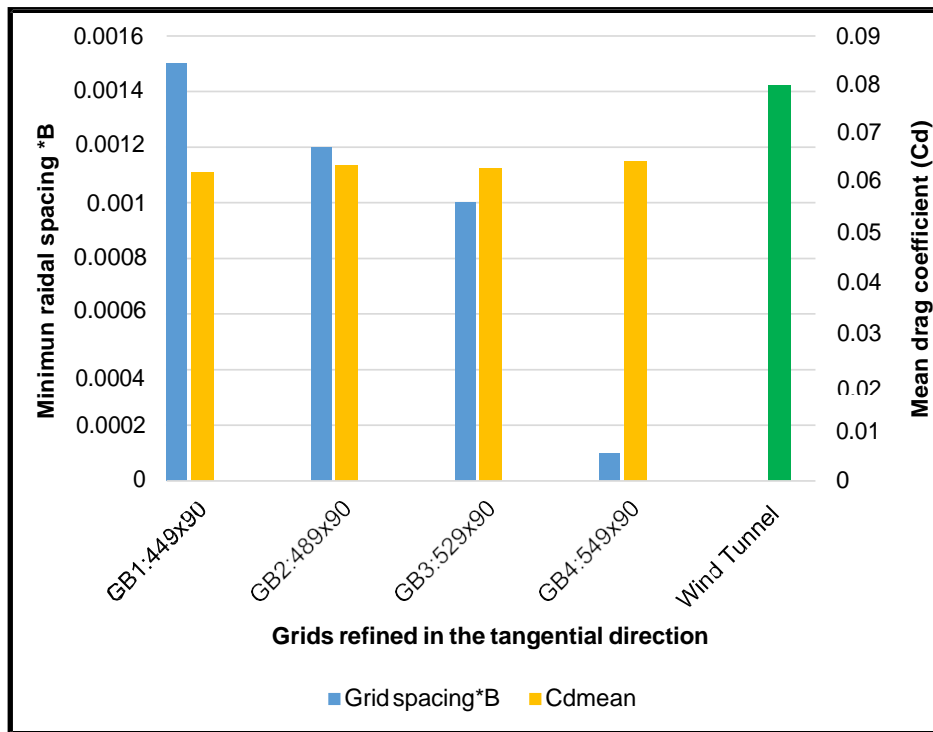


Figure 5-22: Variation of mean drag coefficient with tangential grid spacing, B is the bridge width

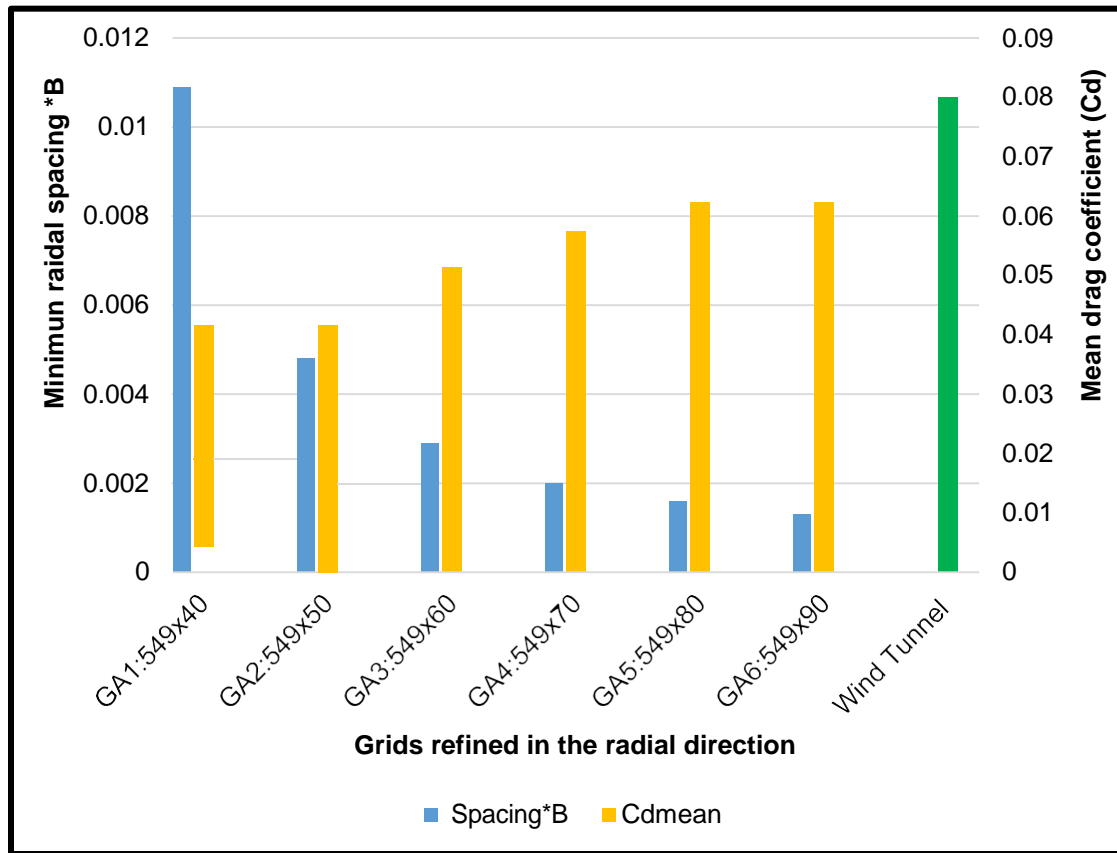


Figure 5-23: Variation of mean drag coefficient with radial grid spacing, B is the bridge width

5.4.3. Pressure contour

The pressure contour plot of Figure 5-12 and Figure 5-13 displayed the pressure distribution around the bridge section. Positive maximum pressure are concentrated on the bridge windward face (corner point) and negative ones on the bridge leeward and bottom face. The contour plots accurately represent the predicted pressure distribution discussed in section 3.2.1: the bridge leeward face is subjected to suction or negative pressure and the windward face to pressure. As the grid is more refined in the radial direction, the pressure distribution is more developed on the bottom and side of the bridge deck section.

5.4.4. Result summary

Except for the lift coefficient where the discrepancy with wind tunnel experiment is higher than 50% (Table 5-6 and Table 5-7), the drag coefficient and the Strouhal number are in comparison with previous studies: Reinhold et al. (1992), Larsen & Walter (1998), Selvam & Govindaswamy (2002), Bruno & Chris (2003) and Patro et al. (2013). Grid refined in the radial direction gives higher result of the Strouhal number while grid refined in the tangential direction give higher drag coefficient (Figure 5-24 and Figure 5-25).

The current model with that of Selvam & Govindaswamy (2002) demonstrate some similarities and differences as illustrated in Table 5-8. During the grid generation process, a single domain region is used instead of two regions in Selvam & Govindaswamy (2002). A single domain is advantageous in term of initial amount of information to provide, parallel computing process and computational loads involved. In the present work, the user only provide, the coordinates of 8 points that define the bridge cross section shape and perimeter. Previously 16 points coordinates were needed. During processing, output data from the pre-processing must be formatted; formatting may increase error for an unfamiliar user since all the data are crucial the processing and post processing. It should also be noted that the present model can be used for both parallel and serial computing; however, only parallel computing was implemented in this work. Further differences between the two models are shown in Table 5-8 to demonstrate how the current model improved Selvam & Govindaswamy (2002) model.

Table 5-6: Error (in percentage), current work result with literature

Researchers	Radial refinement (GA5:549X80)			Tangential refinement (GB4:549X90)		
	Cd/Cdmean	St	CI	Cd/Cdmean	St	CI
Reinhold et al. (1992)	22.00	33.61	98.10	19.38	0.00	98.00
Larsen & Walter (1998)	22.00	28.57	99.73	19.38	34.12	99.71
Selvam et al. (2002)	0.65	41.18	-	4.03	20.00	-
Bruno & Chris (2003)	12.11	31.09	~	9.15	9.68	~
Patro et al. (2013)	0.95	20.17	-	2.38	0.00	-

Table 5-7: Summary of flow parameter for different studies

Researchers	Nodes	Minimum spacing	Cd/Cdmean	St	CI	
Reinhold et al. (1992)	Wind tunnel tests		0.08	0.109 - 0.158	0.01	
Larsen & Walter(1998)			0.08	0.17	0.07	
Larsen & Jacobsen(1992)			0.57 & 0.59	-	0.067 & -0.05	
Selvam et al. (2002)	14805	0.0015B	0.062	0.14	-	
Bruno &Chris (2003)	-	0.00022B	0.071	0.124 - 0.164	-0.195	
Braun & Auruch (2008)	8400	0.003B	0.65	-	0.05	
Patro et al. (2013)	18615	0.001B	0.063	0.11-0.19	-	
Current work	GA5:549x80	43920	0.001B	0.0624	0.238	0.00019
	GB4:549x90	49410	0.0001B	0.0645	0.112	0.0002

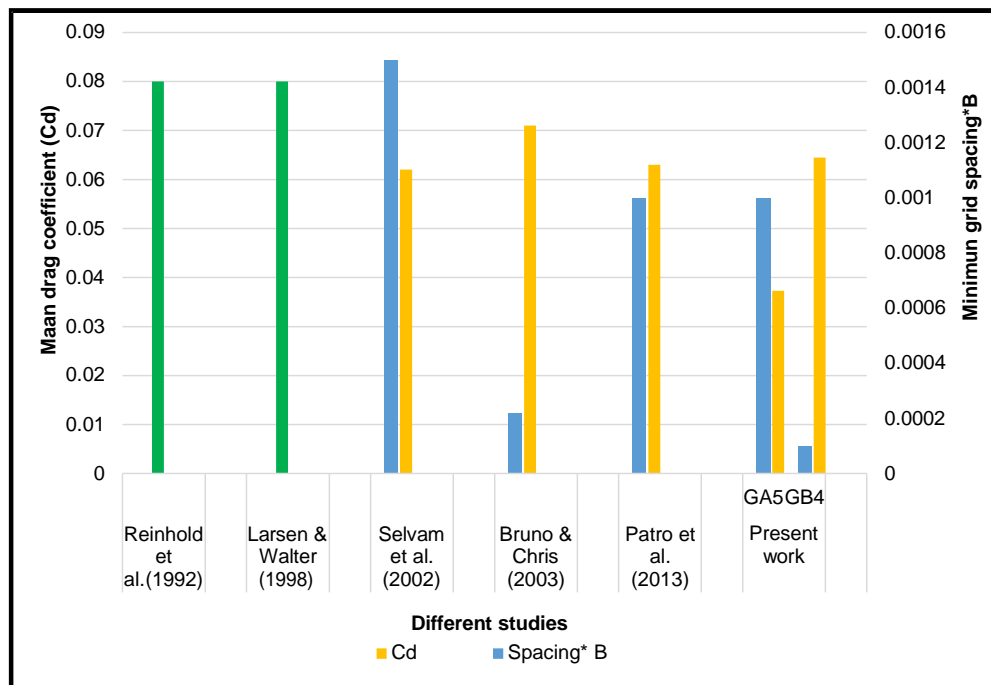


Figure 5-24: Mean drag coefficient chart for different studies, B is the bridge width

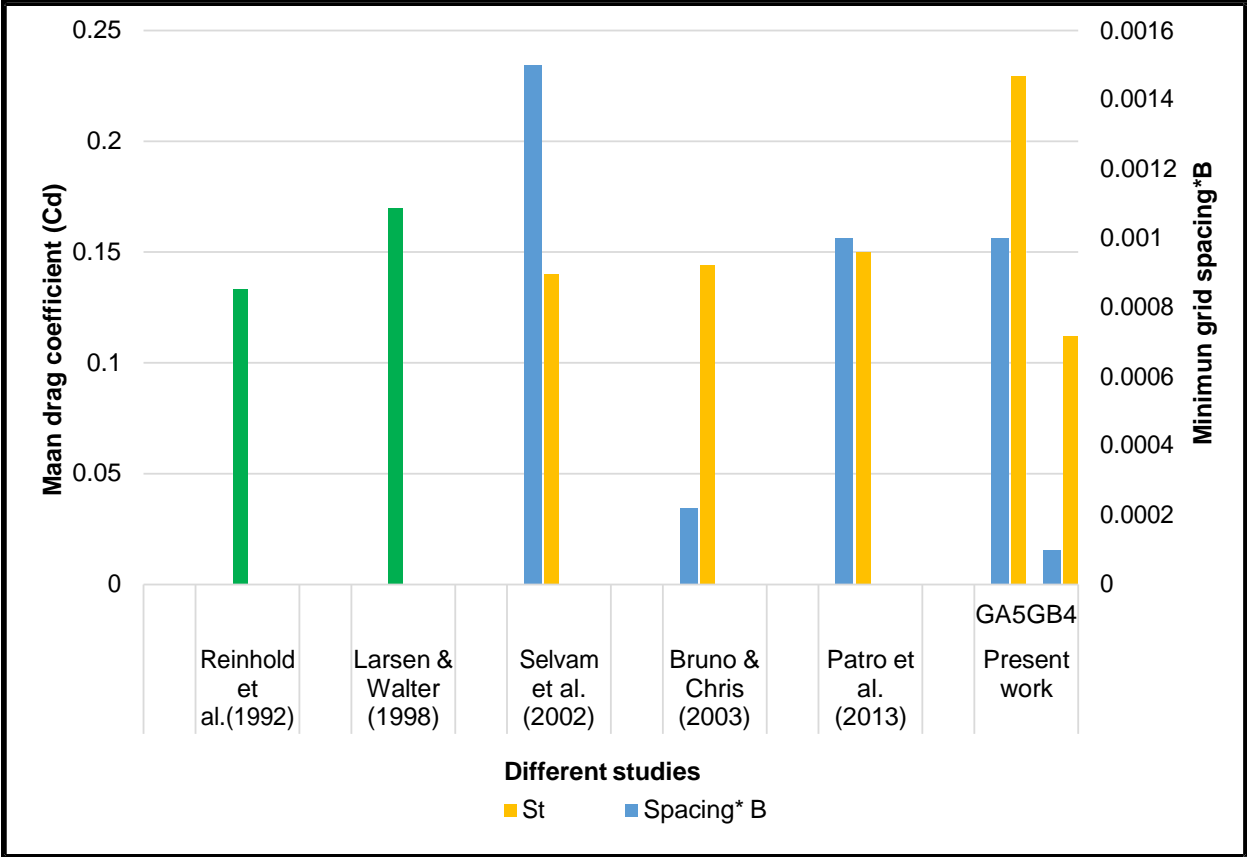
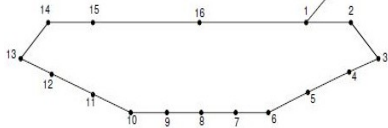

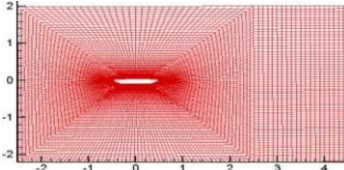
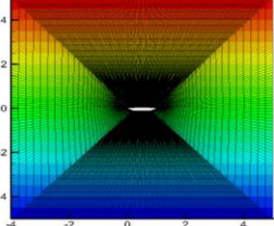


Figure 5-25: Strouhal number chart for different studies, B is the bridge width

Table 5-8: Comparison and contrast of the current work with Selvam & Govindaswamy (2002)

Parameter	Selvam & Govindaswamy (2002)	Present work
Type of bridge	GBEG suspension span	GBEG suspension span
Pre-processing		
Grid type	Structured and Unstructured(body fitted)	Structured (body fitted)
Domain	2 regions:main and extended(4Bx7B)	1 region(9Bx10B)
	required regions to match and merge	Single region with no matching required
Number of point required for the grid generation	16	8
		
Grid/domain geometry		
Processing(Bridge Solver)		
Numerical model	Finite Element Method and Large Eddy Simulation (FEM & LES)	Finite Difference Method and Large Eddy Simulation (FDM & LES)
Parallel computing	no	yes, automatic region division amount processor
Serial computing	yes	yes, but not use in the present work
Bridge type	fixed and moving	fixed
Computational time	4 days on a 8-400Mhz/4Mb external CPU and 4Gb memory microsystem enterprise computer	1.5h to 30 min on a 2 CPU Intel Xeon E5-2630v2 computer with 3TB memory
Input data	Data formating required	No data formating required
Results		
Grid Size	216x63	549x90
Number of nodes	14805	49410
Minimun grid spacing	0.001B	0.0001B
Mean drag coefficient (Cd)	0.062	0.0645
Strouhal number (St)	0.14	0.112
Lift coefficient (Cl)	-	0.0002
Statut with wind tunnel test	In good agreement	In good agreement

6. CONCLUSION

6.1. Summary and conclusion

Numerous methods for the wind induced loads analysis on bridges exist. Probabilistic methods, linear and nonlinear approaches, computational fluid dynamics methods and experimental methods have been widely explored for this purpose. A review of these methods was carried in order to investigate the current trend in bridge aerodynamics and identify the challenges within CFD methods. One challenge is a lack of clear and exact range of grid resolution for accurate force coefficient prediction in the grid generation process of CFD methods. Indeed, once results close to wind tunnel test are predicted with a certain level of grid resolution, there are no concerns about the result behavior if better grid refinements are achieved.

“UofA Bridge Code” software package for bridge analysis, a FDM/LES, intends to reduce the computational time involves in the simulation and provide level of grid refinement needed for good results to avoid in future works random choice of grid parameters. Currently, the effects of grid refinement on vortex shedding, aerodynamic parameters are presented and the model parallel performance is demonstrated. With parallel computing, the current model allowed to conduct bridge analysis in approximatively 30 minutes which is beneficial for project management. Some issues faced by Selvam & Govindaswamy, (2002) model are solved in the present work, thus demonstrate the user friendliness of the model. From the present research the following conclusions can be made:

- Grid refinement in radial direction influences the number of vortices formation in the wake of the bridge (Figure 5-8 and Figure 5-10).

- When the grids are more refined in the tangential direction, the discrepancies between wind tunnel tests and the present work for the mean drag coefficient are 2.62 % reduced (22 % and 19.38% of error for grids refined respectively in radial and tangential direction, Table 5-6). Indeed, tangential refinements reduce the space between nodes located on the bridge perimeter ; for this reason, better results were achieved since grid refinements on the side of the bridge influence the drag force.
- With less refinements close to the bridge wall, the current work was able to achieve higher drag coefficient than Selvam & Govindaswamy (2002) (Table 5-7, grid GB4:549x90).
- For accurate result of the drag coefficient we recommend the designer to reduce the minimum grid spacing in the tangential direction(side of the bridge). We recommend a minimum grid spacing close to the bridge wall ranging from 0.0013B to 0.002B in radial direction to predict a drag coefficient comparable to wind tunnel experiment.
- Concerning the Strouhal number both radial and tangential refinements influence its value. A decrease of the Strouhal number with decrease in grid spacing is observed in Figure 5-20 and Figure 5-21; however an unusual change occurred for grid GA5:549x80 and GB3:529x90 which might be due to numerical instability
- The present work ,with the lowest minimum grid spacing close to the bridge wall of 0.0001B (Figure 5-24 and Figure 5-25), was able to predict result comparable to wind tunnel experiment of Larsen & Walther (1998) and Reinhold et al. (1992). A discrepancy of 19.38% and 34.12% (respectively drag coefficient and Strouhal number) for the former and 19.38% and 0% for the latter were thus achieved (Table 5-6).
- The lift coefficient were not comparable to wind tunnel results and were not reported.

6.2. Model limitations and recommendation

Implementation of parallel computing had numerous issues: firstly, the high numerical dispersion which was responsible for the force parameter divergence with increase of grid refinement. Secondly, the moving bridge method used by Selvam & Govindaswamy (2002) could not be utilized with the current model limiting the critical wind speed prediction of for flutter instability. The method is investigated for bridge aerodynamics use. During the simulation, numerous processes are involved (grid generation, bridge solver and post processing) and several type of file with name restriction exist, and this can be challenging for the user. The model do not predict accurately the lift coefficient; thus, this area needs more investigations in future work. As the number of grid increases the computational time become larger; this might be the result of small time step usage with the explicit method. The usage of large time step associates with parallel computing might solve this issue.

Investigation of the Reynold number and domain size influence on force coefficients might be considered for future works. Moreover, the model assesment for different bridge cross sections is also a possible scope for upcomming researches.

7. USER MANUAL FOR “UofA Bridge Code” PACKAGE

7.1. Introduction

“UofA Bridge Code” is a software package used for the computer modeling and analysis of flow around bridges. The package contains three main parts that the user needs to follow according to the set structure. The package different parts are:

1. Grid generation
2. Bridge solver
3. Visualization and data processing

For an efficient usage of “UofA Bridge Code” software package, some background in Linux and Fortran is needed. Nevertheless, some key concepts for an ease code use are mentioned in the following sections to help the user.

7.1.1. Grid Generation

In this first step the user needs to provide data to generate the bridge geometry and computational domain. The data consist of points coordinates named bridge key/ inner points and outer point. Bridge key/ inner points are used for the bridge geometry and outer point for the computational domain. Since the main goal of the grid generation is to split the domain of study in sub-domains, spacing around the bridge perimeter and distance between node located within each inner and outer points are needed; this is called tangential and radial grid refinement. Depending on the level of accuracy the user needs to obtain, the grid can be refined by decreasing the distance between points. From the grid generation, data are generated for the bridge finite difference analysis. The grid generation software also enables to visualize bridge shape, domain, sub-domain and nodes interconnected.

7.1.2. Bridge Solver

With the domain discretized in the previous grid generation process, the flow Navier Stokes equation and the structural dynamics equations for the bridge motion are solved with the Bridge Solver. A fixed Bridge Solver in which the bridge is restricted from any movement is implemented in the package and enables to obtain the aerodynamic force coefficients. CFD methods with FDM and LES are used for this purpose. The solving process consists of numerous iterations ending when the solution convergence (set up by the code developer) is reached. Data in non-dimensional and graphic forms are provided after few minutes runs (force coefficients, pressure and vorticity contours, etc.). Each part of “UofA Bridge Code” is interconnected with other; thus, the output files from the bridge solver are useful for the following step.

7.1.3. Visualization and Data Processing

Results from the Grid Generation and Bridge Solver are analyzed, and proper conclusions are deduced. Graphic plots are visualized, and observations on the behavior of the bridge subjected to wind induced load are made. The Strouhal number is calculated from the frequency versus amplitude plot. With the data processing, the user can compare the result of the analysis and validate the model.

7.2. User Manual for the Grid Generation Code

A grid is a set of points (nodes) and elements related to each other which help to discretize a computational domain to solve a problem numerically. The grid generation is also known as pre-processing in CFD code. The **acbrg-i.txt** and **inp.txt** constitute the input files, the program is executed using **acbrg.exe** for the final mesh. It should be noted that the user only

need to have access to internet and be connected to any browser and that the online page enable to generate only the input file (**acbrg-i.txt** and **inp.txt**) for the grid generation and not the grid itself. The steps to generate the grid follow:

7.2.1. Step 1: Pre-processing, preparation of the input data: acbrg-i.txt

1- Go to <http://comp.uark.edu/~btmbiand/> click on Grid generation

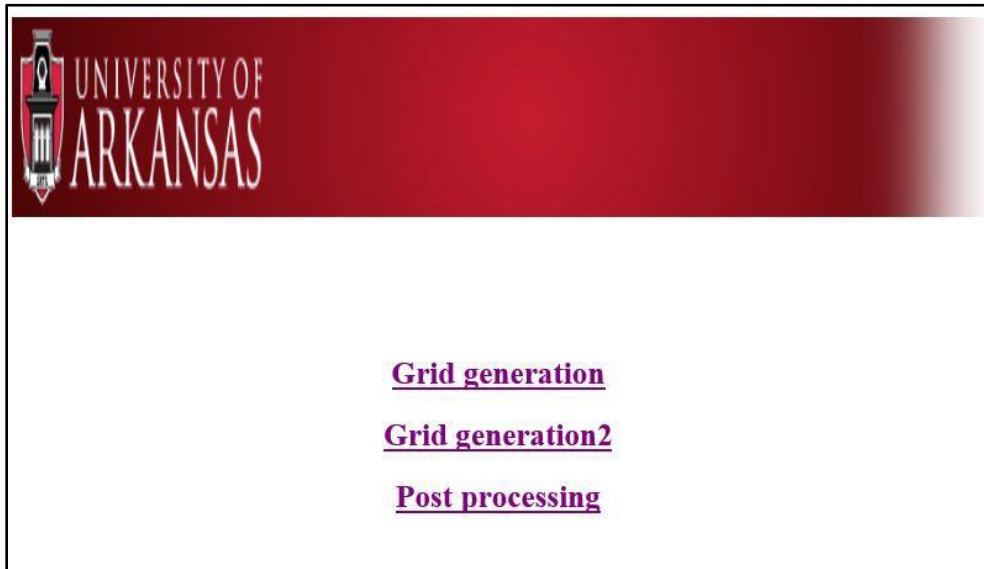


Figure 7-1: General window interface for pre and post processing

2- Enter the different data as display in Figure 7-2

Figure 7-2: Window interface for the acbrg-i.txt file generation

Input 1: enter value of the number of bridge inner points and number of radial points respectively in the first and second boxes

Input 2: Enter number of space between tangential point

- Value 1: number of space between point 1 and 2
- Value 2: number of space between point 2 and 3
- Value 3: number of space between point 3 and 4

Note: Points 1, 2 and 3 are bridge inner points and represented in Figure 7-5, value 3 must be an even number since the number of space will be equally divided for the spacing between point 6, 7 and 8

Drmin: Enter the minimum grid spacing in the radial direction

Drmax: Enter the maximum grid spacing in the radial direction

Gf: Enter the growth factor for the radial spacing development Gf is recommended to be between 1 and 1.2

Bridge and domain coordinates: Enter in the first two columns boxes (8 rows) the bridge inners points coordinates and in the two last rows enter the coordinates of the domain points

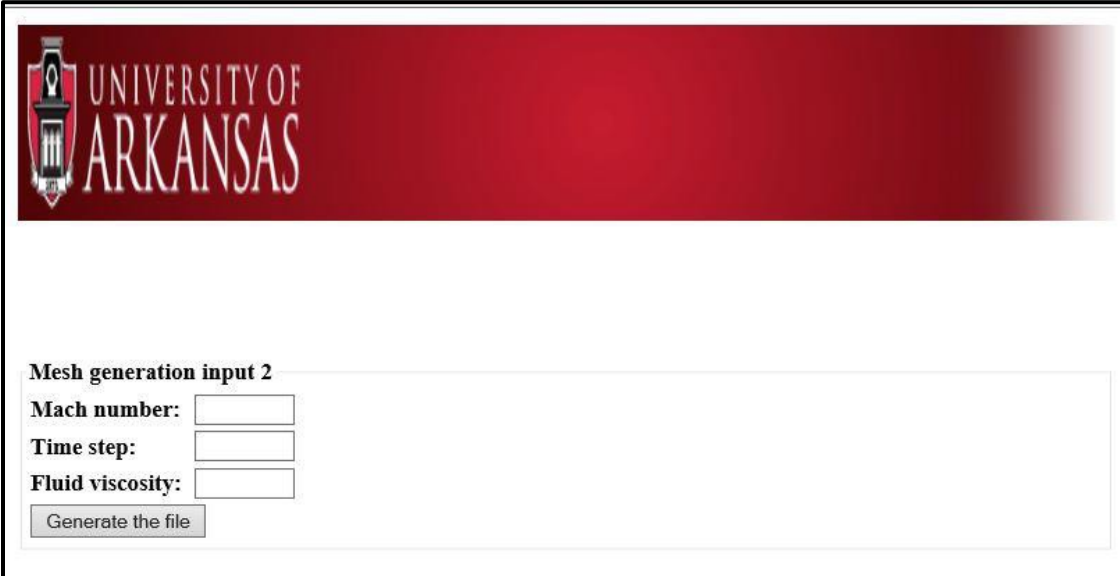
3- *Click on the box “Generate the file” and save the file*

By clicking on “generate the file”, a text file is created with the first input data **acbrg-i.txt** for the grid generation. Simply save the file using **acbrg-i.txt** name.

7.2.2. Step 2: Pre-processing, preparation of the second input data inp.txt

1- *Go to <http://comp.uark.edu/~btmbiand/> and click on Grid generation 2*

Use the link above to access to the general window interface in Figure 7-1, after clicking on Grid generation 2 a screen similar to Figure 7-3 will appear on the user fill the boxes and generate the inp.txt file.



The screenshot shows a web-based interface for mesh generation. At the top, there is a red banner with the University of Arkansas logo and the text "UNIVERSITY OF ARKANSAS". Below this banner, the main content area is white and contains the following elements:

- A title "Mesh generation input 2" in bold black text.
- Three input fields, each with a label and a text box:
 - "Mach number:" followed by an empty text box.
 - "Time step:" followed by an empty text box.
 - "Fluid viscosity:" followed by an empty text box.
- A button labeled "Generate the file" located at the bottom left of the input area.

Figure 7-3: *Grid generation input file 2 window interface*

Mach number: enter the Mach number

Mach number is a dimensionless number used to express the flow speed when analyzing systems that involved high speed gas flow. $Mach = V/C$ where V is the speed of flow and C is the speed of sound

Mach number=0.3 in our case, indeed for Incompressible flow $Mac < 0.3$ (Cengel & Cimbala, 2006) and for reasonable flow, $0.3 < Mach < 0.7$ (Song & Chen, 1996)

Time step: Enter the time step for the iteration, time step in our case 0.0001

Fluid Viscosity: Enter the wind/air viscosity, in the present work the fluid viscosity in 10^{-5}

7.2.3. Step 3: Processing, run the code acbrg.exe

Here the user can either double-click on the file **acbrg.exe** or use DOS system to run the code. Using DOS system, one needs to follow these step:

- Open the command prompt windows: use the window search engine and type **cmd** or go to all *program* -> *accessories* -> *cmd prompt*
- In the command prompt windows, write: **cd->copy and paste the file name path->write the file name(acbrg.exe) and press enter key**

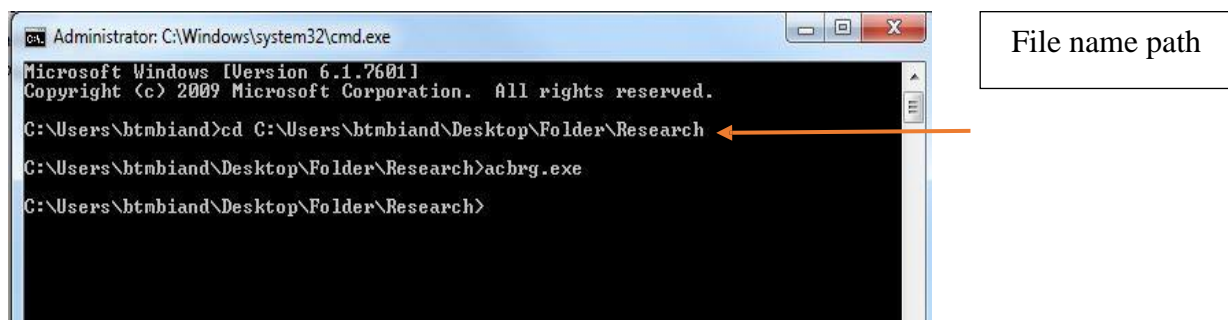


Figure 7-4: Dos windows to run acbrg.exe code

7.2.4. Step 4: Post-processing, visualization of the output file

Once the program **acbrg.exe** is executed two files are generated:

- **acbrg-o.plt** for the mesh visualization
- **acbr.txt**, input file for the Bridge Solver. This file displays:

the number of tangential points (im), radial points (jm), total number of iteration, viscosity value, time step, Mach number and ib_1, ib_2, ib_3 respectively. The total number of grid points going counterclockwise from the first domain point to the same point as shown in the Figure 7-5.

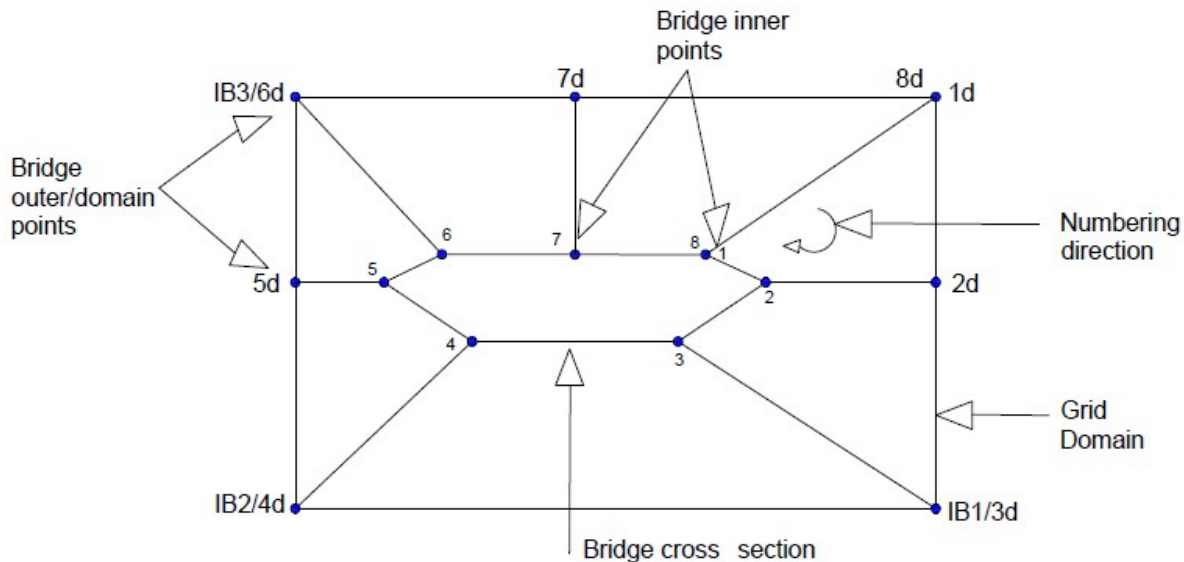


Figure 7-5: Sample Grid domain and boundary points

7.2.5. Examples

For a better understanding of the grid generation code, example of grid input and output file is given as well as illustrative pictures in figure A1 and A2 of appendix 1. Depending on the target level of accuracy, a more refined grid can be done, an example is shown in appendix 2.

a- Sample acbrg-i.txt

```

8, 10,13,25,37
.93548 3.2258e-2 5.0 5.0
1.0 0.0 5.0 0.0
.80645 -9.6774e-2 5.0 -5.0
.19355 -9.6774e-2 -4.0 -5.0
0.0 0.0 -4.0 0.0

6.4516e-2 3.2258e-2 -4.0 5.0

.5 4.3145e-2 .5 5.0
.93548 3.2258e-2 5.0 5.0
5 7 12 7 5 6 6
.0000000E+00 .1000000E-02 .2100000E-02 .3310000E-02 .4641001E-02
.6105101E-02 .7715611E-02 .9487173E-02 .1143589E-01 .1357948E-01
Total=10

```

Input 1: 8 bridges points; 10 radial points; 13, 25, 37 grids points between point 1d and IB1, IB1 and IB2, IB2 and IB3 respectively

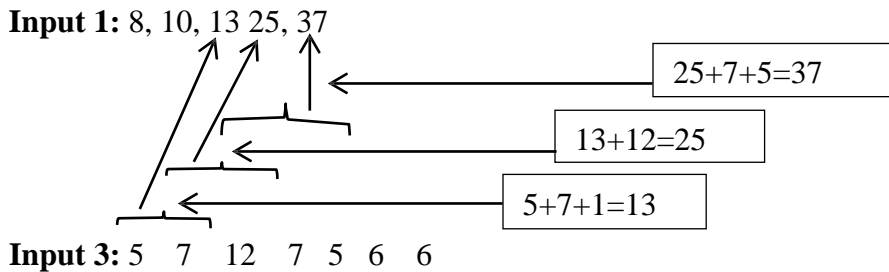
Input 2: x, y, xd, yd: coordinates of grid inner points with their corresponding outer point (8 points in total)

Input 3: spacing between the grid inner points. The number represent respectively the spacing between point 1-2,2-3,3-5,5-6,6-7,7-8,8-1.this is the same spacing between grid outer point and 1d,ib1,ib2 ,6d, ib3, 8d and 1d.

Input 4: Spacing between radial points (10 points in our case)

Note:

- Input 1 and Input 3 are related, the user should defined input 3 first before having the 3 last values of input 1. In our case we have:



- Input 4 helps for the grid development which schematic is provided in Figure 7-6 to aid in discussion of the grid. The first radial node location (R_1) is set up by the key point 2 of the bridge and therefore the first radial spacing is specified as 0. The second radial spacing (Δr_0) is specified for the location of the second radial node (R_2). The spacing between the second and third radial node (R_3) is computed as $\Delta r_1 = \Delta r_0 * Gf = (R_2 - R_1) * Gf$, where Gf is a growth factor ($1 < Gf < 1.2$). Utilizing this format, the radial dimension of the grid is increased to a maximum spacing (Δr_{max}). It should be noted that the

aforementioned grid spacing is proportionally distributed within the distance from each bridge inner point to the domain point (for instance from point 1 to 1d, 3 to 3d etc.in Figure 7-6). Utilizing the website, the user only provide Δr_0 , Δr_{max} and G_f , the input 4 is hence automatically generated.

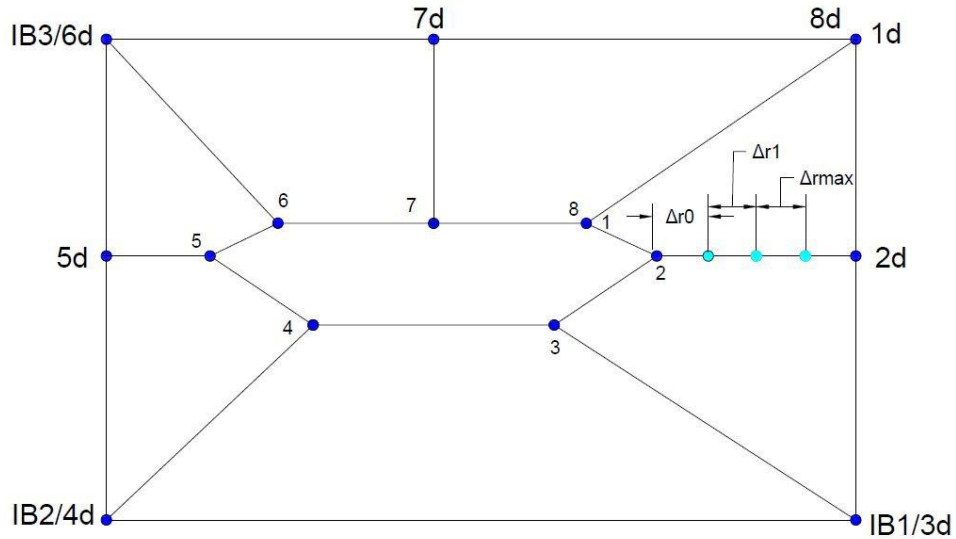


Figure 7-6: Schematic of the radial grid points development

b- Sample of inp.txt file

600000 1.e-5 0.0001 0.3

Number of iteration= $60/0.0001=600000$, for $T=60$ and $DTT=0.0001$

Fluid viscosity = 10^{-5}

Time step= 0.0001

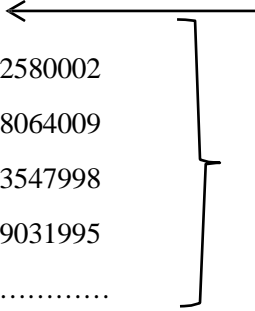
Mach number= 0.3

c- Sample output file:

1- acbr.txt file

49 10 150000 9.99999975E-006 9.99999975E-005 0.300000012

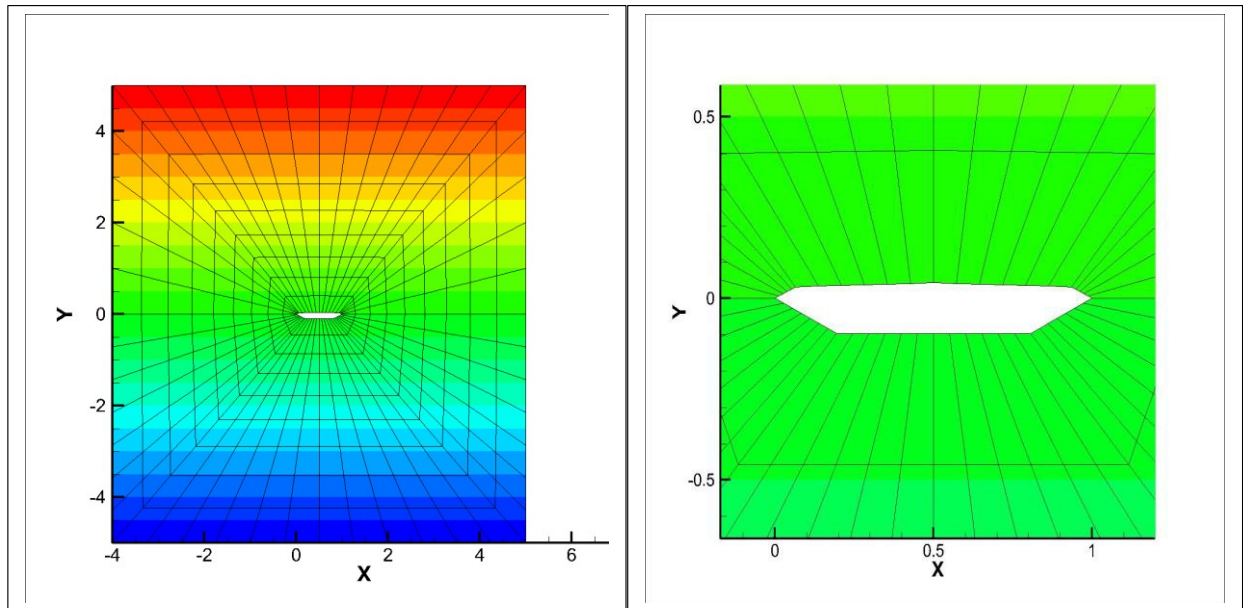
13 25 37
 0.935479999 0.0322580002
 0.948383987 0.0258064009
 0.961287975 0.0193547998
 0.974192023 0.0129031995



Output 1: 49 tangential points; 10 radial points;
 150000 iteration; 9.99×10^{-6} viscosity; 9.99×10^{-5} time
 step; 0.3 Mach number; 13,25,37 grids points between
 point 1d and ib1, ib1 and ib2, ib2 and ib3 respectively

Output 2: The coordinates x and y of the whole
 region domain points.

2- acbrg-o.plt file



a) Whole grid

b) Close up view

Figure 7-7: Sample grid visualization

7.3. User Manual for the Bridge Code

The FDM bridge analysis is done through the code **pacbrf13.out**. The code use as input file the **acbr.txt** output file generated in the grid generation (code: **acbrg.exe**) as explained in the previous section. The files obtained after the running job are:

- **acbr-o.plt** with time, drag ,lift and moment coefficient data
- **acbr-p.plt** for the visualization of the contour, pressure and vorticity plot

The program can be run using processor in parallel to reduce the computational time. Using Linux operating System, the steps to follow are:

- Create a folder in a Linux account and locate the file **acbr.txt** and **pacbrf13.out**. To create a folder in Linux use the following *command a* :

Command a: **mkdir** (press space key once) **folder name** (press enter key)

- Copy and paste the **acbr.txt** and **pacbrf22.out** in the previously created folder
- Run the **pacbrf22.out** code on Linux using the *command b*, a number assigned by the system to the job will appear on the command window as well as a **dum** file in the file transfer file window (Figure 7-9 and Figure 7-10)

Command b: **nohup** (press space key once) **mpirun** (press space key once) **-np** (press space key once) **x** (press space key once) **pacbrf13.out** (press space key once) **> dum** (press space key once) **&**

- Check if the running process is done through the *command c* and download the folder by simply copy it from the file transfer windows and paste it to the desire location.

Command c: **ps** (press space key once) **-ef**

Note:

1) **Command a:** `mkdir` stands for make a directory

To verify if the folder have effectively been created the user can type `ls`=list content of current directory, as follow:

`ls` (press enter key) or `ls` (press space key once)-`l`(press enter key)

Example: The folder “test “have been create in the user account btmbiand in Linux

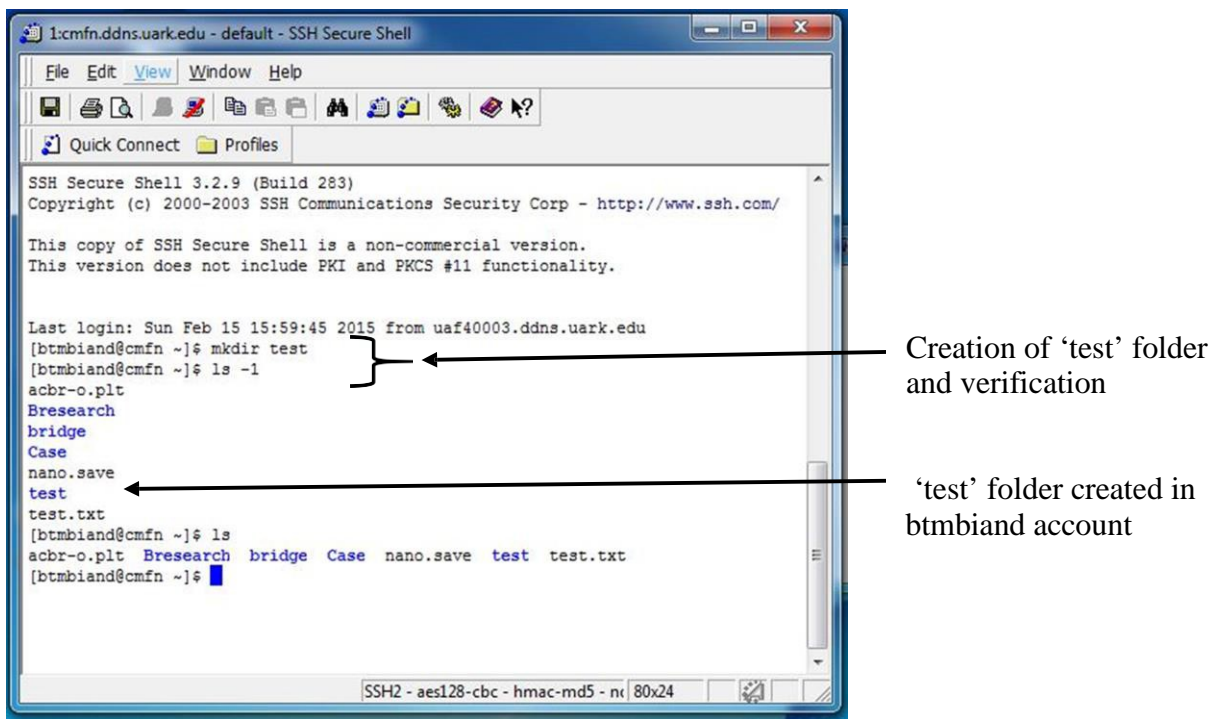
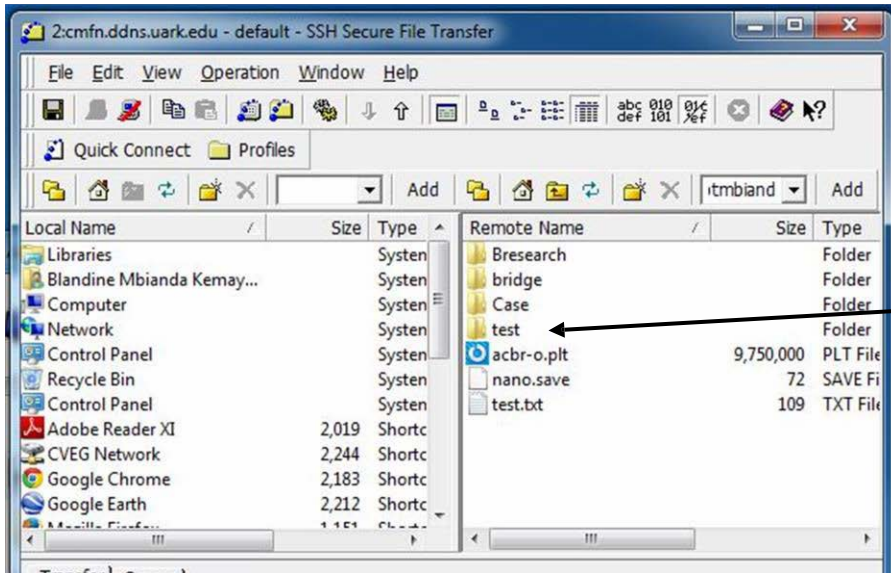


Figure 7-8: Sample creation of a folder in Linux account



'Test' previously
created

Figure 7-9: File transfer window 1

2) Command b:

nohup: continue background processes after log off, this command is optional.

mpirun: run mpi program

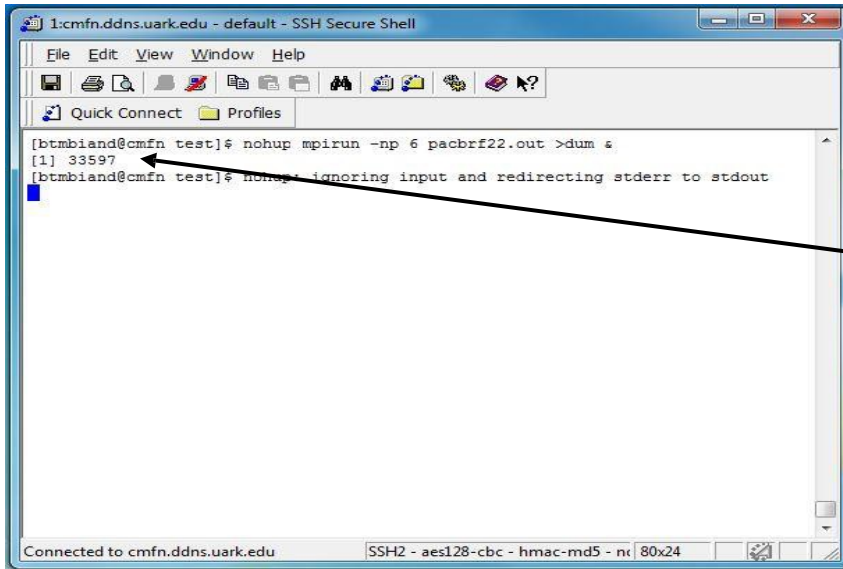
np: number of processor to run on

x: number of processor the user need to specify the number of processor he will use to run the code

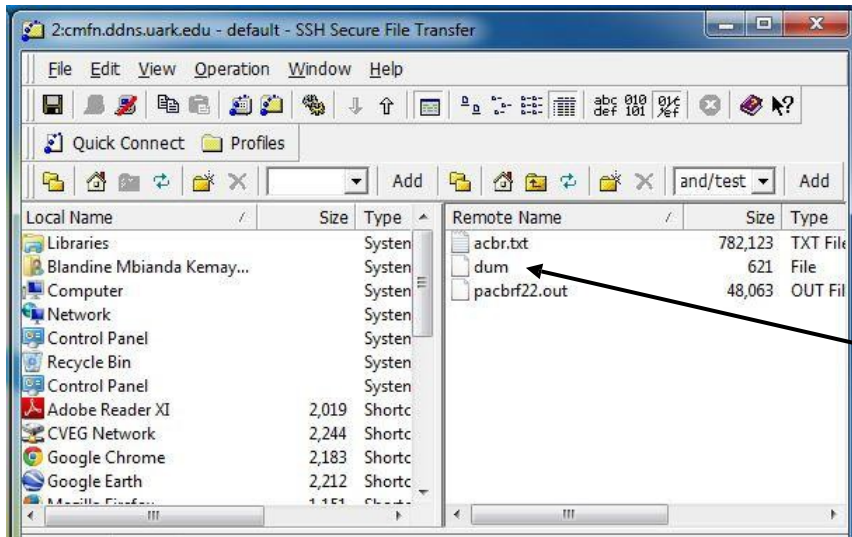
pacbrf13.out: Bridge Solver code

dum: file create to back up the output file. Once the running process begin, this file appears in the folder initially created, it also helps to ensure that the code is currently running and contains the total computational time.

Example:



Number assigned to the running job



dum file automatically created when the program is running

Figure 7-10: File transfer window 2

3) Command c:

ps -ef: shows status of background processes and the running jobs

7.4. User Manual for Post Processing

In the post processing part, data from the Bridge Solver output files are extracted, graph are plotted for instance the frequency versus amplitude, results are deduced and conclusions are made. In this section explanations on how to plot the frequency against amplitude graph will be provided since for the visualization of vector, contour, pressures and vorticity plot, the user only need to open the **acbr-p.plt** output file.

To plot the frequency against amplitude graph, the **acbr-o.plt** file obtained in the previous step is used as an input file. The first ten units has to be removed and replaced by the line containing the data stored in **dft-i.txt** file. Indeed, these units are strongly affected by the impulsive initial condition and cause a lot of fluctuation and perturbations in the results. To smooth the result the user need to follow the step below:

➤ **Step 1:** Generate the **dft-i.txt** input file

1- Go to <http://comp.uark.edu/~btmbiand/> click on Post processing

Use the link above to access to the general window interface in Figure 7-1, after clicking on post processing a screen similar to Figure 7-11 will appear; the user fill the boxes ,generate the dft-i.txt file and save if in the desired location.

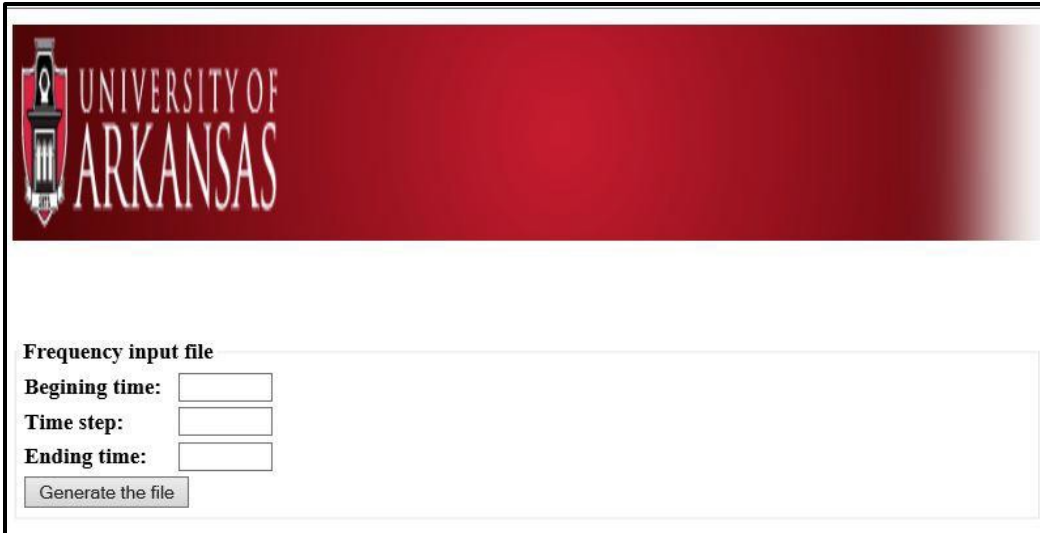


Figure 7-11: Windows interface for the *dft-i.txt* post processing file generation

Beginning time: Time beginning, with the first 10 units removed, it is recommended to use 10 as a beginning time.

Notes:

The first 10 non-dimensional time units are withdraw from the **acbr-o.plt** input file as explained in previous section. Bruno & Chris (2003) recommended a minimum sampling extent of 30 non-dimensional time units which is required in order to assume stationary signal

Time step: enter the same time step used in the **inp.txt** file

Ending time: Time ending, this is the initial time unit choose for the analysis

Example of dft-i.txt file

500001, 10.0, 60.0, 0.1,150,2,100000

$np = (60-10)/Dtt + 1 = 50/0.0001 + 1 = 500001$

Beginning time =10

Ending time=60

nf1=0.1

nf2=150

idir=2

nstart=10/DTT=10/0.0001=100000

Notes:

np: The number of iteration remaining when the first 10 nondimensional time units are withdraw from the **acbr-o.plt** input file

nf1 and nf2: Parameter used for the frequencies calculation,

idir: columns number containing the drag coefficient and used to compute the mean drag coefficient. idir=2

nstart: number of iteration or line to skip in order to delete the first 10 units time

nstart=10/DTT

➤ **Step2:** Run **dft-p.exe** file

Run the file **dft-p.exe** by a left click on it; the **fr-i.txt** file is obtained and will be used for the frequency versus amplitude plot. The **average.txt** file is also generated and contains the mean drag coefficient.

Example of fr-i.txt file and average.txt file

- **fri.txt file**

```

500001 10. 60. 1 150 2
10. 0.09205451 -0.2886517
10.0001 0.09206569 -0.2886605
10.0002 0.09207683 -0.2886692
10.0003 0.09208794 -0.2886778
.....

```

→ Data insert from the **dft-i.txt** file

} Time, Cd and Cl (drag and lift coefficient) for each iteration

- **average.txt file**

0.3131 → A single value of the mean drag coefficient

➤ **Step3:** Run **freq3.exe** code using **fr-i.txt** as input.

When running **freq3.exe** file, the **fr-o.plt** file is generated. By opening the **fr-o.plt** file, a frequency against amplitude plot as in Figure 7-12 is displayed.

Notes to run **dft-p.exe** and **freq3.exe** code the user needs **dft-i.txt** and **fr-i.txt** files respectively.

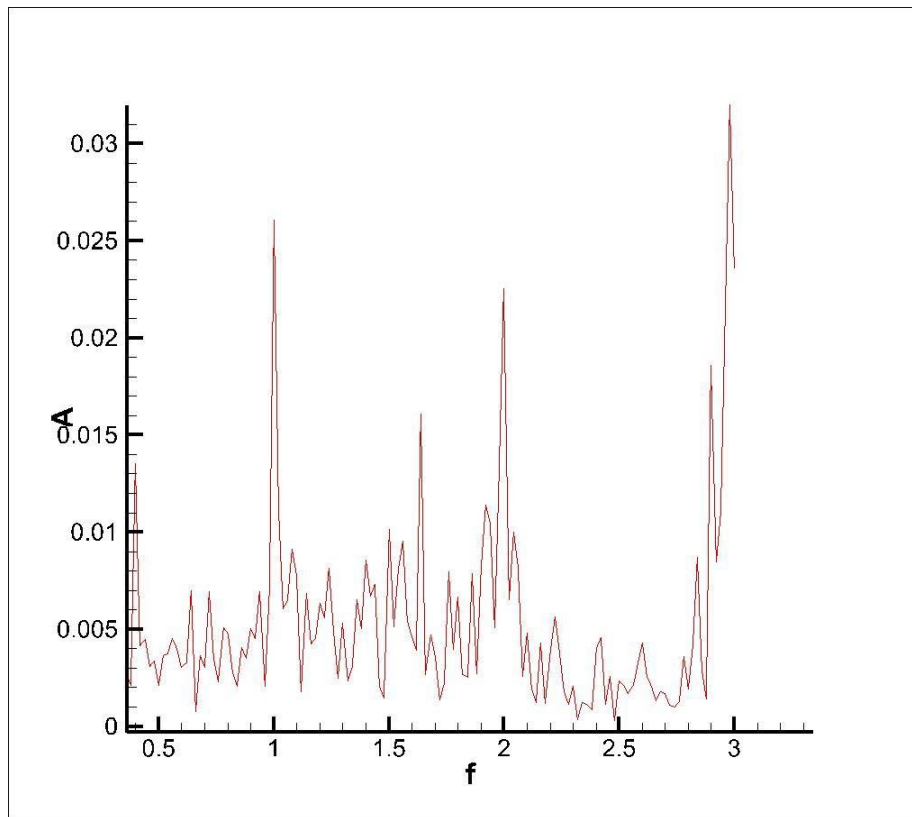
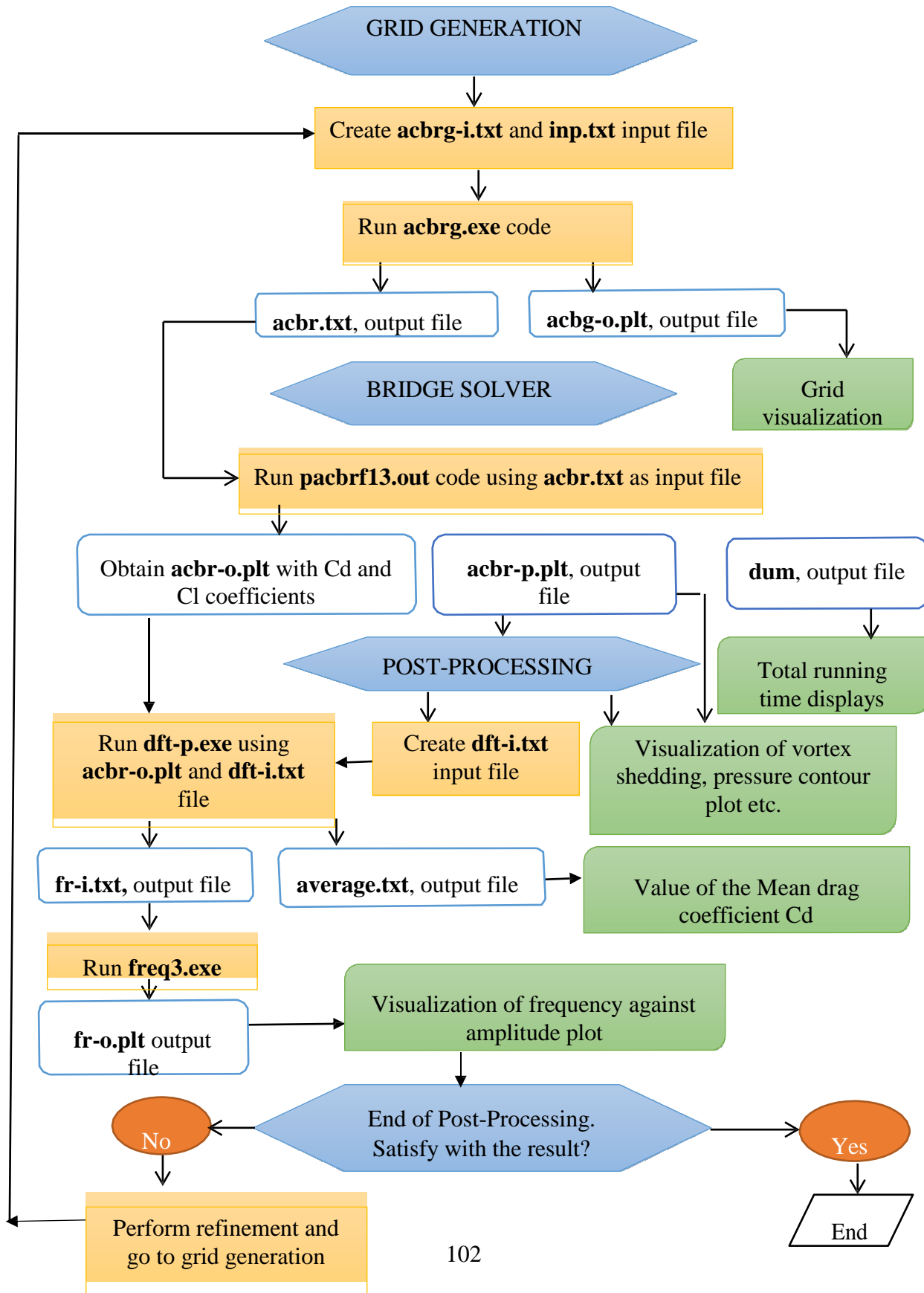


Figure 7-12: Frequency versus amplitude plot from *fr-o.plt* file

7.5. Flowchart of the design process using the package “UofA Bridge Code”



REFERENCES

- Anderson, J. (1995). *Computational Fluid Dynamics*. McGraw-Hill.
- Bai, Y., & Sun, D. (2010). 3-D aerodynamic analysis of long-span bridge deck sections ,using DES and block iterative coupling. *Earth and Space 2010:Engineering,Science ,Construction,and operations in Challenging Environments*, pp. 2152-2160.
- Bienkiewicz, B., & Kutz, R. (1993). Applying the discrete vortex method to flow around bluff bodies. *Journal of wind engineering and Industrial aerodynamics*, 36, 1011-1020.
- Blazek , J. (2001). *Computational Fluid Dynamics:Principles and applications*. Oxford England.
- Bosch, H., & Oneyemelukwe, O. (1993). Numerical simulation of wind flow patterns and wind-induced forces on bridges deck section models. Proceeding:7th US national Wind Engineering Conference, (pp. 493-501). Los Angeles,June 27-30.
- Braun, A., & Awruch, A. (2003). Numerical Simulation of the wind Action on a long-span bridge deck. (A. d. Neto, Ed.) *Journal of the brazillian society of Mechanic,Science and Engineering*, XXV(4), 352-363.
- Braun, A., & Awruch, A. (2008). Finite element simulation of the wind action over bridge sectional models:Application to the Guama River Bridge (Para state,Brazil). *Finte Elements in Analysis and Design* , 44, 105-122.
- Bruno, L., & Khris, S. (2003). The validity of 2D Numerical simulations of Vortical Structure around a bridges deck. *Mathematical and computer Modelling*, 37, 795-828.
- Cengel, Y., & Cimbala, J. (2006). *Fluids Mechanics:Fundamentals and applications*. McGraw Hill.
- Chen, C., & Jaw, S. (1998). *Fundamentals of turbulence modeling*. Washington DC: Taylor & Francis.
- Chetverushkin, B., Churbanova, N., Trapeznikova, M., & Romanyukha, N. (2004). Solution of computational fluid dynamics problems on parallel computers with distributed memory. In B. Chetveruskin, A. Ecer, J. Periaux, N. Satofuka, & P. Fox (Ed.), *Parallel computational fluid dynamic:Advanced numerical methods software and applications*, (pp. 489-496). Moscow Russia.
- Davenport, A., King, J., & Larose, G. (1992). Taut strip model tests. In A. Larsen (Ed.), *Aerodynamics of Large Bridges* (pp. 113-124). Balkema ,Rotterdam.
- Diana, G., Fiammenghi, G., Belloli, M., & Rocchi, D. (2013). Wind tunnel tests and numerical approach for long span bridges:the Messina bridge. *Journal of Wind Engineering and Industrial Aerodynamics*, 122, 38-49.

- Diana, G., Rocchi, D., & Muggiasca, S. (2008). Aerodynamics Instability of a bridge deck section model: Linear and non linear approach to force modelling. *BBA VI Internationnal Colloquium on :Bluff Bodies Aerodynamics & Apllications*. Milano, Italy.
- Fan Liaw, K. (2005). *Simulation of flow around bluff bodies and bridge Deck sections using CFD*. Phd thesis, University of Nottingham, School of Civil Engineering.
- Ferziger, J., & Peric, M. (1999). *Computational Methods for Fluid Dynamics* (2nd ed.). Springer.
- Frandsen, J. (2004). Numerical bridge deck studies using finite elements. Part I: flutter. *Journal of fluids and structures*, 19, 171-191.
- Frandsen, J. (2004). Numerical bridge deck stuides using finite elements. Part I: flutter. *Journal of fluids and structures* , 19, 171-191.
- Fujiwara, A., Kataoka, H., & Ito, M. (1993). Numerical simulation of flow field around an oscillating bridge using finite difference method. *Journal of wind Engineering and Industrial aerodynamics*, 46&47, 567-575.
- iClickfun. (n.d.). *Top 10 longest suspension bridges*. Retrieved 11 16, 2015, from www.iclickfun.com: <http://www.iclickfun.com/top-10-longest-suspension-bridges/>
- Kemayou, B., Selvam, P., Bosch, H., & Nawfal, A. (11-14 November 2015). Aero Elastic analysis of bridge deck sections by FDM using LES: Improving the performance through implementation of parallel computing. *XIX National Engineering Convention of Civil engineering*, (pp. 1-8). Huaraz-Peru.
- Kiris, C., Housman, J., & Kwak, D. (n.d.). *Comparison of artificial compressibility Methods*. California.
- Kuroda, S. (1997). Numerical simulation of flow around a box girder of a long span suspension bridge. *Jouranal of wind engineering and Industrial aerodynamics*, 67&68, 239-252.
- Larsen, A., & Walther, J. (1997). Aeroelastic analysis of bridge girder sections based on discrete vortex simulations. *Journal of Wind Engineering and Industrial Aerodynamics*, 67&68, 253-265.
- Larsen, A., & Walther, J. (1997). Aeroelastic analysis of bridge girder setions based on discrete vortex simulations. *Journal of wind Engineering and industrial Aerodynamics* , 67&68, 253-265.
- Larsen, A., & Walther, J. (1998). Discrete Vortecx Simulation of flow around five generic bridge deck sections. *Journal of Wind engineering and Industrial Aerodynamics*, 77&78, 591-602.
- Lewis, R. (1991). *Vortex Element Methods for Fluid Dynamics Analysis of Engineering Systems*. Cambridge University Press.
- Liu, H. (1991). *Wind engineering a hand book for structural engineers*. New Jersey: Prentice-Hall .

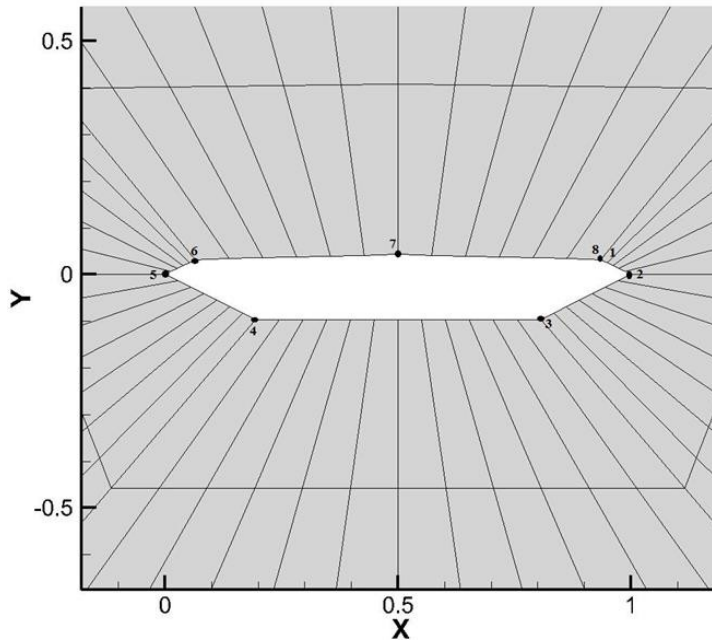
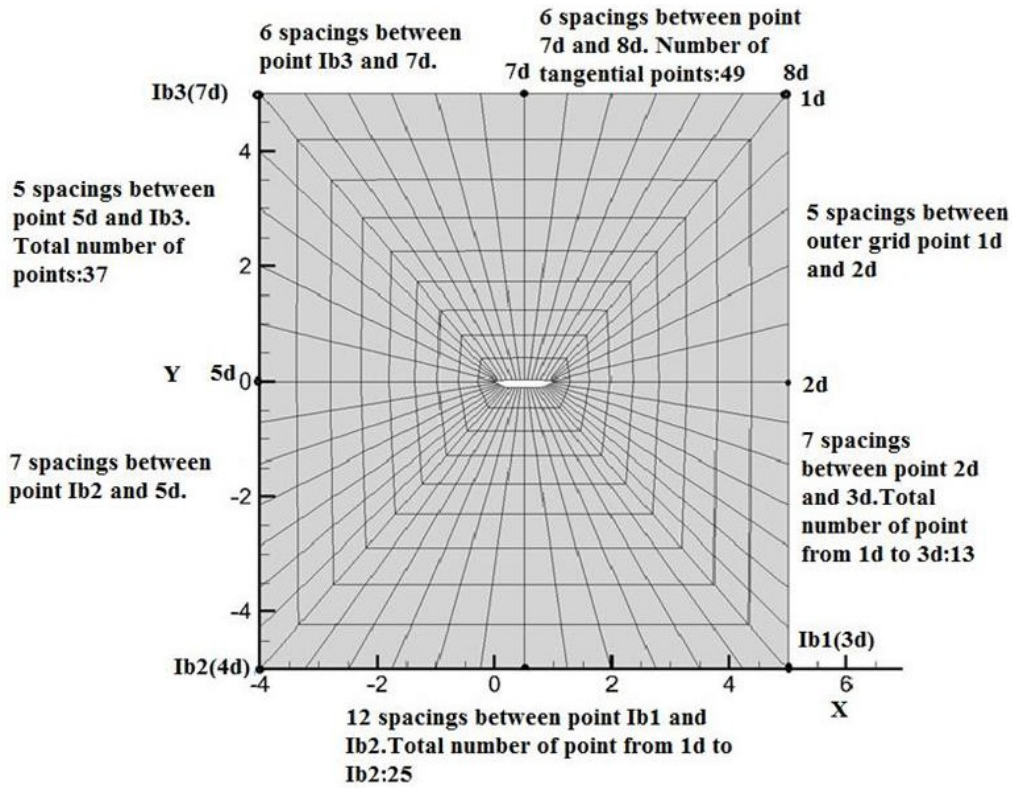
- Madsen, H. O., & Ostenfeld, P. (1992). Wind criteria for long span Bridges. In A. Larsen (Ed.), *Proceedings of the first International symposium on Aerodynamics of Large Bridges* (pp. 33-43). Denmark: Balkema Rotterdam.
- McNamara, G., & Zanetti, G. (1998). Use of the Boltzmann equation to simulate Lattice gas automata. *Physical Review Letters*, *61*, 2332-2335.
- Menter, F., & Kuntz, M. (2001). Development and application of a zonal DES turbulence for CFX-5. *ANSYS CFX Validation Report, CFX-VAL17/0703*, 1-34.
- Mohammadi, S., & Mukherjee, R. (2013). *Wind loads on bridges analysis of a three span bridge based on theoretical methods and Eurocode 1*. Master thesis, Royal Institute of Technology(KTH), Department of Civil and Architectural Engineering, Stockholm, Sweden.
- Morgenthal, G. (2000). *Fluid-Structure Interaction in Bluff-body Aerodynamics and Long-Span Bridges Design: Phenomena and Methods*. Technical Report, University of Cambridge, Department of Engineering.
- Morgenthal, G., & McRobbie, A. (2002). A comparative study of numerical methods for fluid structure interaction analysis in long-span bridge design. *Wind and structure*, *5*(2), 101-114.
- Morgenthal, G., & McRobbie, A. (2002). A comparative study of numerical methods for fluid structure interaction analysis in long-span bridge design. *Wind and structure*, *5*(2), 101-114.
- Ostenfeld, K., & Larsen, A. (1992). Bridges Engineering and Aerodynamics. In A. Larsen (Ed.), *Proceeding of the first International Symposium on Aerodynamics of Large Bridges* (pp. 3-22). Denmark: Balkema Rotterdam.
- Parson. (n.d.). *Tacoma Narrows bridge project*. Retrieved 11 10, 2015, from <http://www.bing.com/images/search?q=full+tacoma+narrow+bridge+wind+tunnel+test+images&view=detailv2&&id=EDB1256817593BC2C402274E72A66BC88498A034&selectedIndex=5&ccid=q4%2fucg9X&simid=608033439746361805&thid=JN.HbPuMubgUwLPyQSIYADwdQ&ajaxhist=0>.
- Patro, S., Selvam, P., & Bosch, H. (2009). H-adaptive FEM and moving grids for bridge aerodynamics. *11th American conference on wind Engineering*, (pp. 1-11). San Juan, Puerto Rico.
- Patro, S., Selvam, P., & Bosch, H. (2009). H-adaptive FEM and moving grids for bridges Aerodynamics. *11th Americas Conference on Wind Engineering June 22-26*. San Juan, Puerto Rico.
- Patro, S., Selvam, R., & Bosch, H. (2013). Adaptive h-finite element modeling of wind flow around bridges. *Engineering Structures*, *48*, 569-577.
- Reinhold, T., Brinch, M., & Damsgaard, A. (1992). Wind Tunnel test for the Great Belt Link. In A. Larsen (Ed.), *Aerodynamics of Large Bridges* (pp. 255-267). Rotterdam Balkema.

- Rhie, C., & Chow, W. (1983). A numerical study of turbulent flow past an isolated airfoil with trailing edge separation. *AIAA*, 1525-1532.
- Sarwar, M., & Ishihara, T. (2010). Numerical study on suppression of vortex-induced vibrations of box girder bridge section by aerodynamics countermeasures. *Journal of Wind Engineering and Industrial Aerodynamics*. doi:10.1016/j.jweia.2010.06.001
- Selvam, R., & Govindaswamy, S. (2002). *A report on Aeroelastic analysis of bridge girder section using computer modelling*. University of Arkansas, Civil Engineering, Fayetteville.
- Selvam, P. (2014). *Computational fluid dynamics*. Classnotes, University of Arkansas, Civil engineering, Fayetteville.
- Selvam, R. (1998). Computational procedure in grid based computational bridge aerodynamics. In A. Larsen, & S. Esdahl (Ed.), *Proceeding of the International symposium advances in bridge aerodynamics* (pp. 327-337). Denmark: A.A Balkema/Rotterdam/Brookfield.
- Selvam, R. (2010). Building and bridge Aerodynamics Using computational wind Engineering. *The international workshop on Wind Engineering Research and Practise, May 28-29*. Chapel Hill, NC, USA.
- Selvam, R. (2010, May 28-29). Building and bridge Aerodynamics using computer wind engineering. *International Workshop on Wind engineering Research and practise*. NC: Chapel Hill.
- Selvam, R., & Bosch, H. (1999). Finite element Modelling of flow around bridges. (A. Larsen, & G. Larose, Eds.) *Wind engineering into the 21st century*, 2, 1321-1327.
- Selvam, R., & Govindaswamy, S. (2001). *Aeroelastic Analysis of bridge girder section using computer modeling*. Master Thesis, University of Arkansas, Department of Civil engineering, Fayetteville.
- Selvam, R., Bosch, H., & Govindaswamy, S. (2001). *Aeroelastic Analysis of bridge deck sections by finite element methods and moving grids*. Fayetteville: Lendis Corporation project work.
- Selvam, R., Bosch, H., & Joshi, R. (2010). Comparison of 2D and 3D CFD modeling of bridge aerodynamics. *The fifth International symposium on computational Wind engineering (CWE 2010)*. North Carolina: Chapel Hill.
- Selvam, R., Govindaswamy, S., & Bosch, H. (2002). Aeroelastic analysis of bridge using FEM and moving Grid. *Wind and Structure*, 5(2-4), 257-266.
- Selvam, R., Tarini, M., & Larsen, A. (1997b). Computer modelling of flow around bridges using LES and FEM. *Journal of Wind Engineering and Industrial Aerodynamics*, 77-78, 643-651.
- Selvam, R., Tarini, M., & Larsen, A. (1998). Computer modelling of flow around bridges using LES and FEM. *Journal of Wind Engineering and Industrial Aerodynamics*, 77&78, 643-651.

- Simiu, E., & Scanlan, R. (1986). *Wind effects on Structures*. Maryland: John Wiley & Sons, Inc.
- Song, C., & Chen, X. (1996). Compressibility boundary layer and computation of small Mach number flows, Hydrodynamics theory and application. *Second International Conference on Hydrodynamics*. Hong Kong.
- Song, C., & Chen, X. (1996). Compressibility boundary layer and computation of small Mach number flows. In Lee, & Leung (Eds.), *Hydrodynamics*. Balkema, Rotterdam.
- Sorensen, N. (1995). *General Purpose flow solver applied to flows over Hills*. Riso National Laboratory. Roskilde, Denmark: RISO-R-827(EN).
- Stathopoulos, T. (1997). Computational wind engineering: Past achievements and future challenges. *Journal of Wind Engineering and industrial aerodynamics*, 67&68, 509-532.
- Strommen, E. (2010). *Theory of Bridge Aerodynamics* (2nd ed.). Norway: Springer.
- Tamura, T., & et al. (1993). On the reliability of two-Dimensional Simulation for the unsteady flows around a cylinder-type structure. *Journal of Wind Engineering and Industrial Aerodynamics*, 35, 275-298.
- Tanaka, H. (1992). Similitude and modelling in bridge aerodynamics. In A. Larsen (Ed.), *Aerodynamics of Large Bridges* (pp. 83-94). Balkema, Rotterdam.
- Theodorsen, T. (1935). *General theory of aerodynamic instability and the mechanism of flutter*. Technical Report 496, NACA.
- Ubertini, F. (2008). *Wind effects on bridges: Response, stability and control*. PhD thesis, University of Pavia, Department of Civil Engineering, Pavia, Italy.
- Uphoff, S., Geller, S., & Krafczyk, M. (2012). *Study of flow around a bridge cross section with a Lattice Boltzmann LES model*. Institute for Computational Modeling in Civil Engineering TU Braunschweig, Braunschweig.
- Wu, T., & Kareem, A. (2014). Simulation of nonlinear bridge aerodynamics: A sparse third-order Voleterra model. *Journal of Sound and vibration*, 333, 178-188.
- Yang, J., & Balaras, E. (2006). An embedded-boundary formulation for large-eddy simulation of turbulent flows interacting with moving boundaries. *Journal of Computational Physics*, 215, 12-40.

Appendix 1: Grid details with inner and outer points

Section 7.2.5 example: 10 radial and 49 tangential points, 8 inner and outer points



Appendix 2: Sample input and output file for more refined grid

1- Sample input file for a more refined grid (90x471)

8, 90, 47,167,213	←	Input 1: 8 bridges points; 90 radial points; 47,167,213 grids points between point 1d and IB1, IB1 and IB2, IB2 and IB3 respectively
.93548 3.2258e-2 5.0 5.0	}	Input 2: x, y, xd, yd: coordinates of grid inner points with their corresponding outer point (8 points in total)
1.0 0.0 5.0 0.0		
.80645 -9.6774e-2 5.0 -5.0		
.19355 -9.6774e-2 -4.0 -5.0		
0.0 0.0 -4.0 0.0		
6.4516e-2 3.2258e-2 -4.0 5.0		
.5 4.3145e-2 .5 5.0		
.93548 3.2258e-2 5.0 5.0		
21 25 120 25 21 60 60	←	Input 3: spacing between the grid domain (d) outer points. The number represent respectively the spacing between point 1d and 2d,2d and Ib1,ib1 and ib2,ib2 and point 6d,6d and ib3,ib3 and 8d,8d and 1d.

.0000000E+00 .1000000E-02 .2100000E-02 .3310000E-02 .4641001E-02	}	Input 4: Spacing between radial points (90 points in our case)		
.6105101E-02 .7715611E-02 .9487173E-02 .1143589E-01 .1357948E-01				
.1593743E-01 .1853117E-01 .2138429E-01 .2452272E-01 .2797499E-01				
.3177249E-01 .3594974E-01 .4054471E-01 .4559918E-01 .5115911E-01				
.5727502E-01 .6400252E-01 .7140277E-01 .7954305E-01 .8849736E-01				
.9834710E-01 .1091818E+00 .1211000E+00 .1342100E+00 .1486310E+00				
.1644941E+00 .1819435E+00 .2011379E+00 .2222517E+00 .2454768E+00				
.2710245E+00 .2991270E+00 .3300397E+00 .3640437E+00 .4014480E+00				
.4425929E+00 .4878522E+00 .5376374E+00 .5924011E+00 .6526413E+00				
.7189054E+00 .7917960E+00 .8719757E+00 .9601732E+00 .1057191E+01				
.1163910E+01 .1263910E+01 .1363910E+01 .1463910E+01 .1563910E+01				
.1663910E+01 .1763910E+01 .1863910E+01 .1963910E+01 .2063910E+01				
.2163910E+01 .2263910E+01 .2363909E+01 .2463909E+01 .2563909E+01				
.2663909E+01 .2763909E+01 .2863909E+01 .2963909E+01 .3063909E+01				
.3163909E+01 .3263909E+01 .3363909E+01 .3463908E+01 .3563908E+01				
.3663908E+01 .3763908E+01 .3863908E+01 .3963908E+01 .4063908E+01				
.4163908E+01 .4263908E+01 .4363908E+01 .4463908E+01 .4563908E+01				
.4663908E+01 .4763907E+01 .4863907E+01 .4963907E+01 .5063907E+01				
Total=90				

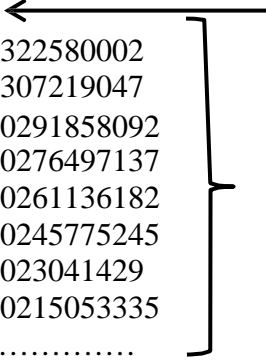
2- Output file for a more refined grid (90x333)

a) acbr.txt file

```
333 90 600000 9.99999975E-006 9.99999975E-005 0.300000012
```

```
47 167 213
```

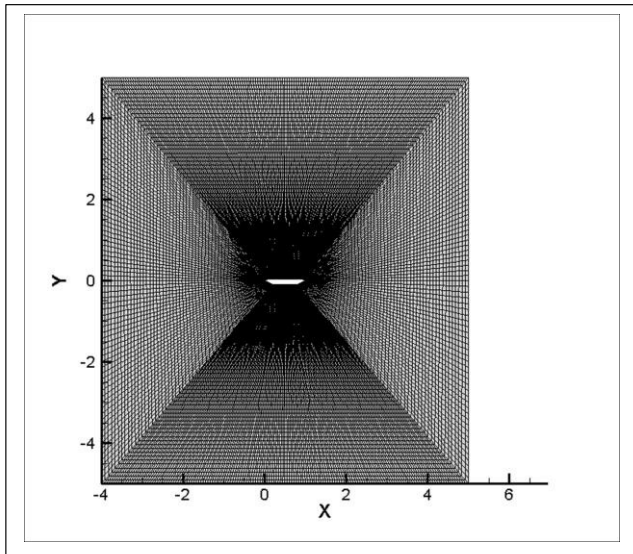
```
0.935479999 0.0322580002
0.93855238 0.0307219047
0.941624761 0.0291858092
0.944697142 0.0276497137
0.947769523 0.0261136182
0.950841904 0.0245775245
0.953914285 0.023041429
0.956986666 0.0215053335
.....
```



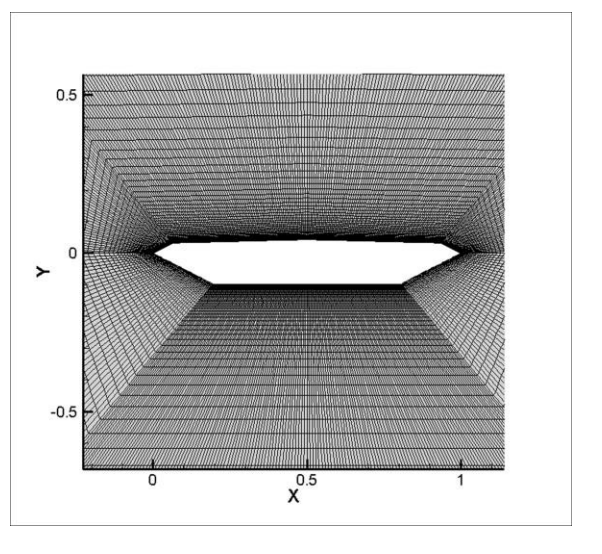
Output 1: 471 tangential points; 90 radial points; 150000 iteration; 9.99×10^{-6} viscosity; 9.99×10^{-5} time step; 0.3 Mach number; 76,236,311 grids points between point 1d and ib1, ib1 and ib2, ib2 and ib3 respectively

Output 2: The coordinates x and y of the whole region domain points.

b) acbrg-o.plt file



a) Whole grid



b) Close up view